International Scientific-Technical and Production Journal

The Paton WELDING JOURNAL

April 2010 # 4

English translation of the monthly «Avtomaticheskaya Svarka» (Automatic Welding) journal published in Russian since 1948

Founders: *E.O. Paton Electric Welding Institute of the NAS of Ukraine*
International Association «Welding»

Publisher: *International Association «Welding»*

Editor-in-Chief B.E.Paton

Editorial board:

Yu.S.Borisov, V.F.Khorunov, A.Ya.Ishchenko, I.V.Krivtsun, B.V.Khitrovskaya, L.M.Lobanov, V.I.Kirian, A.A.Mazur, S.I.Kuchuk-Yatsenko, Yu.N.Lankin, I.K.Pokhodnya, V.N.Lipodaev, V.D.Poznyakov, V.I.Makhnenko, K.A.Yushchenko, O.K.Nazarenko, A.T.Zelnichenko, I.A.Ryabtsev

International editorial council:

N.P.Alyoshin (Russia), U.Diltey (Germany), Guan Qiao (China), D. von Hofe (Germany), V.I.Lysak (Russia), N.I.Nikiforov (Russia), B.E.Paton (Ukraine), Ya.Pilarczyk (Poland), P.Seyffarth (Germany), G.A.Turichin (Russia), Zhang Yanmin (China), A.S.Zubchenko (Russia)

Promotion group:

V.N.Lipodaev, V.I.Lokteva, A.T.Zelnichenko (exec. director)

Translators:
A.A.Fomin, O.S.Kurochko, I.N.Kutianova, T.K.Vasilenko, PE «Melnik A.M.»

Editor
N.A.Dmitrieva

Electron galley:
D.I.Sereda, T.Yu.Snegiryova

Address:
E.O. Paton Electric Welding Institute,
International Association «Welding»,
11, Bozhenko str., 03680, Kyiv, Ukraine
Tel.: (38044) 287 67 57
Fax: (38044) 528 04 86
E-mail: journal@paton.kiev.ua
http://www.nas.gov.ua/pwj

State Registration Certificate
KV 4790 of 09.01.2001

Subscriptions:
$324, 12 issues per year,
postage and packaging included.
Back issues available.

All rights reserved.
This publication and each of the articles contained herein are protected by copyright. Permission to reproduce material contained in this journal must be obtained in writing from the Publisher.
Copies of individual articles may be obtained from the Publisher.

CONTENTS

SCIENTIFIC AND TECHNICAL

Slivinsky A.A. Analysis of factors of subsolidus crack formation in welding metals with fcc-structure of crystalline lattice (Review) 2

Ryabtsev I.A., Kondratiev I.A., Chernyak Ya.P., Gordan G.N., Solomijchuk T.G. and *Godzyra N.F.* Structure and properties of high-manganese deposited metal 7

Ternovoj E.G., Bulatsev A.R., Solomijchuk T.G. and *Shulym V.F.* Repair of pipelines using orbital TIG welding inside inhabited space objects 10

Dyadin V.P. Evaluation of temperature shift depending upon the specimen thickness by the force and deformation criteria of fracture mechanics 14

Dzykovich V.I., Zhudra A.P. and *Bely A.I.* Properties of tungsten carbide powders produced by different technologies 22

Borisova A.L., Adeeva L.I., Tunik A.Yu., Tsymbalistaya T.V. and *Grishchenko A.P.* Plasma ZrO_2 coatings with metallic bond coat of alloy AlCuFe 25

INDUSTRIAL

Pokhodnya I.K. and *Kotelchuk A.S.* Advance of ferrous metallurgy and welding consumables production in PRC (Review) 30

Kuchuk-Yatsenko V.S., Nakonechny A.A. and *Sakhatsky A.G.* Resistance welding of steel reinforcement using composite insert 34

Poklyatsky A.A., Ishchenko A.Ya., Chajka A.A. and *Labur T.M.* Friction stir welding as an effective method to improve structure performance 37

Zalevsky A.V., Galinich V.I., Protsenko N.A. and *Kukharenko V.V.* Code designations of locally manufactured fluxes and flux + wire combinations in keeping with international standards 42

BRIEF INFORMATION

Lankin Yu.N. Influence of working frequency on dimensions of transformers for AC resistance welding 49

News 51

© PWI, International Association «Welding», 2010

ANALYSIS OF FACTORS OF SUBSOLIDUS CRACK FORMATION IN WELDING METALS WITH FCC-STRUCTURE OF CRYSTALLINE LATTICE (Review)

A.A. SLIVINSKY
NTUU «Kiev Polytechnic Institute», Kiev, Ukraine

The paper gives terminological analysis of the phenomenon of subsolidus cracking in welding. Structural and technological factors affecting subsolidus crack formation in welding of various materials with fcc-structure of the crystalline lattice are considered. The need for generalizing the current concepts on this issue with application of modern physical models from the field of dislocation theory of plastic deformation and brittle fracture mechanisms at high-temperature creep is noted.

Keywords: *fusion welding, subsolidus cracks, austenitic steels, nickel, aluminium, copper alloys, terminological analysis*

In keeping with the generally accepted concepts, a separate kind of brittle intercrystalline (intergranular) fracture of weld and HAZ metal is called subsolidus cracks in welding. They initiate after completion of solidification in completely solidified metal, but at high temperatures, sufficient for predominant development of viscoplastic deformation in it [1–5]. In foreign publications, including several normative documents (DVS 1004-1, DIN 8524-3 and DIN EN ISO 6520-1), this type of hot cracks are usually called ductility dip cracks (DDC).

In terms of the widely accepted N.N. Prokhorov deformation-kinetic theory of technological strength [6–11] it is not quite correct to call hot cracks of only a certain type like that, as any cases of cracking in welding are related to the joined metal staying in the appropriate temperature range of lower ductility, so-called brittle temperature range (BTR). On the other hand, the phenomenon of an abrupt ductility drop in steels and alloys suitable for high-temperature plastic deformation during their staying in the temperature range of $(0.5–0.8)T_{melt}$ and the thus caused cracking at hot forming (forge rolling, stamping, press-forging treatment) or heat treatment has been known for many years [12–14], which is exactly what led to inclusion of the term of «ductility dip cracks» into the international welding terminology.

Despite a long-time study of the phenomenon of ductility dip or subsolidus cracks, the mechanism of their formation in welding is not completely clear yet. Proceeding from analysis of published sources, we can unambiguously state only the presence of a number of common features, characteristic of subsolidus crack formation. Numerous studies of subsolidus crack surface fractography [1, 15, 16] point to their development at high temperatures, as well as the brittle, intergranular or intercrystalline nature of fracture at the moment of initaition and growth of these defects. However, these investigations, as a rule do not give any grounds to state the presence of liquid inclusions on grain boundaries during cracking.

In addition, presence of a subsolidus brittle temperature range in a certain material, unlike the «solidification BTR», is not objectively attributable to the very specifics of the fusion welding process. While potential susceptibility to solidification cracking is demonstrated by all the structural alloys at any welding processes, as well as with some other pressure welding processes, accompanied by material overheating above the solidus temperature, initiation of subsolidus cracks requires running of special structural and phase transformation in the solid metal, the probability of which essentially depends on its composition. The most susceptible to formation of subsolidus hot cracks in welding or heat treatment are metallic materials with face-centered cubic (fcc) crystalline lattice: austenitic class steels [16–18], nickel- [2, 4, 13, 19–24], aluminium- [25], copper- [26], gold- and platinum-base [27] alloys.

Results of numerous studies of weldability of these materials point to a set of certain predominantly structural factors, influencing subsolidus cracking in welding. They include grain size, type, geometry and orientation of intergranular boundaries in relation to acting stresses, presence of precipitates of other phases, segregation of impurities or higher concentration of dislocated atoms on intergranular boundaries, as well as welding heat input and temperature rate of deformation.

Thermally activated grain coarsening increases the extent of BTR and reduces the material deformability [28, 29], and also intensifies the processes of intergranular slipping [2] under the impact of welding stresses, thus promoting crack initiation. On the other hand, the results of investigations conducted by the authors of [30] with nickel alloys of different structure and composition, do not point to the presence of a strict interrelation between the susceptibility to subsolidus cracking and base metal grain size.

© A.A. SLIVINSKY, 2010

Grain coarsening as a result of selective recrystallization caused by welding heat leads to straightening of intergranular boundaries. By the data of numerous sources subsolidus cracks propagate predominantly along rectilinear «flat» boundaries [2, 4, 31].

Contrarily, curvature, «waveviness» of intergranular boundary prevents slipping of neighbouring grains over it and makes crack initiation more difficult.

The role of microchemical heteromogeneity of intergranular boundaries in subsolidus crack initiation remains ambiguous and not fully understood so far. The adverse influence of intergranular boundaries contamination by such segregated impurities as sulphur [32, 33], phosphorus [33], oxygen [34] and surface-active elements such as boron, selenium etc. on their strength is a widely known fact [35]. On the other hand, alloying elements, the segregation of which along the boundaries between the grains or crystallites promotes curving of the latter, enhance the alloy resistance to initiation of subsolidus cracks. In stable austenitic steels and alloys such an effect is demonstrated by niobium [33, 36], and in niobium alloys — by zirconium and tungsten [2]. In the opinion of the authors of [33], alloying of austenitic alloys by elements with atomic radius greater than that of elements of the solid solution base (iron, chromium, nickel), leads to suppression of selective recrystallization and promotes curving of intergranular boundaries, which is favourable for weld metal resistance to subsolidus cracking.

Assessment of the role of hydrogen dissolved in the weld metal in initiation of intergranular cracks of subsolidus type is a subject for a separate discussion. Despite the high solubility and relatively low rate of atomic hydrogen diffusion in a crystalline structure with fcc-lattice, some cases of failure of welded structures made from copper, aluminium or nickel alloys due to hydrogen embrittlement or the so-called hydrogen disease of welded joint metal are known from practical experience [37–40]. Investigation of weldability of a number of nickel alloys showed that the destructive action of hydrogen is not limited to the known cases of corrosion cracking, for instance, of nuclear reactor primary circuit steam piping. So, by the data of [41], increase of hydrogen concentration in shielding gas composition in welding a number of alloys of Ni–Cr–Fe system causes an essential lowering of weld metal resistance to subsolidus crack initiation. Fractographic analysis of crack surfaces, in addition to flat nature of fracture, also revealed individual cavities, similar to micropores [42].

Increased susceptibility of dispersion-hardening nickel alloys to formation of subsolidus cracks in welding and heat treatment made several researchers look for causes for these defects development in the processes of coagulation, or dissolution and re-precipitation, predominantly along the boundaries between the grains and crystallites, of strengthening phases, present in the structure of these alloys, namely carbides and γ′-phase of $Ni_3(Al, Ti)$ type. According to [43, 44], subsolidus cracks initiate on the boundary between the phase and grain of the solid solution as a result of higher concentration of stresses in these regions, thus causing formation of microprotrusions and their further opening into cracks during intergranular slipping under the impact of temperature stresses. Taking into account the results of processing numerous crack resistance tests in [45, 46], it is proposed to assess the nickel alloy susceptibility to subsolidus cracking, depending on their content of the main γ′-forming elements, namely aluminium and titanium. It is assumed that in alloys with a low intensity of dispersion-hardening, when the overall content of aluminium and titanium does not exceed 3–4 %, formation of subsolidus cracks during their processing in welding is improbable.

A similar opinion is expressed by the authors of [47]. Studying crack resistance of Ni–20–30 % Cr alloys, they put forward the hypothesis that the cause for subsolidus cracking in welding of these materials is contribution of additional stresses localized along grain boundaries to macroscopic action of welding stresses. These additional stresses are due to thermal ageing of the alloys with the resulting precipitation along the grain boundaries of carbide particles of the type of $(Cr, Fe)_{23}C_6$, partially coherent with the matrix crystalline lattice. Here it is stated that these are exactly the partially coherent precipitates of $(Cr, Fe)_{23}C_6$ carbides, that cause the appearance of local elastic stresses along the boundaries between the matrix grains and carbide phase particles. Non-coherent precipitates of carbides of MeC or Me_7C_3 type do not show such an effect.

On the other hand, there are numerous publications, in which the «carbide hypothesis» of subsolidus crack initiation is disproved. In [22] it is shown that the carbides distributed along the intergranular boundaries prevent boundary straightening during recrystallization and, thus, complicate the intergranular slipping and crack formation. This viewpoint is confirmed by the results of microstructural investigations [30] of the edges of subsolidus cracks formed in welds of a number of nickel alloys. It is shown that the carbide precipitates along the boundaries inhibit crack propagation instead of initiating it. More over, in [30, 48] it is established that in a number of alloys subsolidus cracks form in the high temperature range, when the carbide phase is completely dissolved or is present in an extremely insignificant amount.

A well-grounded view point on the role of $Me_{23}C_6$ type carbides and γ′-phase in formation of subsolidus cracks is given in [49, 50]. Authors of these studies showed for various dispersion-hardening nickel alloys that a local decrease of ductility of these materials under the action of welding heat is due to diffusion redistribution between the grain and intergranular

boundary of alloying elements involved in formation of the carbides and γ′-phase. As a result, in the near-weld zone near the fusion line the boundary grain portions are softened because of their depletion in γ′-phase, while grain boundaries are enriched in carbide precipitates and particles of surface-active impurities. As a result, the difference between the values of strength of intergranular boundary and grain (near it) takes critical values, this being exactly what simplifies formation of subsolidus type cracks during intergranular slipping.

Practically all the researchers of the problem of subsolidus cracks in welding of polycrystalline materials are of the opinion that development of this type of intergranular fracture occurs predominantly along the boundaries located at an angle of 45–90° relative to the weld longitudinal axis [2, 3, 27, 36, 41]. This fact is in good agreement with the decisive role of the process of intergranular slipping in subsolidus crack initiation, during which these are exactly the grain boundaries located at an angle of 45–90° to the direction of longitudinal welding stresses that are exposed to the action of maximum cleavage stresses.

In addition to the «macroscopic» spatial orientation of grain boundaries relative to the direction of the action of welding stresses, crystallographic orientation of neighbouring grains also has a certain role in subsolidus crack initiation. As is known, the angle of mismatch of crystalline lattices of the neighbouring grains determines the potential energy of the boundary between them, and, thus, the degree of its saturation with impurities. This leads to different crystallite boundaries demonstrating different deformation resistance, which, in its turn, leads to non-uniform distribution of intercrystalline deformation in welding. By the data of [2, 31], the most intensive intergranular slipping and formation of subsolidus cracks occur along the strongly disoriented, so-called regular boundaries, along which the angle of mismatch of spliced crystalline lattices is greater than 15°. The above-noted is confirmed by experimental studies on the influence of the type of intergranular boundaries on the susceptibility of metal of high-temperature nickel alloy welded joint to formation of subsolidus cracks conducted by the authors of [23]. More over, application of special stepped thermodeformation treatment of base metal before welding, which increases the volume fraction of special low-angle boundaries with a low level of free energy, allowed a considerable increase of the material ductility margin within the anticipated subsolidus BTR.

Welding heat input is a generally known technological factor of controlling welded joint metal susceptibility to hot cracking of all types. According to numerous recommendations [27, 43, 44, 51] reduction of heat input causes a narrowing of subsolidus BTR, increase of the metal ductility margin within BTR and, thus, is a rational technique for subsolidus crack prevention. As welding heat input is inversely proportional to the rate of cooling of welded joint metal, the positive effect of reduction of the heat input is most often attributed to reduction of the time of the metal staying in the range of temperatures of predominant development of intergranular plastic deformation. For instance, by the data of [27], the intensity of intergranular slipping is linearly dependent on the time of the metal staying in the high temperature range. In welding of nickel alloys, forced cooling is sometimes used for an effective reduction of this parameter and prevention of cracks in the near-weld zone [52].

Unlike the welding heat input the role of deformation increase rate in subsolidus crack formation is described in publications in a somewhat contradictory manner. The authors of [53], proceeding from the proportionality of the cooling rate to deformation rate in welding, note that decrease of deformation rate increases the intergranular slipping and promotes formation of subsolidus cracks. Similarly, by the data of [44], deformability of welded joint metal within the subsolidus BTR, increases at increase of deformation rate.

On the other hand, work [2] states the opposite — with increase of deformation rate the critical velocity of integranular slipping, sufficient for subsolidus crack initiation, decreases.

Thus, proceeding from the conducted analysis of factors of subsolidus crack formation in welding of austenitic steels and alloys, we can note their diversity and ambiguous, based on different published data, nature of their influence. On the other hand, proceeding from the intergranular nature of local fractures, which subsolidus cracks are in polycrystalline materials, it is obvious that intercrystalline plastic deformation in the form of intergranular slipping has the decisive role in their initiation.

In addition to intensive slipping of neighbouring grains, the following should be also regarded as the necessary conditions for subsolidus crack formation: stress localizing along the individual grain boundaries, non-uniform deformation of boundary portions of grains, weakening of intergrnular boundaries and adjacent grain portions by the specific nature of structural and phase transformation in welding and gradual accumulation of submicrodefects — crack nuclei — near the submicrodefect interface. This, in its turn, allows projecting the known physical models of brittle fracture of metals and alloys at high-temperature creep on the mechanism of subsolidus crack initiation in welding or heat treatment of welded joints.

CONCLUSIONS

1. Subsolidus cracks, proceeding from the totality of features, such as brittle intergranular (intercrystalline) nature of fracture, as well as temperature-time range of formation (below the solidus temperature, but above $(0.5–0.8)T_{melt}$), initiate directly under the influence of thermodeformational cycle of welding on

the material and are a separate subtype of hot cracks in welding.

2. Increased susceptibility to formation of subsolidus type cracks is found in metals and alloys with fcc-lattice and absence of allotropic transformations.

3. Influence of the following structural and technological factors on subsolidus cracking is the best studied: grain size, type, geometry and orientation of intergranular boundaries relative to the acting stresses, presence of precipitates of other phases on the intergranular boundaries, chemical inhomogeneity, as well as welding heat input and temperature rate of deformation. On the other hand, the influence of these factors has not been generalized, and by the data of various publications it is sometimes contradictory.

4. Necessary conditions for initiation of subsolidus cracks are intercrystalline plastic deformation in the form of intergranular slipping and stress localizing along the individual grain boundary portions, weakened by the specific nature of structural and phase transformations in welding. In order to construct a generalized physical model of subsolidus cracks, it is necessary to involve the modern concepts from the field of dislocation theory of plastic deformation and mechanisms of brittle fracture at high-temperature creep.

1. Hemsworth, B., Boniszewski, T., Eaton, N.F. (1969) Classification and definition of high temperature welding cracks in alloys. *Metal Const. and British Welding J.*, **2**, 5–16.
2. Shorshorov, M.Kh., Erokhin, A.A., Chernyshova, T.A. (1973) *Hot cracks in welding of heat-resistant alloys*. Moscow: Mashinostroenie.
3. Nissley, N.E., Lippold, J.C. (2003) Ductility-dip cracking susceptibility of austenitic alloys. In: *Proc. of 6th Int. Conf. on Trends in Welding Research* (15–19 April, 2002, Pine Mountain). ASM Int., 64–69.
4. Lippold, J.C., Nissley, N.E. (2007) Further investigations of ductility-dip cracking in high chromium Ni-base filler metals. *Welding in the World*, 51(**9/10**), 24–30.
5. Lancaster, J.F. (1993) *Metallurgy of welding*. London: Chapman & Hall.
6. Prokhorov, N.N. (1956) Problem of strength of metals in welding during crystallization process. *Svarochn. Proizvodstvo*, **6**, 5–11.
7. Prokhorov, N.N. (1958) Strength of metals in welding. In: *Proc. of All-Union Sci.-Techn. Meeting on Problems of Welding*. Ed. by K.V. Lyubavsky. Moscow.
8. Bochvar, A.A., Rykalin, N.N., Prokhorov, N.N. et al. (1960) To problem of «hot» (crystallization) cracks. *Svarochn. Proizvodstvo*, **10**, 3–4.
9. Prokhorov, N.N. (1962) Technological strength of metals during crystallization process in welding. *Ibid.*, **4**, 1–5.
10. Rykalin, N.N., Prokhorov, N.N., Shorshorov, M.Kh. et al. (1971) State-of-the-art and tasks in development of technological strength during crystallization process in welding. *Ibid.*, **6**, 3–5.
11. Prokhorov, N.N. (1979) *Technological strength of welds during crystallization process*. Moscow: Metallurgiya.
12. Bengough, G.D. (1912) A study of the properties of alloys at high temperatures. *Institute of Metals*, **7**, 123–174.
13. Yenisavich, W.A. (1966) Correlation of Ni–Cr–Fe alloy weld metal fissuring with hot ductility behavior. *Welding J.*, **8**, 344–356.
14. Dzugutov, M.Ya. (1971) *Plastic deformation of high-alloy steels and alloys*. Moscow: Metallurgiya.
15. Matsuda, F., Nakagawa, H. (1977) Some fractographic features of various weld cracking and fracture surfaces with scanning electron microscope. Report 1: Studies on fractography of welded zone. *Transact. of JWRI*, 6(**1**), 81–90.
16. Matsuda, F., Nakagawa, H., Ogata, S. et al. (1978) Fractographic investigation on solidification crack in the varestraint test of fully austenitic stainless steel. Pt 3: Studies on fractography of welded zone. *Ibid.*, 7(**1**), 59–70.
17. Nissley, N.E., Lippold, J.C. (2003) Development of the strain-to-fracture test. *Welding J.*, 82(**12**), 355–364.
18. Lippold, J.C., Kotecki, D.J. (2005) *Welding metallurgy and weldability of stainless steels*. John Willey & Sons.
19. Yushchenko, K.A., Lipodaev, V.N., Belchuk, M.V. et al. (1986) Resistance of welded joints of heat-resistant alloy of Hastelloy H type to hot cracking. *Avtomatich. Svarka*, **9**, 10–12.
20. Bagdasarov, Yu.S., Yakushin, B.F. (1991) Effect of microchemical heterogeneity on near-weld cracking of nickel alloy welded joints in dispersion solidification. *Svarochn. Proizvodstvo*, **8**, 37–40.
21. Collins, M.G., Lippold, J.C., Kikel, J.M. (2002) Quantifying ductility-dip cracking susceptibility in nickel-base weld metals using the strain-to-fracture test. In: *Proc. of 6th Int. Conf. on Trends in Welding Research* (15–19 April, 2002, Pine Mountain). ASM Int., 586–590.
22. Ramirez, A.J., Lippold, J.C. (2004) High-temperature behavior of Ni-base weld metal. Pt 2: Insight into the mechanism for ductility-dip cracking. *Materials Sci. and Eng. A*, **380**, 245–258.
23. Dave, K., Cola, M.J., Kumar, M. (2004) Grain boundary character in alloy 690 and ductility-dip cracking susceptibility. *Welding J.*, 83(**1**), 1–5.
24. Yushchenko, K.A., Savchenko, V.S., Chervyakova, L.V. et al. (2005) Investigation of weldability of nickel superalloys and development of repair technology for gas turbine blades. *The Paton Welding J.*, **6**, 2–5.
25. Horikawa, K., Kuramoto, S., Kauno, M. (2000) Sources of a trace amount of sodium, and its effect on hot ductility of an Al–5 mass % Mg alloy. *Light Metals Review*, **7**, 18–23.
26. Wilken, K., Bauer, S. (1998) Eignung von MVT- und PVR-Versuch zur Bestimmung der Mikrorissanfaelligkeit. *Schweissen und Schneiden*, 50(**3**), 160–165.
27. Stepanov, V.V., Chernyshova, T.A., Shevelev, V.V. (1975) About intergranular sliding in welding of platinum alloys and local intercrystalline fractures in near-weld zone. *Svarochn. Proizvodstvo*, **8**, 1–3.
28. Ozgowicz, W. (2005) The relationship between hot ductility and intergranular fracture in an CuSn6P alloy at elevated temperatures. In: *Proc. of 13th Int. Sci. Conf. on Achievements in Mechanical and Material Eng.* (16–19 May, 2005, Gliwice-Wisla), 503–508.
29. Kazennov, Yu.I., Stepankov, V.N., Protsenko, L.N. (1982) Recrystallization and fine structure of near-weld zone of welded joints of austenitic sheet steel. *Svarochn. Proizvodstvo*, **5**, 7–9.
30. Noecker, II F.F., DuPont, J.N. (2009) Metallurgical investigation into ductility dip cracking in Ni-based alloys. Pt 2: Microstructural and microchemical development is characterized during simulated weld reheat thermal cycle and correlated to ductility dip cracking susceptibility. *Welding J.*, 88(**3**), 62–77.
31. Collins, M.G., Ramirez, A.J., Lippold, J.C. (2004) An investigation of ductility dip cracking in nickel-based filler materials. Pt 3: The characteristics of weld metal grain boundaries associated with elevated-temperature fracture are investigated. *Ibid.*, 83(**2**), 39–49.
32. Nakao, Y., Shinozaki, K., Ogawa, T. et al. (1993) Effect of Cr and S on ductility-dip cracking susceptibilities in the reheated weld metals of Ni–Cr–Fe ternary alloys. Pt 2: Study on microcracks in multipass weld metals of Ni-base alloys. *Transact. of JWS*, 24(**2**), 101–106.
33. Kazennov, Yu.I., Reviznikov, L.I. (1978) Effect of additive and alloying elements on weldability of steel with stably austenitic structure. *Svarochn. Proizvodstvo*, **11**, 29–32.
34. Yushchenko, K.A., Starushchenko, T.M. (1981) Role of oxygen in crack formation during welding of invar. *Avtomatich. Svarka*, **8**, 21–24.
35. Yushchenko, K.A., Savchenko, V.S. (2008) Classification and mechanism of cracking in welding high-alloy steels and nickel alloys in brittle temperature ranges. In: *Hot cracking phenomena in welds II*. Ed. by Th. Bollinghaus et al. Berlin; Heidelberg: Springer, 147–170.
36. Shorshorov, M.Kh., Chernyshova, T.A., Loseva, G.I. (1973) On migration of grain boundaries and intergranular sliding in weld metal of nickel alloy welded joints. *Svarochn. Proizvodstvo*, **4**, 6–8.
37. Quadrini, E., Mengucci, P. (1992) Influence of microstructure on the hydrogen embrittlement of Al–Li–Cu–Mg–Zr alloys. *J. Mater. Sci.*, **27**, 1391–1396.
38. Hicks, P.D., Altstetter, C.J. (1992) Hydrogen-enhanced cracking of superalloys. *Metall. Transact. A*, **23**, 237–249.

39. Symons, D.M. (1997) Hydrogen embrittlement of Ni–Cr–Fe alloys. *Ibid*., **28**, 655–663.
40. Lynch, S.P. (1986) A fractographic study of hydrogen-assisted cracking and liquid-metal embrittlement in nickel. *J. Mater. Sci*., **21**, 692–704.
41. Collins, M.G., Lippold, J.C. (2003) An investigation of ductility dip cracking in nickel-based filler materials. Pt 1: The strain-to-fracture test has been used to develop temperature-strain relationship for ductility dip cracking. *Welding J*., 82(**10**), 288–295.
42. Collins, M.G., Ramirez, A.J., Lippold, J.C. (2003) An investigation of ductility dip cracking in nickel-based filler materials. Pt 2: Fracture behavior and fracture surface morphology are related to microstructure, composition and temperature. *Ibid*., 2(**12**), 348–354.
43. (1979) *Welding in machine-building*: Refer. Book. Vol. 3. Ed. by V.A. Vinokurov. Moscow: Mashinostroenie.
44. Yakushin, B.F. (1981) State-of-the-art and problems of hot cracks in welded joints. In: *Proc. of 1st Symp. on Cracks in Welded Joints of Steels* (13–17 April, 1981, ChSSR). Moscow: N.E. Bauman MVTU, 22–36.
45. Sorokin, L.I., Tupikin, V.I. (1985) Classification of heat-resistant nickel alloys by their resistance to cracking in heat treatment of welded joints. *Avtomatich. Svarka*, **5**, 23–25.
46. Sorokin, L.I. (2004) Weldability of heat-resistant nickel alloys (Review). Pt 2. *Svarochn. Proizvodstvo*, **5**, 23–25.
47. Young, G.A., Capobianco, T.E., Penik, M.A. et al. (2008) The mechanism of ductility dip cracking in nickel-chromium alloys. *Welding J*., 87(**2**), 31–43.
48. Noecker, II F.F., DuPont, J.N. (2009) Metallurgical investigation into ductility dip cracking in Ni-based alloys. Pt 1: Quantifying cracking susceptibility during the first thermal cycle using the Gleeble(r) hot ductility test. *Ibid*., 88(**1**), 7–20.
49. Slivinsky, A.A., Veit, P. (2003) Structure and properties of welded joints of nickel based heat-resistant alloy. *The Paton Welding J*., **5**, 6–12.
50. Yushchenko, K.A., Savchenko, V.S., Chervyakov, N.O. et al. (2004) Character of formation of hot cracks in welding cast heat-resistant nickel alloys. *Ibid*., **8**, 35–40.
51. Aoh, J.N., Yang, C.H. (2003) Cracking susceptibility study of Inconel 600 alloy using Varestraint and hot ductility test. In: *Proc. of 6th Int. Conf. on Trends in Welding Research* (15–19 April, 2002, Pine Mountain). ASM Int., 597–602.
52. Bagdasarov, Yu.S., Sorokin, L.I., Yakushin, B.F. et al. (1983) Influence of technological procedures on resistance of welded joints of nickel alloys to crack formation in heat treatment. *Svarochn. Proizvodstvo*, **4**, 23–26.
53. Mnushkin, O.S., Potapov, B.V., Kopelman, L.A. et al. (1974) About influence of temporary deformations on decrease of resistance of near-weld zone to local fractures. *Ibid*., **2**, 1–3.

Main conference topics:

- analysis of titanium market in CIS countries and in the world
- national programs of industry development
- dynamics of development of titanium applications
- new achievements in the field of metal science and metallurgy of titanium
- development of raw material base of titanium industry
- analysis of ferrotitanium market

Site for registration: http://titan-association.com/conference.html

STRUCTURE AND PROPERTIES OF HIGH-MANGANESE DEPOSITED METAL

I.A. RYABTSEV[1], I.A. KONDRATIEV[1], Ya.P. CHERNYAK[1], G.N. GORDAN[1], T.G. SOLOMIJCHUK[1] and N.F. GODZYRA[2]
[1]E.O. Paton Electric Welding Institute, NASU, Kiev, Ukraine
[2]I.N. Frantsevich Institute of Problems of Materials Science, Kiev, Ukraine

Effect of charge materials, containing ultra-dispersed carbides, on properties of metal deposited by flux-cored wire PP-AN105 was investigated. It was found that application of ultra-dispersed carbides leads to refining of deposited metal structure and more uniform distribution of alloying elements, thus improving its cold workability and wear resistance.

Keywords: *arc hard-facing, flux-cored wires, high-manganese deposited metal, properties of deposited metal, microstructure, ultra-dispersed carbides*

The high-carbon high-manganese Hadfield steel 110G13 is widely used for casting teeth and buckets of excavators, dredge buckets, dredgers, jaws, crushing heads, railway frogs and other similar parts [1, 2], that is explained by its capability to undergo impact loads. As a result of cold working the hardness of a surface layer of steel is increased from *HB* 180–250 up to 450–500, thus this layer has a good resistance to abrasive wear at intensive impact loads. The purely austenite structure and cold workability are acquired by steel 110G13 after hardening (heating up to 950–1100 °C, cooling in water). Castings from steel 110G13 have, as a rule, a coarse-grain structure that has a negative influence on crack resistance, and also on mechanical and service properties of steel [3].

To perform hard-facing of parts of steel 110G13, the E.O. Paton Electric Welding Institute has developed a flux-cored wire of PP-AN105 type, which produces the deposited metal, almost similar by chemical composition to the parent metal, additionally alloyed by nickel for improvement of the austenite stability [4]. However, the heating and delayed cooling at 800–500 °C temperature in hard-facing (welding) of parts of steel 110G13 leads to the decay of austenite and precipitation of a carbide phase at the grain boundaries, that reduces its crack resistance and also mechanical and service properties [1, 2]. The application of a special technique of hard-facing (deposition of narrow beads with a minimum heat input and their subsequent peening) allows preventing the precipitation of a carbide phase at the grain boundaries, but it is not almost managed to avoid the formation of a coarse-grain columnar structure of the deposited metal.

It was found from the results of investigations carried out by us [5], that application of ultra-dispersed carbide compositions in charge of flux-cored wires contributes to refining of structure of the deposited metal corresponding to tool steels. The aim of the present work was the investigation of effect of ultra-dispersed carbide compositions, added to the charge of the flux-cored wire PP-AN105, on the structure and properties of austenite deposited metal of 110G13N type. The ultra-dispersed carbide compositions were produced by high-temperature treatment of mixture of powders of metallic manganese, iron powder and natural colloid graphite in CO_2. As a result the powder contained 3.7 wt.% C; 12.6 wt.% Mn; the rest — Fe.

Specimens for study of structure and wear resistance of the deposited metal were hard-faced by self-shielding flux-cored wire with a charge, containing the treated powder PP-AN105op (tested), and standard charge PP-AN105. Hard-facing was made in four layers using wires of 2 mm diameter at similar conditions (I = 230–240 A; U_a = 24–26 V).

In investigation of a cold workability of metal deposited by both wires, firstly the Brinell hardness of deposited metal was determined, and then the Rockwell hardness was measured in the made dent. It was established that the metal deposited by standard wire PP-AN105 had hardness *HB* 163–170 directly after deposition, and after cold working it was of *HRC* 34–36, and metal deposited by test wire PP-AN105op had, respectively, *HB* 179–187 and *HRC* 38–40.

The microstructure of metal, deposited by wires of both types, was also evaluated. Specimens for metallographic examinations were manufactured by a standard procedure. To reveal the microstructure, they were subjected to etching in 20 % water solution of chromic acid. Mircohardness of deposited metal was determined in the LECO hardness meter M-400 at 1 N load, the content of δ-ferrite was determined using the ferrite meter FERRITGEHALTME SSER-1.053.

It was found that in both cases the deposited metal has an austenite structure with a negligible content of δ-ferrite. Microhardness of austenite matrix of metal deposited by a test wire is *HV*01 264–292, and by a standard wire — *HV*01 258–285 MPa. Metal, deposited by the test wire (Figure 1, *a*) has the finer-

© I.A. RYABTSEV, I.A. KONDRATIEV, Ya.P. CHERNYAK, G.N. GORDAN, T.G. SOLOMIJCHUK and N.F. GODZYRA, 2010

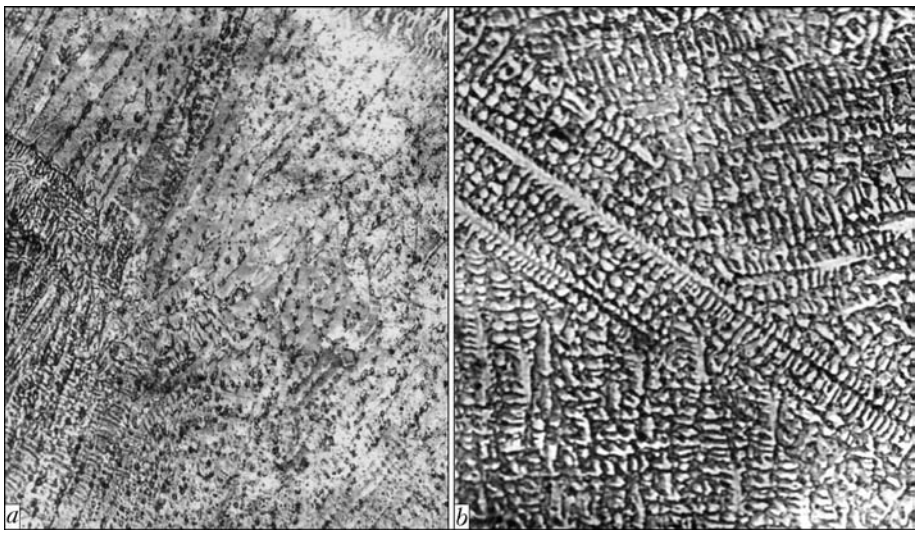

Figure 1. Microstructures (×200) of the forth layer of the deposited metal produced in hard-facing with flux-cored wires PP-AN105op (*a*) and PP-AN105 (*b*)

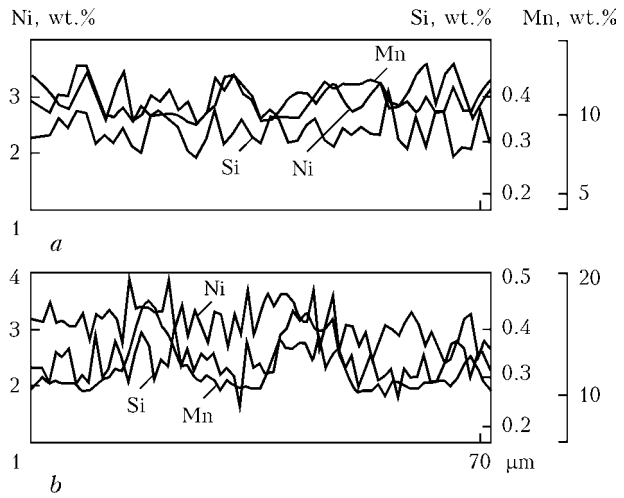

Figure 2. Distribution of alloying elements in metal deposited with flux-cored wires PP-AN105op (*a*) and PP-AN105 (*b*)

grain structure as compared with that deposited by the standard wire (Figure 1, *b*).

The metal, deposited by the test wire, contains 1.0–1.5 wt.% of δ-ferrite, while that by the standard wire — 0.2–0.3 wt.%. It is known that in welding of chrome-nickel austenite steels the presence of 2.0–3.0 wt.% of δ-ferrite in steel structure allows successful prevention of crystalline cracks [6]. Probably, in hard-facing the austenite steel 110G13 the δ-ferrite should play its positive role.

The uniformity of distribution of main alloying elements in the deposited metal was determined using X-ray diffraction microanalyzer Camebax SX50 at the depth of about 70 μm from the surface of deposited metal, parallel to it, in the automatic mode at the interval of about 1.01 μm (Figure 2).

The distribution of alloying elements in metal deposited by the test wire PP-AN105op (Figure 2, *a*) is more uniform than in metal deposited by PP-AN105 wire with a standard charge (Figure 2, *b*). This is clearly observed on the example of manganese, the main alloying element.

The wear resistance of specimens of metal, deposited by flux-cored wires PP-AN105op and PP-AN105, was determined at dry friction of metal on metal at room temperature by the shaft–plane scheme (Figure 3). Specimens of 3 × 15 × 25 mm size were cut out from the deposited metal so that the test plane entered the upper layers of the deposited metal. Shaft-mating body of 40 mm diameter was manufactured of steel 45 and hardened up to *HRC* 42 hardness. During

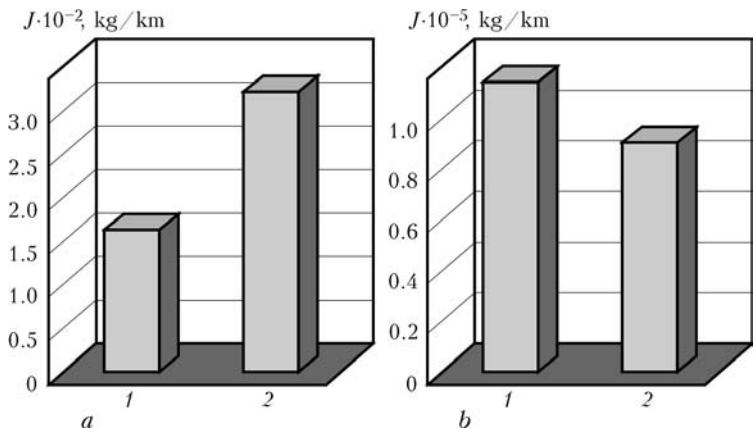

Figure 3. Wear *J* of specimens (*a*) and mating bodies (*b*) deposited by wires PP-AN105op (*1*) and PP-AN105 (*2*)

tests the specimen is pressed against the mating body by a plane which has 3 × 25 mm size. As a result, a dent is formed on the test plane, and a path is formed on the mating body. Here, the following test condition was selected: sliding rate — 1 m/s; load — 30 N; rotation frequency of mating body — 30 rpm. This condition provided stabilization of tribotechnical characteristics of all test specimens. The use of system of positioning allowed repeating tests of each deposited specimen not less than 3 times on new areas of friction of the specimen and on the path of mating body friction.

The tests showed that the wear of metal deposited by the test wire PP-AN105op is 2 times lower than that of metal deposited by the standard wire PP-AN105 (Figure 3, *a*). The wear of rings-mating bodies which were tested in pair with specimens deposited by the test wire PP-AN105op is 2 times higher than that in those which were tested with specimens deposited by a standard wire PP-AN105 (Figure 3, *b*). However, the total wear resistance of a pair of friction: test deposited metal–ring-mating body was higher than in pair of friction: standard deposited metal–ring-mating body.

Thus, the application of charge materials, containing the ultra-dispersed carbides in the flux-cored wire PP-AN105, leads to refining of structure of deposited metal of 110G13N type and more uniform distribution of alloying elements in it.

In dry sliding friction the metal deposited by flux-cored wire PP-AN105, whose charge contains ultra-dispersed carbides, is subjected to cold working to a larger degree and results in 2 times higher resistance than the metal deposited by the standard wire PP-AN105.

1. Gasik, M.I., Petrov, Yu.N., Semyonov, I.A. et al. (1990) *Metallurgy of high-manganese steel*. Kiev: Tekhnika.
2. Zhitnov, S.V., Davydov, N.G., Bratchikov, S.G. (1995) *High-manganese steels*. Moscow: Metallurgiya.
3. Astafiev, A.A. (1997) Influence of grain size on properties of manganese austenitic steel 110G13L. *Metallovedenie i Termich. Obrab. Metallov*, **5**, 18–20.
4. Ryabtsev, I.A., Kondratiev, I.A. (1999) *Mechanized electric arc surfacing of metallurgical equipment parts*. Kiev: Ekotekhnologiya.
5. Ryabtsev, I.A., Kondratiev, I.A., Godzyra, N.F. et al. (2009) Effect of ultradispersed carbides contained in flux-cored wires on properties of heat-resistant deposited metal. *The Paton Welding J.*, **6**, 10–13.
6. (1974) *Technology of fusion electric arc welding of metals and alloys*. Ed. by B.E. Paton. Moscow: Mashinostroenie.

International Scientific-and-Technical Conference

ADVANCED TECHNOLOGIES AND DEVELOPMENT OF WELDING SCIENCE AND PRACTICE

(under the auspices of exhibition «Welding-2010»)

20–21 May 2010, St.-Petersburg

Organised by

National Welding Committee of the Russian Academy of Sciences — **NKS RAN**
DVS — German Welding Society
Engineering-Technological Centre «Alliance of Welders of St.-Petersburg and North-Western Region» — **SPAS**

National Agency for Control and Welding — **NAKS**
IIS — Italian Welding Institute
OJSC «LENEXPO»
MESSE ESSEN GmbH

Subjects of the Conference

- Advanced welding technologies and related processes
- Automation, robots and positioning systems
- Welding equipment
- Welding consumables, raw materials, equipment for manufacture and inspection of welding consumables
- Training of staff, advanced training
- Qualification, certification and standardisation in welding industry
- Diagnostics, destructive and non-destructive testing of welded joints and structures, remaining life
- Ecology and safety in welding industry

For further information, please contact:
http://alians-weld.ru
LENEXPO, St.-Petersburg — Tel./Fax: +7(812) 321 26 31

REPAIR OF PIPELINES USING ORBITAL TIG WELDING INSIDE INHABITED SPACE OBJECTS

E.G. TERNOVOJ, A.R. BULATSEV, T.G. SOLOMIJCHUK and **V.F. SHULYM**
E.O. Paton Electric Welding Institute, NASU, Kiev, Ukraine

Investigations on application of equipment and technology for orbital TIG welding to repair pipelines inside functioning space objects were carried out. Properties and structural peculiarities of 12Kh18N12T steel tubular joints made by auto-pressing under conditions of decreased effect of the Earth gravitation were studied.

Keywords: *orbital TIG welding, pipelines, stainless steel, position welds, decreased gravitation, microchamber, tubular joints, mechanical properties, macro- and microstrucutre, microhardness*

In performance of repair works on the board of International Space Station (ISS) under space conditions the problem of welding of position welds of different-purpose pipelines has become challenging. The analysis of service of space objects, operating for a long time under conditions of orbital flight, in particular, the Russian complex «Mir», proves that one of the most vulnerable units are technological pipelines. It is supposed that after 6–10 years from the beginning of operation of ISS the need in their repair, as well as in methods and equipment for its realization, can arise.

In the opinion of authors of the works [1, 2] the argon arc welding with non-consumable tungsten electrode (TIG) is one of the basic methods of welding and repair of pipelines under space conditions using specialized captive chambers with a controllable atmosphere. TIG method both with filler materials feeding and also without it found wide application in manufacturing structures in different fields of industry [3–5].

Without filler material the auto-pressing method is usually used for welding of butt joints with edges flanging, overlap joints, and also butt joints without edges flanging (mainly tubular ones) [6–9]. In this method the multipass welding is applied which is performed in continuous and pulsed mode and also with activating additions [10–13]. In spite of existing opinion about detrimental influence of reheats in multipass TIG welding, the increase in strength of joints is observed in comparison with welds, welded with feeding of filler wire whose composition corresponds to that of the base metal [14]. Different enterprises of CIS and also many international companies are dealing with the development of technology and equipment for these purposes. However, there are no equipment and technologies for welding and repair of pipelines directly in space.

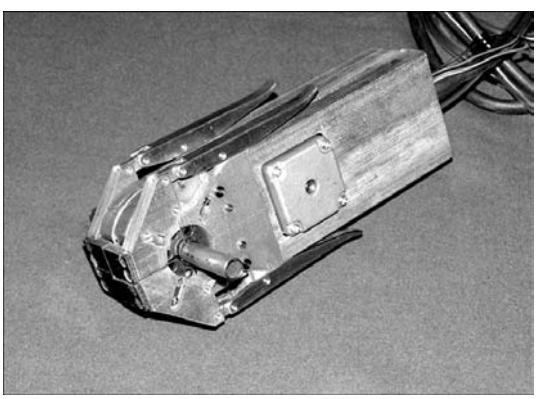

Figure 1. Appearance of captive microchamber for orbital TIG welding of pipelines under microgravity conditions

In this work the application of method of orbital TIG welding for repair of pipelines inside functioning space stations is considered and properties of multipass butt tubular joints, produced during testing the preliminary technology as applied to the conditions of microgravity, are studied.

During experiments the inverter power source GUSMI-160 for TIG welding was applied. As specimens, the steel 12Kh18N12T pipes of 10 mm diameter and 1 mm wall thickness were butt welded without filler materials. Here, the tungsten electrode of WT20 grade of «Binzel» company of 1.6 mm diameter with 60° sharpening angle and 0.5 mm blunting was used. As the shielding gas, the argon of the highest quality (GOST 10157–79) was used, the consumption of which was 4–6 l/min.

At the first stage the downhill welding at stationary arc heating source and horizontally positioned rotating tube was performed. Such choice of spatial position and method of performance of welding process assumes minimal influence of gravitation field of the Earth on molten weld pool [15–18].

At the second stage the orbital welding by horizontal welds in vertically positioned stationary pipe using captive chamber was performed (Figure 1).

As a result of carried out works the optimal welding modes of single- and multipass welding for both variants, properties and structural peculiarities of joints produced without feeding of a filler wire were defined.

The quality of produced butt joints were estimated by visual inspection, as well as according to macro and microsections. The chemical composition of base

© E.G. TERNOVOJ, A.R. BULATSEV, T.G. SOLOMIJCHUK and V.F. SHULYM, 2010

Table 1. Conditions of TIG welding of butt joints of 12Kh18N12T steel tubes of ∅ 10 × 1 mm (welding speed is 15 m/h)

Number of specimen	Number of passes	Arc current, A, in making a pass				Macrosection of joint
		One	Two	Three	Four	
30	One	28	–	–	–	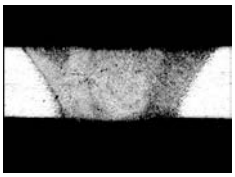
41	Two	28	22	–	–	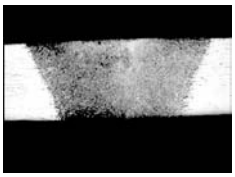
56	Three	28	22	18	–	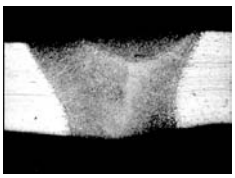
58	Four	28	22	18	15	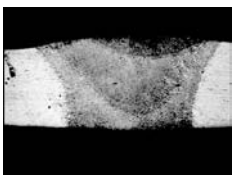

metal (BM) and weld metal were studied by a spectral analysis using spectrometer DFS-36. Tensile strength of welded joints was determined by mechanical tests of tubular specimens in rupture machine TsDM-4 at temperature +20 °C. Metallographic examinations, photographing of geometry and structure of metal both of the whole joint, and also of its single areas were performed in optical microscope «Neophot 32». Size of grains was measured by visual comparison with references of scales in accordance with GOST 5639–82. Vickers hardness of joints at 1 N load was measured on tubular transverse microsections using the LECO microhardness meter M-400 at 0.3 mm pitch. The structural components were revealed by electrochemical etching in 20 % water solution of chromic acid at the voltage 20 V during 10 s.

To set welding conditions of butt tubular joints the penetrations on solid tubular specimens of steel 12Kh18N12T was initially performed. Then, the butt joints were welded by single- and then multipass welds.

The TIG downhill and orbital welding conditions of butt tubular joints were similar (Table 1). Here the first pass was performed by a through penetration and next depositing passes on the first weld were made without through penetrations. It was established as a result of conducted experiments that selected TIG welding conditions with through penetration of butt tubular joints of steel 12Kh18N12T allow producing circumferential welds for one pass with reinforced root bead and negligible weakening of a face part of the weld (see macrosection of specimen 30 in Table 1). The next pressing passes allow producing of welds with reinforcement of an upper part of the weld, which is seen on macrosections of specimens 41, 56, 58 in Table 1.

The analysis of macrosections of joints showed that by selection of main and pressing modes of welding one

Table 2. Chemical composition (wt.%) of base and weld metal produced by orbital TIG multipass welding on 12Kh18N12T steel tubes

Number of specimen	Number of passes	Si	Mn	Cr	Ni	Ti	Cu
1 (BM)	–	0.63	1.15	18.0	11.6	0.85	0.22
27	One	0.62	1.14	18.0	11.4	0.86	0.21
42	Two	0.62	1.13	17.8	11.5	0.85	0.21
50	Three	0.62	1.12	18.0	11.4	0.85	0.22
57	Four	0.62	1.12	17.8	11.6	0.85	0.22

Table 3. Results of tensile tests of BM and joints of 12Kh18N12T steel tubes of ∅ 10 × 1 mm produced by orbital TIG welding and downhill welding

Number of specimen	Number of passes	Site of fracture	Test results σ_t, MPa	
			BM	Welded joint
1, 2, 3	–	BM	782–788	–
72, 76, 79 28, 29, 31	One	Weld	–	605–635 610*–630*
82, 84, 85 43, 44, 45	Two	HAZ	–	638–657 635*–660*
87, 89, 90 51, 52, 53	Three	Same	–	635–647 638*–650*
92, 93, 98 60, 61, 62	Four	»	–	612–637 608*–642*

*Specimens were made by downhill welding.

can achieve optimum geometry and satisfactory formation of upper and root reinforcing beads both for downhill welding and also for the orbital one. The uniformity of penetration of root weld and its reinforcement are achieved as a result of stable welding speed which is provided by step motor KRS392S-4015-Z121-W60, controlled by a drive KRD1250i and stabilization of welding current of inverter power source GUSMI-160. A metal of the first pass and HAZ are repeatedly heated by next (pressing) passes which were performed by the arc of a lower capacity. Here the metal is subjected to local plastic deformation (buckling) under the influence of inner compressveg stresses up to the temperatures of plastic and elastic-plastic state of metal in heating zone. Thus, the weld reinforcement is obtained without applying the external compressive forces and filler material for both variants.

The chemical composition of weld metal of joints produced for one, two, three and four passes without filler material is not almost differed from BM (Table 2).

Having compared the values of tensile strength of butt joints of pipes of ∅ 10 × 1 mm of steel 12Kh18N12T produced for variants of downhill and orbital welding, at different amount of welding passes (Table 3), it is necessary to note that the smallest value of strength was obtained after the first and fourth passes.

The most suitable results were obtained after second and third passes — $(0.80–0.84)\sigma_t$ of BM.

Investigations of nonmetallic inclusions in 12Kh18N12T steel joints produced without filler wire for variants of downhill and orbital welding showed that single and line oxides are observed in BM (Figure 2, *a, b*), and in weld metal after the first pas — single inclusions of corundum and tiny silicates of a globular shape (Figure 2, *c*).

It is also necessary to note the presence of inclusions of titanium nitrites in weld metal after the first pass and in the fusion zone.

After the second and next passes the nonmetallic inclusions in welds and in the fusion zone were observed more rarely.

Macrostrucutre of weld metal produced in orbital welding for four passes is given in Table 1 (specimen 58), where weld has a reinforcement both on the external surface, and also in its root part. The weld metal is dense, without pores, cracks and other defects, weld shape is symmetric, microstructure of this joint is shown in Figure 3.

The cast weld structure represents a two-phase system: austenite and δ-ferrite. Weld metal structure after the first pass is dispersed. The contents of δ-ferrite in weld metal is about 1.0–1.5 %. After the second pass the austenite grain is increased and amount of δ-ferrite is reduced (down to 0.5–1.0 %). After the third and fourth passes the weld metal structure is more fine-dispersed than after the first pass. Nonmetallic inclusions in a weld and fusion zone are observed more rarely than in weld metal after the first pass.

In HAZ metal the typical austenite structure is observed on the both sides of a weld (Figure 4).

Small amount of δ-ferrite (up to 0.5 %) was revealed at the areas adjacent to fusion line. Size of grain at the area of coarse grain of HAZ on the both sides is the same and corresponds to the size No.5 (line 3). At the area of fine grain the size of grains corresponds to the size No.8 (line 3). Microstrucutre of BM is composed of austenite grains of size No.6 (line 3) and represents austenite and δ-ferrite with distinctly expressed texture of rolling. Along the fibers of rolling the nonmetallic inclusions and also carbide particles are observed. Grain size at the bound-

Figure 2. Microstructures (×500) of base and weld metal with nonmetallic inclusions in them: *a* — chains of oxides in BM along the rolling; *b* — sulphides in BM elongated along the rolling; *c* — inclusions of corundum and silicates in a single-pass metal

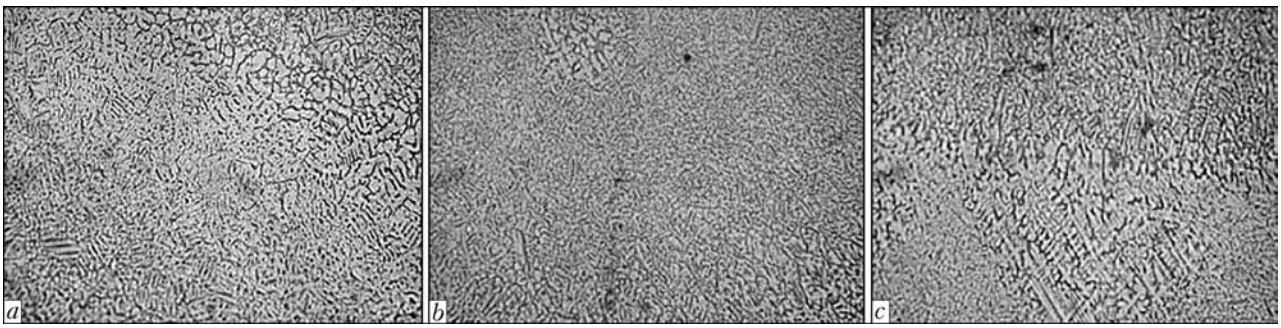

Figure 3. Microstructure (×320) of weld metal of 12Kh18N12T steel tubular joint produced by orbital TIG welding for four passes: *a, b* — weld metal, respectively, after the first and second passes; *c* — at the boundary of the third and fourth passes

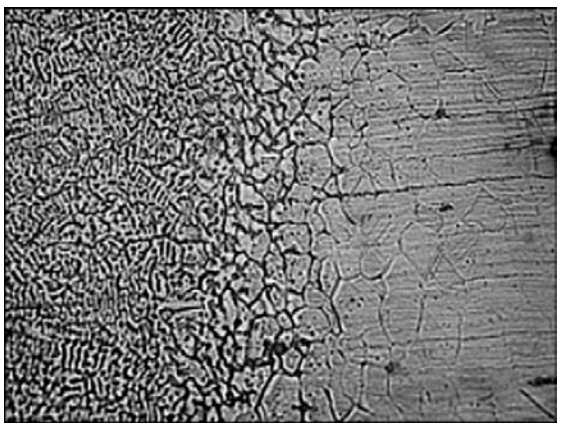

Figure 4. Microstructure (×500) of HAZ metal of 12Kh18N12T steel joint made by TIG welding for four passes

ary of BM, i.e. the area of incomplete recrystallization, corresponds to size No.7 (line 3).

Microhardness of joints was measured in upper cuts of external surfaces of pipes in perpendicular direction towards the weld.

The values of hardness of weld metal, HAZ and BM are differed between each other. Besides, the number of welding passes also influences the values of hardness. Figure 5 shows distribution of microhardness for welded tubular joints produced for one, two, four passes, where maximum microhardness is 2750 MPa in the center of a single-pass weld and minimum value in the same joint at the region of a coarse grain is 1650 MPa in HAZ metal. In welds with two passes the character of distribution of microhardness remained the same as after the first pass, however the values of microhardness become somewhat lower. And after third and especially fourth passes the distribution of microhardness is more stable along the whole weld section and reaches the value of 2500 MPa.

Thus, the feasibility of producing quality welded joints of thin-wall pipes of stainless steel 12Kh18N12T at repair of pipelines using orbital TIG welding was experimentally shown.

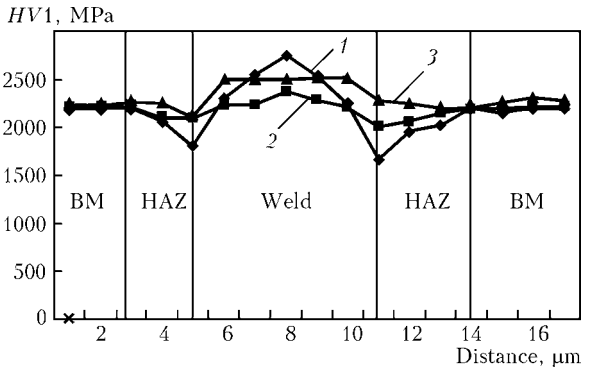

Figure 5. Distribution of microhardness of 12Kh18N12T steel tubular joints (specimen 47) made by orbital TIG welding for one (*1*), two (*2*) and three (*3*) passes

1. Paton. B.E., Lapchinsky, V.F., Stesin, V.V. et al. (1977) Some principles of design of equipment for technological operations in space. In: *Transact. of 4th Gagarin Lectures on Technology in Space*. Moscow: MAI, 16–23.
2. Paton, B.E., Dudko, D.A., Bernadsky, V.N. et al. (1976) Application of welding for repair of space objects. In: *Space investigations in Ukraine*, Issue 9, 3–5.
3. Russo, V.L. (1984) *Inert-gas arc welding*. Leningrad: Sudostroenie.
4. (1977) *Current technologies in production of gas-turbine engines*. Ed. by A.G. Bratukhin et al. Moscow: Mashinostroenie.
5. Abramov, E.V., Lyashenko, V.I., Semyonov, V.A. (1975) Automatic welding of small-diameter thin-wall pipes from steel and titanium. In: *Advanced methods of treatment of metals and alloys*. Leningrad: LDNTP.
6. (1978) *Welding in machine-building*: Refer. Book. Vol. 1. Ed. by N.A. Olshansky. Moscow: Mashinostroenie.
7. Grinenko, V.I., Belkin, S.A., Astafurova, N.I. (1963) Position welding of 1Kh18N9T steel pipes by auto-pressing. *Svarochn. Proizvodstvo*, **10**, 27–29.
8. Roshchin, V.V., Akulov, L.I., Grinenko, V.I. et al. *Method of auto-pressing welding*. USSR author's cert. 212409. Int. Cl. B 23 K 9/16, 37/2. Publ. 1968.
9. Novikov, O.M., Morochko, V.P., Tokarev, V.O. et al. *Method of shielded-gas arc welding of position joints of pipelines*. USSR author's cert. 1593828. Int. Cl. B 23 K 9/16. Publ. 1990.
10. Roshchin, V.V., Ishchenko, Yu.S., Bukarov, V.A. et al. Automatic arc welding of joints of pipelines by auto-pressing method. In: *Problems of nuclear science and technology*. Welding in nuclear technology Series, Issue 1, 73–81.
11. Ishhenko, Yu.S., Grinenko, V.I., Pavlov, Yu.S. (1965) Pulsed consumable electrode argon arc welding of position joints of 1Kh18N9T steel. *Svarochn. Proizvodstvo*, **12**, 16–18.
12. Bukarov, V.A., Ishchenko, Yu.S., Loshakova, V.G. (1982) *Method of fusion welding of butt joints*. USSR author's cert. 899296. Publ. 1982.
13. Savitsky, M.M., Savitsky, O.M., Melnichuk, G.M. et al. (2006) Combined technology of position orbital welding of pipelines. In: *Problems of resource and service safety of structures, constructions and machines*. Ed. by B.E. Paton. Kyiv: PWI.
14. Roshchin, V.V., Ishchenko, U.S., Bukarov, V.A. et al. (1985) Properties of weld joints made by self-compression method. *IIW Doc. XII-901–85*.
15. Ishchenko, Yu.S. (2002) Physical-technological principles of weld formation in arc welding. In: *Transact. of NIKIMT*. Ed. by L.N. Shchavelev. Vol. 2. Moscow: IzdAT, 204–237.
16. Ishchenko, Yu.S., Grechishkin, V.I. (1966) Evaluation of weld pool weight and geometrical sizes of penetration zone. *Svarochn. Proizvodstvo*, **11**, 30–31.
17. Paton, B.E., Nazarenko, O.K., Lokshin, V.E. et al. (1972) Peculiarities of electron beam welding in different spatial positions. *Avtomatich. Svarka*, **6**, 1–4.
18. Kajdalov, A.A. (2004) *Electron beam welding and related technologies*. 2nd ed. Kiev: Ekotekhnologiya.

EVALUATION OF TEMPERATURE SHIFT DEPENDING UPON THE SPECIMEN THICKNESS BY THE FORCE AND DEFORMATION CRITERIA OF FRACTURE MECHANICS

V.P. DYADIN
E.O. Paton Electric Welding Institute, NASU, Kiev, Ukraine

Relationships between impact toughness *KCV* and crack resistance characteristics of a material, derived by the E.O. Paton Electric Welding Institute, are applicable for a case where the plane-strain state forms within the defect zone. If this condition is violated, evaluation of crack resistance of structural members is not always optimal. To solve this problem, it is suggested that temperature shift in basic curves of fracture toughness characteristics should be evaluated depending upon the thickness of an object under investigation. It is shown that, in addition to thickness of a specimen, the temperature shift should also be evaluated by allowing for strength properties of a material and its welded joints.

Keywords: *impact toughness, Charpy specimen, crack resistance characteristics, plane strain, thickness effect, temperature shift, strain hardening of material*

Relationships between impact toughness *KCV* and crack resistance characteristics of a material (δ_{Ic}, K_{Ic}), derived by the E.O. Paton Electric Welding Institute, are applicable for a case where the plane-strain state forms within the defect zone [1, 2]. If this condition is violated, such evaluation of crack resistance of structural members is not always optimal.

In practice, when using fracture mechanics approaches, there are cases where it is necessary to specify conditions of transition from the plane strain (PS) to plane-stress state (PSS) in the presence of developed plastic strains, when strain characteristic δ_{Ic} or J_{Ic}-integral can be applied.

For critical crack opening displacement δ_{Ic} and J_{Ic}, unlike critical stress intensity coefficient K_{Ic}, conditions of transition from PS to PSS are little studied as yet. For example, it is suggested in technical literature that the measured level of values of fracture toughness at plane strain, depending upon thickness t of a specimen, should be limited by the following expression:

$$t > m\delta_{Ic} \approx mJ_{Ic}/H\sigma_y, \quad (1)$$

where H and m are the coefficients, the values of which vary from 1 to 2 and from 25 to 100, respectively.

It follows from (1) that at different values of coefficients H and m the limiting requirements to specimen thickness can change 8 times. Such substantial deviations indicate that the authors are uncertain in adequacy of the choice of the suggested requirement to the specimen thickness for determination of the PS to PSS transition conditions in the case of through cracks. Probable errors in this case may lead both to catastrophic consequences with a conservative estimation of crack resistance, and to a groundless rise in cost of a structure because of the non-optimal choice of materials.

A step toward elimination of uncertainties in condition (1) was made in standard ASTM E 1921–97 [3] in the form of an attempt to relate the PS to PSS transition conditions to a tough-brittle transition temperature for specimens of different thicknesses.

For ferritic steels with a yield stress of 275 to 825 MPa, the following approximation of temperature dependence of K_{jc} was made from the results of testing specimens with a thickness of up to 100 mm:

$$K_{jc(\text{mean})} = 30 + 70 \exp [0.019(T - T_0)] \ [\text{MPa}\sqrt{\text{m}}], \quad (2)$$

where $K_{jc(\text{mean})}$ is the mean value of K_{jc} determined on 25 mm thick specimens; and T_0 is the temperature corresponding to K_{jc} = 100 MPa$\sqrt{\text{m}}$, which was determined in testing 25 mm thick specimens, °C.

As follows from the recommendations of standard ASTM E 1921–97, temperature $T^{(t)}_{100}$ for specimens with a thickness of about 100 mm, when the K_{jc} = = K_{Ic} = 100 MPa$\sqrt{\text{m}}$ condition is met, corresponds to temperature $T_{28\ \text{J}}$, at which the fracture energy of Charpy specimens is equal to 28 J, i.e. in fact, it is the case of using the relationship between impact toughness of the Charpy specimens and criterion K_{Ic} given in study [1].

For specimens of a smaller thickness, the PS to PSS transition occurs at lower temperatures. To find the $K^{(t)}_{jc}$ = 100 MPa$\sqrt{\text{m}}$ value, this circumstance is taken into account by using corresponding temperature shift $T^{(t)}$:

$$T^{(t)} = T_{28\ \text{J}} + C, \quad (3)$$

where C is the recommended temperature shift depending upon the size of standard specimens with a

© V.P. DYADIN, 2010

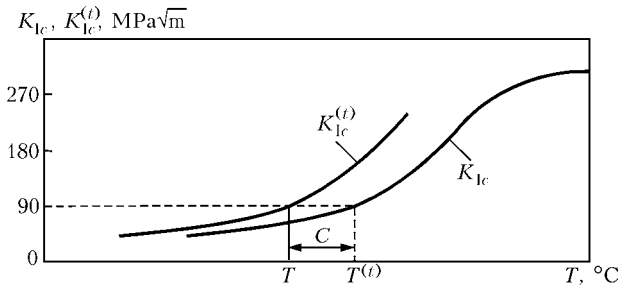

Figure 1. Graphic interpretation of temperature shift from formula (3), where the C value was obtained with decrease in specimen thickness

thickness of 10, 12.5, 25, 50, 75 and 100 mm for three-point bending or eccentric tension tests; and the values of C are assumed to be equal to −32, −28, −18, −8, −1 and +2 °C, respectively.

This approach makes it possible to evaluate resistance of a material to propagation of a through crack, allowing for characteristic violations of the PS condition with decrease in thickness of a structural member.

Drawbacks of this method include a rigid, regulated form of the temperature dependence of K_{jc} (2), which may be different in different materials.

This study suggests using, instead of expression (2), the temperature dependencies of K_{Ic} (Figure 1) derived from the results of impact toughness tests of a material corrected for structural members of different thicknesses, like condition (3).

Relationships between impact toughness of the Charpy specimens and criterion K_{jc}, developed by the E.O. Paton Electric Welding Institute [1], can be rewritten with allowance for a thickness correction:

$$K_{Ic}^{(t)} = (AEa_V^{(t)}/(1 - \nu^2))^{0.5}, \quad (4)$$

where $K_{Ic}^{(t)}$ is the calculated characteristic of crack resistance in propagation of a through crack in a structural member with thickness t and temperature T; A is the correlation coefficient; E is the elasticity modulus; $a_V^{(t)}$ is the impact toughness of the Charpy specimens at corrected temperature $T^{(t)}$, allowing for a specimen thickness; and ν is the Poisson's ratio;

$$T^{(t)} = T + \Delta T, \quad (5)$$

where ΔT is the temperature shift at a limited thickness of structural members ($10 < t < 100$ mm), which is determined from expression (3) and assumed to be equal to C.

The approach suggested resembles the Makhutov's method of a shift of second critical brittle temperatures [4], the substantial difference being that the shift of fracture toughness characteristics, rather than fracture stresses, opens up considerably wider opportunities for calculation of crack resistance of structures. A more detailed analysis of the results of the shift of the second critical brittle temperatures depending upon the specimen thickness is also of high interest.

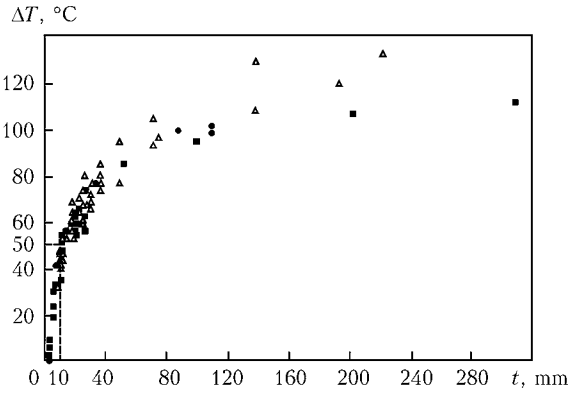

Figure 2. Dependence of critical brittle temperature shift upon the specimen thickness related to a specimen with thickness t = 10 mm, derived from formula (6) at $t_{cr} > 10$ mm

Figure 2 shows the generalised results of experimental data on the shift of the second critical temperatures depending upon the thickness of specimens of low-carbon and low-alloy steels in tensile tests [5]. Specimens with a section width exceeding their thickness 4–5 or more times were tested. An important point here is that the second critical brittle temperatures increase with increase in a specimen thickness, this being indicative of a risk of brittle fracture of thick-walled large-size structures. In this case, a relative shift of the critical brittle temperatures, ΔT_{cr}, for a 10 mm thick specimen can be described by the following relationship:

$$\Delta T_{cr} = 50(t_{cr} - 10)/t_{cr}, \quad (6)$$

where t_{cr} is the current thickness of a specimen, mm.

As seen from Figure 2, the temperature shift stabilises with increase in the specimen thickness and reaches approximately 50–55 °C (for a 10 mm thick specimen), which is a bit higher than the values recommended by standard ASTM E 1921–97.

To compare relationships (3) and (6), rewrite them in the following form:

$$C = T^{(t)} - T_{28\,J}; \quad (7)$$

$$C_{cr} = 50(t_{cr} - 10)/t_{cr} - 50, \quad (8)$$

where C_{cr} is the critical shift of the second critical temperatures depending upon the specimen thickness.

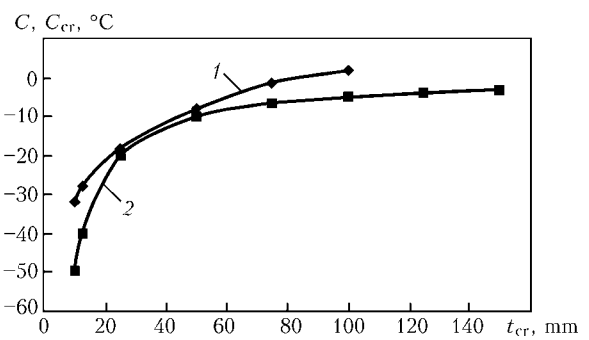

Figure 3. Dependence of C recommended by ASTM E 1921–972 (*1*) and critical C_{cr} (*2*) from formula (2) of temperature shifts upon specimen thickness t_{cr}

As seen from Figure 3, the shifts of the second critical brittle temperatures and toughness characteristics according to ASTM E 1921–97, corresponding to $K_{jc} \approx 100$ MPa$\sqrt{\text{m}}$, almost coincide over a wide range of specimen thicknesses. Moreover, the observed difference between the temperature shifts for specimens with a thickness of 10–15 mm is more likely to be associated with different sections of the specimens. Similar values of the temperature shifts are also noted in standard ASTM E 1921–97, where temperature shift C equal to –50 °C is recommended for static bending tests of a Charpy specimen with a fatigue crack.

Therefore, it can be expected that introducing the $K_{Ic}^{(t)}$ characteristic will make it possible to use the force criterion more rationally, as it relates it to temperature $T_{28\ J}$ with allowance for dependence upon the thickness of a structural member.

Temperature shift ΔT can be used in other cases as well, for example, in the case of a change in the PS to PSS transition conditions as a result of dynamic ageing of a material within the zones of concentration of thermoplastic strains, in formation of quenching structures, case hardening of metal during operation, etc. As far as the surface cracks are concerned, for this case the PS conservation conditions are little studied.

It can be concluded on the basis of numerical and experimental studies [6] that stresses and strains near the crack apex in a real three-dimensional body depend upon the stress-strain state in two regions: region located in the immediate proximity to the crack apex, where the local restraining effect shows up, and region that is more distant from the crack apex, where strains correspond to the PSS conditions and depend upon the general stress-strain state of a section weakened by a crack.

In the first of the above regions, the degree of restraint of plastic strains can be characterised by coefficient $\beta = \sigma_{max}/\sigma_{0.2}$ (where σ_{max} is the maximal stress ahead of the crack apex, and $\sigma_{0.2}$ is the yield strength with a uniaxial stress), which amounts to 2.57 in the plane-strain state.

In the second region, the degree of restraint of a strain can be expressed by the following formula:

$$L = \sigma_{s.m}/\sigma_{0.2}, \qquad (9)$$

where $\sigma_{s.m}$ are the mean stresses in a specimen section weakened by a defect, which correspond to the beginning of yield (general yield stress).

Naturally, at $L = \beta$ there is no reason to expect violation of the plane-strain condition at any level of fracture toughness of a material, as the degrees of restraint of plastic strains under conditions of local and general yield are identical. On the contrary, at $L < \beta$ it may be expected that a gradual transition from PS to a state characteristic of the entire weakened section ($\beta \to L$) will occur in development of the plastic zone and, particularly, at the beginning of a general yield. For these cases it is necessary to determine conditions providing invariance of characteristic δ_{Ic} both in experimental measurements and in calculations. Such investigations were carried out by V.S. Girenko. The point is as follows. Crack opening displacement δ_c, like other crack resistance criteria, is not a constant in quasi-brittle states of a material. Therefore, in practice it is necessary to be guided by characteristic δ_{Ic}.

For shallow and short surface defects, this leads to an error that is allowed for in the safety factor for crack resistance and strength. However, considering a low accuracy of evaluation of sizes of the defects in non-destructive testing, as well as the probability of their close location to each other, this approach is completely adequate, and separation of conditions of the PS to PSS transition is hardly justifiable at non-admission of a through defect.

In this case, as applied to the technical diagnostics problems, crack resistance characteristic δ_{Ic} should be determined for the most severe case (PS conditions), which can be relatively easily achieved over the entire range of transition temperatures from the results of standard mechanical tests [1, 2]:

$$\delta_{Ic} = 0.5Aa_V/\sigma_{0.2}, \qquad (10)$$

where a_V is the impact toughness of the Charpy specimens at a corresponding test temperature; normally, it is assumed that $A = 0.1$ for low-alloy and low-carbon steels.

As to the use of strain criterion δ_{Ic} for evaluation of through cracks, in analogy with the force criterion (4) the strain curve can also be written down in the following form:

$$\delta_{Ic}^{(t)} = 0.5Aa_V^{(t)}/\sigma_{0.2}, \qquad (11)$$

where $\delta_{Ic}^{(t)}$ is the corrected characteristic of fracture toughness with a through crack propagating in a structural member with thickness t at temperature $T^{(t)}$.

Advantages of the crack opening displacement test method, compared to the force criterion, are beyond question. First of all, this is associated with less severe requirements to the specimen thickness, and with a possibility of evaluating crack resistance characteristic δ_c in the quasi-brittle and tough regions.

To check temperature shift ΔT by the strain criterion, worthy of notice are studies [7–9], where the effect of the weld metal thickness on a critical value of δ_c is evaluated using the «restricting plate thickness coefficient β». The authors proceeded from an assumption that the thickness intensity effect on strain along the crack front can be expressed by a model shown in Figures 4 and 5, namely by the ratio of mean stress $\bar{\sigma}_{33}$ to mean strain $\bar{\varepsilon}_{33}$ in a direction of thickness in

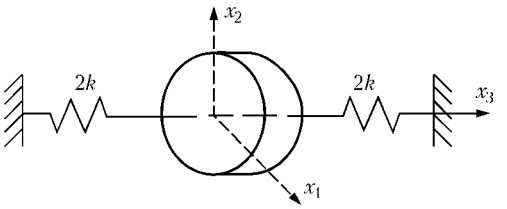

Figure 4. Model of restriction of specimen thickness according to [9]

proportion to a value of k, which is determined as a constant:

$$k = \bar{\sigma}_{33}/\bar{\varepsilon}_{33} = -\frac{2\int_0^{t/2}\sigma_{33}dx_3/t}{2\int_0^{t/2}\varepsilon_{33}dx_3/t}. \quad (12)$$

Setting k by expression

$$k = (1/\beta - 1)\bar{E}, \quad (13)$$

where $\bar{E}$ is the tangent of the angle of inclination of the strain–stress diagram under uniaxial loading in the plastic region, and solving equation (13) by the finite element method [9] yields the following relationship between β and t:

$$\beta = \begin{cases} 10.24/(t + 5.24), & t > 10; \\ 1 - t^2/(20t + 104.9), & t \le 10. \end{cases} \quad (14)$$

By considering a small specimen elongated in a direction of axis x_2 ahead of the crack front (Figure 6) with no allowance for elastic strains, the stress–strain relationship on axis x_1 can be written down as follows:

$$\varepsilon_{22} = \frac{\varepsilon_i^p}{\sigma_i}\left(\sigma_{22} - \frac{\sigma_{33} + \sigma_{11}}{2}\right); \quad (15)$$

$$\varepsilon_{33} = \frac{\varepsilon_i^p}{\sigma_i}\left(\sigma_{33} - \frac{\sigma_{22} + \sigma_{11}}{2}\right), \quad (15a)$$

where σ_i and ε_i^p are the intensities of stresses and plastic strains, respectively.

Express the σ_{11} to σ_{22} ratio in terms of α:

$$\alpha = \sigma_{11}/\sigma_{22}, \quad 0 < \alpha < 1. \quad (16)$$

Then the relationship between crack opening displacement δ_c and strain ε_{22} can be written down in the following form:

$$\delta_c = C_1\varepsilon_{22}, \quad (17)$$

where C_1 is the constant value.

When using the fracture mechanics approaches, it seems reasonable to limit the real strains and stresses at the crack apex to the values that correspond to the loss of plastic stability of a material. And since the latter at the moment of the neck formation is usually not in excess of 20 % of the strain, in our case it is

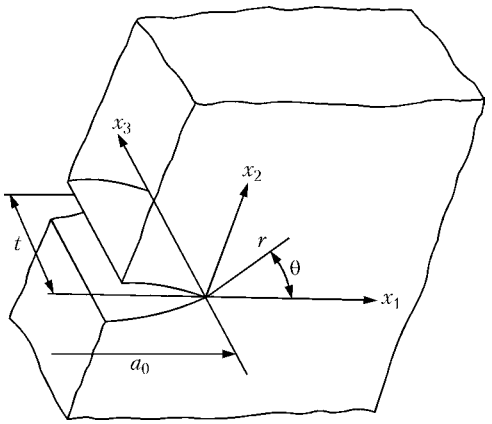

Figure 5. Location of coordinate axis ahead of the crack front: a_0 — crack length

possible to use the exponential law of strain hardening of the material:

$$\sigma_i = \sigma_{0.2}(\varepsilon_i^p/\varepsilon_0)^n, \quad (18)$$

where ε_0 is the strain corresponding to material yield stress $\sigma_{0.2}$, and n is the material strain hardening.

Assuming that brittle fracture occurs when the normal stress of an imaginary stressed specimen (Figure 6) amounts to critical fracture stress σ_{cr}, and based on [7–9], the following expression can be written down:

$$\delta_c = C_1\frac{\varepsilon_0}{(\sigma_{0.2})^{1/n}} \times \left[1 - \alpha + \alpha^2 + \frac{(1-\beta)(1+\alpha)}{2}\left\{\frac{(1-\beta)(1+\alpha)}{2} - \alpha - 1\right\}\right]^{(1-n)/2n} \times \left\{1 - \frac{(1-\beta)(1+\alpha) + 2\alpha}{4}\right\}(\sigma_{cr})^{1/n}. \quad (19)$$

Critical crack opening displacement δ_{Ic} at plane strain in this case has the following form:

$$\delta_{Ic} = C_1\frac{\varepsilon_0}{(\sigma_{0.2})^{1/n}}\left(\frac{\sqrt{3}}{2}\right)^{(1/n)+1}(1-\alpha)^{1/n}(\sigma_{cr})^{1/n}. \quad (20)$$

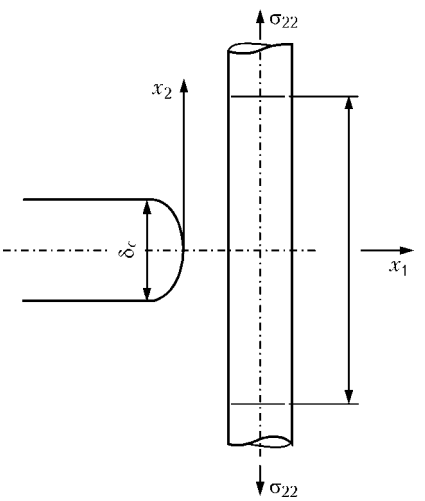

Figure 6. Schematic of conditionally tensioned specimen ahead of the crack apex

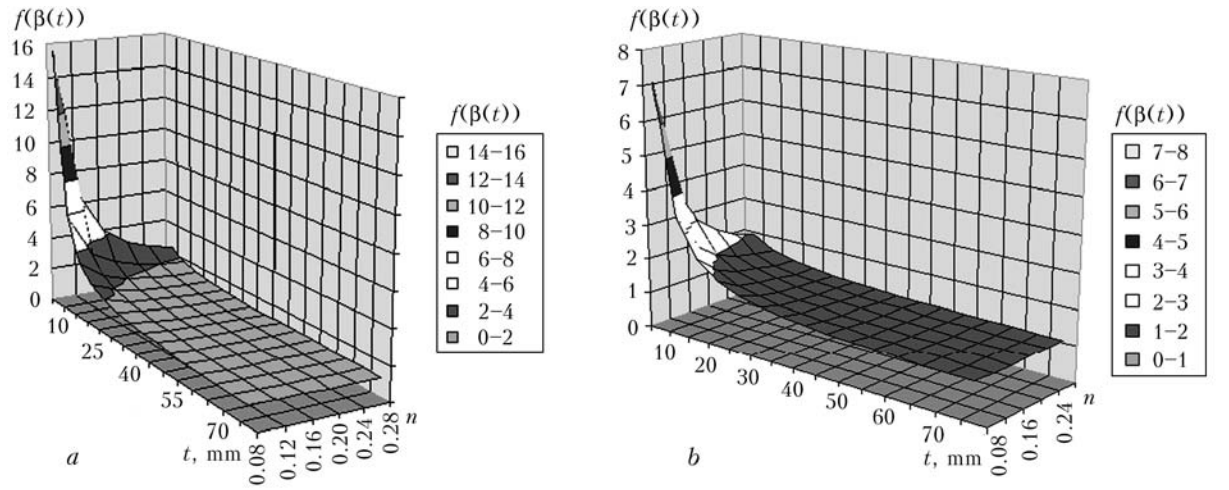

Figure 7. Variations in values of function $f(\beta(t))$ depending upon strain hardening n and thickness t of a specimen at $\alpha = 0.3$ (*a*) and 0.2 (*b*)

By dividing expression (19) by (20), δ_c can be represented in the form of a function of n, β, α and δ_{Ic}:

$$\delta_c = f(\beta)\delta_{Ic}, \tag{21}$$

where

$$f(\beta) = \left(\frac{2}{\sqrt{3}}\right)^{n+1/n} \times$$

$$\times \left[1 - \alpha + \alpha^2 + \frac{(1-\beta)(1+\alpha)}{2}\left\{\frac{(1-\beta)(1+\alpha)}{2} - \alpha - 1\right\}\right]^{(1-n)/2n} \times \tag{22}$$

$$\times \left\{1 - \frac{(1-\beta)(1+\alpha)+2\alpha}{4}\right\} / (1-\alpha)^{1/n}.$$

Proceeding from [10], the value of α in a deformed non-linear zone varies from 0 to 0.6. To simplify further calculations, assume that the value of α in some cases in the plastic zone is equal to 0.3. Then expression (22) can be simplified to some extent:

$$f(\beta) = \left(\frac{2}{\sqrt{3}}\right)^{n+(1/n)} \times$$

$$[0.79 + 0.65(1-\beta)\{0.65(1-\beta) - 1.3\}]^{(1-n)/2n} \times \tag{23}$$

$$\times \{0.85 - 0.325(1-\beta)\} / (0.7)^{1/n},$$

where β can be determined depending upon thickness t of a specimen according to formula (14).

At $t > 10$ mm, dependence (22) in a general form will look as follows:

$$f(\beta) = \left(\frac{2}{\sqrt{3}}\right)^{n+(1/n)} \times$$

$$\times \left[1 - \alpha + \alpha^2 + \frac{(1-10.24)/(t+5.24)(1+\alpha)}{2}\left\{\frac{(1-10.24)/(t+5.24)(1+\alpha)}{2} - \right.\right.$$

$$\left.\left. - \alpha - 1\right\}\right]^{(1-n)/2n} \times \tag{24}$$

$$\times \left\{1 - \frac{(1-10.24)/(t+5.24)(1+\alpha)+2\alpha}{4}\right\} / (1-\alpha)^{1/n}.$$

Figure 7, *a* shows dependence (24) of correction function $f(\beta(t))$ for different values of strain hardening n and thickness t of a specimen at $\alpha = 0.3$.

As seen from the Figure, at a specimen thickness of more than 25 mm, the values of correction function $f(\beta(t))$ vary from 2 to 1. Basically, this is in agreement with general approaches of fracture mechanics to determination of δ_{Ic} at the moment of initiation of crack growth in the transition region. At the same time, this range of values of specimen thicknesses is much higher than that specified by requirement (1). The experiments conducted in study [11] to determine the critical crack opening displacement at room temperature at the moment of beginning of growth of this crack also allowed determining the transverse strain from a replica. As shown by the results, the minimal thickness required to correspond to the PS condition in a tough state should meet condition $t > 25\delta_{Ic}$. Further growth of function $f(\beta(t))$ observed with decrease in the specimen thickness from 25 to 10 mm and in strain hardening n from 0.28 to 0.08 is likely to be associated with decrease in the α value, which in this case is assumed to be equal to 0.3.

To illustrate, Figure 7, *b* shows dependence (28) of correction function $f(\beta(t))$ depending upon strain hardening n and thickness t of a specimen at $\alpha = 0.2$.

It can be seen from Figure 7 that the value of function $f(\beta(t))$ in the given range falls almost 2 times with decrease in α from 0.3 to 0.2. This is indicative of the fact that a change in the stressed state of the plastic zone ahead of the crack front occurs in this range of the specimen thickness values. It should be again noted that the choice of the α value in this case reflects only the probable qualitative jump of function $f(\beta(t))$, which makes it possible to approximately determine the brittle-tough transition region.

Substituting expressions (10) and (24) to (21) yields the following relationship between δ_c and standard mechanical characteristics a_V and $\sigma_{0.2}$ depending upon thickness t of a structural material ($t > 10$ mm):

$$\delta_c = 0.5A \frac{a_V}{\sigma_{0.2}} \left(\frac{2}{\sqrt{3}}\right)^{(n+1)/n} \times$$

$$\times \left[1 - \alpha + \alpha^2 + \frac{(1 - 10.24)/(t + 5.24)(1 + \alpha)}{2} \left\{\frac{(1 - 10.24)/(t + 5.24)(1 + \alpha)}{2} - \right.\right. \quad (25)$$

$$\left.\left. - \alpha - 1\right\}\right]^{(1-n)/2n} \times$$

$$\times \left\{1 - \left(\frac{1 - 10.24)/(t + 5.24)(1 + \alpha) + 2\alpha}{4}\right\}\right/(1 - \alpha)^{1/n}.$$

In this case, the choice of specimen thickness $t > 10$ mm is related to a standard Charpy specimen. Transition to thinner impact specimens with the V-notch does now allow using the earlier developed relationship (10).

However, if results of testing the standard Charpy specimens are known, it is possible to theoretically evaluate strain characteristic δ_c for a specimen of a smaller thickness. Using the second expression of relationship (14) at $t < 10$ mm yields

$$\delta_c = 0.5A \frac{a_V}{\sigma_{0.2}} \left(\frac{2}{\sqrt{3}}\right)^{(n+1)/n} \times$$

$$\times \left\{1 - \frac{(1 - t^2)/(20t + 104.9)(1 + \alpha) + 2\alpha}{4}\right\} \times$$

$$\times \left[1 - \alpha + \alpha^2 + \frac{(1 - t^2)/(20t + 104.9)(1 + \alpha)}{2} \left\{\frac{(1 - t^2)/(20t + 104.9)(1 + \alpha)}{2} - \right.\right. \quad (26)$$

$$\left.\left. - \alpha - 1\right\}\right]^{(1-n)/2n}/(1 - \alpha)^{1/n},$$

where correction function $f(\beta(t))$ is assumed to be equal to

$$f(\beta(t)) = \left(\frac{2}{\sqrt{3}}\right)^{(n+1)/n} \times$$

$$\times \left\{1 - \frac{(1 - t^2)/(20t + 104.9)(1 + \alpha) + 2\alpha}{4}\right\} \times$$

$$\times \left[1 - \alpha + \alpha^2 + \frac{(1 - t^2)/(20t + 104.9)(1 + \alpha)}{2} \times \right. \quad (27)$$

$$\times \left\{\frac{(1 - t^2)/(20t + 104.9)(1 + \alpha)}{2} - \right.$$

$$\left.\left. - \alpha - 1\right\}\right]^{(1-n)/2n}/(1 - \alpha)^{1/n}.$$

As seen from Figure 8, the strongest effect on the $f(\beta(t))$ value is exerted by the characteristic of strain hardening n of a material, in addition to specimen thickness t.

Therefore, dependencies (25) and (26) make it possible to demonstrate the use of strain characteristics δ_c and δ_{ic} in a region of transition temperatures depending upon thickness t of a specimen and strain hardening n.

Given that the value of δ_i in the tough state depends but very slightly upon the specimen thickness, it is necessary to use a corresponding criterion to determine the upper limit of temperature transition proceeding from the following condition:

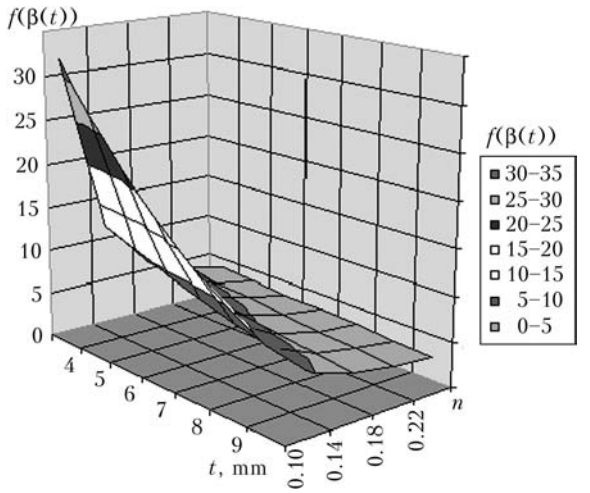

Figure 8. Variations in function $f(\beta(t))$ according to formula (27) depending upon strain hardening n and thickness t of a specimen at $\alpha = 0.3$

$$\delta_i = \delta_c, \quad (28)$$

where δ_i is the critical crack opening displacement at the moment of initiation of a stable growth of the crack in the tough state, and δ_c is determined from formula (25) or (26) depending upon specimen thickness t.

Based on dependence (10), it can be written down that

$$\delta_i = \frac{A}{2} \frac{a_V^{\max}}{\sigma_{0.2}}, \quad (29)$$

where $a_V^{\max}$ is the minimal value of the specific fracture energy of a standard Charpy specimen at the upper shelf.

In this case, allowing for expression (29) dependence (28) will have the following form:

$$\frac{A}{2} \frac{a_V^{\max}}{\sigma_{0.2}} = \frac{A}{2} \frac{a_V^{T_{cr}}}{\sigma_{0.2}^{T_{cr}}} f(\beta), \quad (30)$$

where $a_V^{T_{cr}}$ is the specific fracture energy of the standard Charpy specimen at temperature T_{cr} (Figure 9), and $\sigma_{0.2}^{T_{cr}}$ is the proof stress at temperature T_{cr}.

Upon determining the value of impact toughness $a_V^{T_{cr}}$ from expression (30), find T_{cr} and T_i corresponding to $a_V^{T_{cr}}$ and $a_V^{T\max}$ on the temperature curve of impact

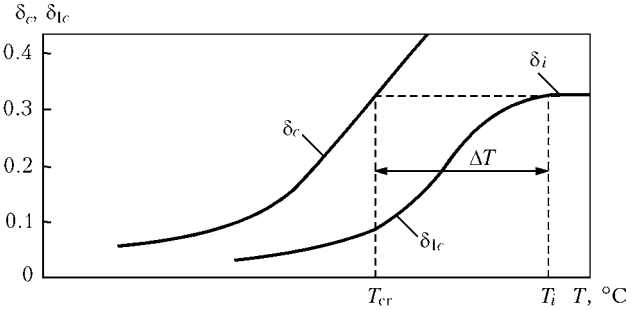

Figure 9. Graphic interpretation of dependencies (28) and (30): $\delta_c = f(\beta)\delta_{1c}$

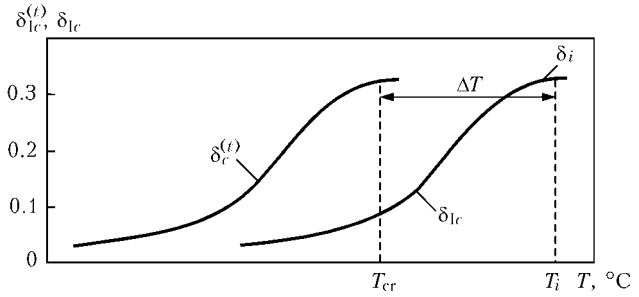

Figure 10. Graphic interpretation of equation (11)

toughness. Temperature difference $T_i - T_{cr}$ yields the required value of shift ΔT, to which it is necessary to displace the basic strain curve at the upper limit (Figure 10).

It follows from expression (30) at a constant value of A that

$$\frac{a_V^{\max}}{a_V^{T_{cr}}} \approx f(\beta) \frac{\sigma_{0.2}}{\sigma_{0.2}^{T_{cr}}}. \quad (31)$$

At a temperature not lower than −60 °C, yield stresses $\sigma_{0.2}$ and $\sigma_{0.2}^{T_{cr}}$ negligibly change as well. In practice, for the most extensively used structural steels such deviations are normally not in excess of 20 %. Hence, it can be assumed that $\sigma_{0.2} \approx \sigma_{0.2}^{T_{cr}}$, this making dependence (31) even simpler:

$$\frac{a_V^{\max}}{a_V^{T_{cr}}} \approx f(\beta). \quad (32)$$

At a small specimen thickness and low values of strain hardening n of a material, function $f(\beta)$ will have high values (Figures 7 and 9). The latter displaces impact toughness $a_V^{T_{cr}}$ to a range of very low values, which can be much lower than a generally accepted value of 35 J/cm^2.

At the same time, the suggested limitation at the upper shelf equal to δ_i is related, first of all, to the probability of a stable growth of the crack in the transition temperature range.

As noted above, depending upon the materials thickness, requirements to force characteristic K_{Ic} can be mitigated at a temperature below $T_{28\,J}$. In this case, the lower temperature limit, where some mitigation can be made when using the strain criterion depending upon the thickness, can also be limited to a value of

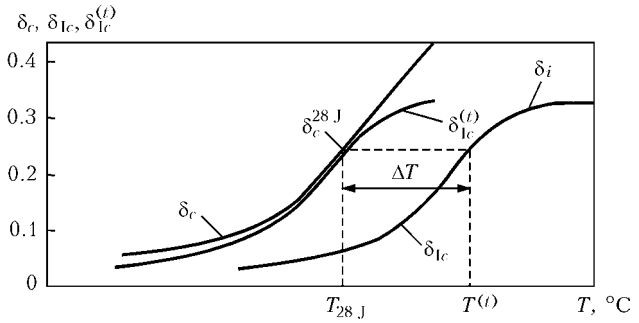

Figure 11. Graphic interpretation of dependence (33): $\delta_c = f(\beta)\delta_{Ic}$

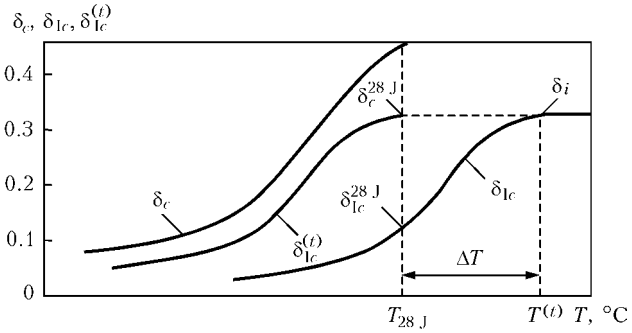

Figure 12. Graphic interpretation of dependence (35) for a case of meeting the inequality: $\delta_i < f(\beta)\delta_{Ic})^{28\,J}$

$T_{28\,J}$. This limitation is of a certain interest, as it allows comparing temperature shifts both by the force and strain criteria with respect to a single point corresponding to $T_{28\,J}$.

Proceeding from dependencies (10), (11) and (21), the value of $\delta_{Ic}^{(t)}$ at the lower limit at temperature $T_{28\,J}$ will be

$$\delta_{Ic}^{(t)} = \frac{A}{2} \frac{a_V^{T_{28\,J}}}{\sigma_{0.2}^{T_{28\,J}}} f(\beta), \quad (33)$$

where $\delta_{Ic}^{(t)}$ is limited on the top by a value of $\delta_i (\delta_{Ic}^{(t)} \le \le \delta_i)$.

Graphic interpretation of dependence (33) for a case of $\delta_i \ge \delta_{Ic}^{(t)} = \frac{A}{2} \frac{a_V^{T_{28\,J}}}{\sigma_{0.2}^{T_{28\,J}}} f(\beta)$ is shown in Figure 11.

As can be seen from the Figure, dependence (33) also comprises condition (3) as a particular case. Using expression (1), reduce dependence (33) to the following form:

$$\frac{A}{2} \frac{a_V^{T^{(t)}}}{\sigma_{0.2}^{T^{(t)}}} = \frac{A}{2} \frac{a_V^{T_{28\,J}}}{\sigma_{0.2}^{T_{28\,J}}} f(\beta), \quad (34)$$

where $a_V^{T^{(t)}} \le a_V^{\max}$.

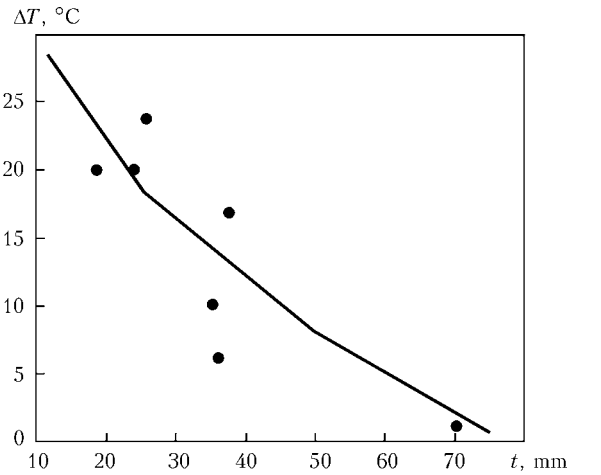

Figure 13. Dependence of temperature shift ΔT on thickness of specimens tested to three-point bending under static loading: *curve* — temperature shift specified by standard ASTM E 1921–97; *points* — experimental data obtained from formula (34)

In analogy with expressions (31) and (32), dependence (34) in the first approximation can also be reduced to the following form:

$$\frac{a_V^{T^{(t)}}}{a_V^{T_{28\,J}}} \le \frac{\sigma_{0.2}^{T^{(t)}}}{\sigma_{0.2}^{T_{28\,J}}} f(\beta), \qquad (35)$$

where, when the inequality is met, the value of $a_V^{T^{(t)}}$ is assumed to be equal to $a_V^{\max}$:

$$\frac{a_V^{T^{(t)}}}{a_V^{T_{28\,J}}} \approx f(\beta) \qquad (36)$$

at $a_V^{T^{(t)}} \le a_V^{\max}$.

This case is illustrated in Figure 12.

Therefore, expressions (34) and (35) allow establishing the necessary requirements to impact toughness of a standard Charpy specimen depending upon its thickness and strength characteristics of a material.

It follows from Figure 12 and formulae (33) and (34) that, to determine temperature shift ΔT depending upon the specimen thickness, it is necessary to know temperature dependencies of impact toughness of the standard Charpy specimen, strength characteristics of a material and strain hardening n.

To illustrate, Figure 13 shows the data obtained from the experimental values of ΔT using formula (34) for specimens of different thicknesses cut from steels 09G2S, St3 and 10KhSND and their welded joints tested to three-point bending, and the recommended temperature shift according to standard ASTM E 1921–97.

It can be seen from the Figure that the temperature shift specified by standard ASTM E 1921–97 is only of a recommendation character, as it limits the temperature range of finding the values corresponding to $K_{jc} = 100$ MPa$\sqrt{\text{m}}$ and describes only the mean values of the experimental data.

Suggested dependencies (34) and (35) also allow for the strain and strength characteristics of a material in determination of the temperature shift, which, along with expression (2), makes it possible to reasonably select the calculation requirements to the temperature shift and determine the temperature transition by taking into account thickness of a structural member.

Detailed experimental verification of the suggested approach to evaluation of the temperature shift and calculation characteristics of fracture toughness of a welded joint, heat-affected zone and base metal is beyond the scope of this article and will be presented in the next study.

Therefore, the coincidence of the temperature shift between the recommended requirement of standard ASTM E 1921–97 and second critical temperature depending upon the specimen thickness has been shown.

The approach has been suggested to evaluation of the temperature shift depending upon the specimen thickness and strength characteristics of a material based on the strain characteristic of fracture toughness δ_{Ic}.

1. Girenko, V.S., Dyadin, V.P. (1985) Relationships between impact toughness and fracture mechanics criteria for structural steels and their welded joints. *Avtomatich. Svarka*, **9**, 13–20.
2. Girenko, V.S., Dyadin, V.P. (1986) Relationships between impact toughness and fracture mechanics criteria for structural materials and their welded joints. *Ibid*., **10**, 61–62.
3. *ASTM E 1921–97*: Standard test method for the determination of reference temperature T_0 for ferritic steels in the transition range. Publ. 1998.
4. Makhutov, N.A. (1973) *Resistance of structural members to brittle fracture*. Moscow: Mashinostroenie.
5. Shiratori, M., Miyoshi, T., Matsushita, H. (1986) *Calculation fracture mechanics*. Moscow: Mir.
6. Hu, W.L., Zin, H. (1976). Crack tip strain. A comparison of finite element method calculations and moire measurements. Cracks and fracture. In: *ASTM STP 601*, 520–534.
7. Kawano, S., Shimizu, S., Nagai, K. (1983) Fracture mechanics approach to thickness effects on brittle fracture toughness under large scale yielding of mild steel. *Naval Architecture and Ocean Eng*., **21**, 113.
8. Kawano, S., Shimizu, S., Nagai, K. et al. (1984) Thickness effects on brittle fracture toughness of HT60 under large scale yielding. *Transact. of West-Japan Society of Naval Architecture*, **68**, 207.
9. Kawano, S., Tada, M., Yajima, H. et al. (1987) Thickness effects on brittle fracture toughness of weld metal of high tensile strength steel. *Ibid*., 18(**1**), 68–76.
10. Paris, P.C. (1977) Fracture mechanics in the elastic-plastic regime. In: *ASTM STP 631*, 3–27.
11. Broek, D. (1980) *Principles of fracture mechanics*. Moscow: Vysshaya Shkola.

PROPERTIES OF TUNGSTEN CARBIDE POWDERS PRODUCED BY DIFFERENT TECHNOLOGIES

V.I. DZYKOVICH, A.P. ZHUDRA and **A.I. BELY**
E.O. Paton Electric Welding Institute, NASU, Kiev, Ukraine

Investigation results are presented on properties of powders containing particles of tungsten carbides WC–W_2C and produced by different technologies. Physical characteristics of the above particles were evaluated. Chemical and X-ray analysis of the investigated powders were carried out.

Keywords: *hard-facing powders, tungsten carbides, technologies for production of powders, spherical tungsten carbide, properties of tungsten carbides, wear-resistant composite coatings*

Traditionally, fused tungsten carbides WC + W_2C are produced by crushing of ingots melted in the Tamman furnace at a temperature of 3100 °C. After crushing, a powder is subjected to separation into fractions. Such grains have mostly fragmented, irregular shape (Figure 1, *a*). Mechanical crushing results in formation of lots of cracks in the grains, this decreasing their strength to a considerable degree [1]. Particles of macrocrystalline tungsten carbide (Figure 1, *b*) produced by the WOKA technology have such drawbacks [2].

Irregular shape of the particles causes a substantial decrease in flowability of the powder, thus reducing its technological capabilities in deposition of highly wear-resistant composite coatings, favouring dissolution of tungsten carbide grains (in application of some technologies) and embrittlement of the alloy matrix, and, as a result, leading to decrease in wear resistance of the composite alloy as a whole.

It is a known fact that in the majority of cases the spherical shape of the particles is most optimal for hard-facing powders, as it provides the maximal flowability of materials and stable operation of feeding devices [3]. One of the methods for producing spherical particles of refractory materials is a process of their spheroidisation using the induction-plasma technology [4–7]. The key advantages of the latter include the possibility of preserving chemical composition of the produced particles owing to elimination of decomposition of the material treated. The technology is applied mostly for materials with a high melting temperature.

The spheroidisation method using the induction-plasma technology, in our opinion, has an important drawback. The particles produced by crushing of ingots melted in a resistance or induction furnace are subjected to fusion (Figure 1, *c*). This technology greatly depends upon the skill of operators. The ingots melted are not always homogeneous across their section and along the length. After crushing and fusion, the particles preserve the above inhomogeneity of an ingot, this affecting the quality of a material.

The E.O. Paton Electric Welding Institute developed and uses to advantage the method for thermal centrifugal spraying of cast tungsten carbide ingots [8, 9]. This method of thermal centrifugal spraying (Figure 1, *d*) provides melting of a rotating billet and formation of a thin film of the melt at the billet tip. Under the effect of the centrifugal force, this film moves to the periphery of the tip along the spiral curves. Diameter of the drops is determined by size of the molten film that constantly covers the billet

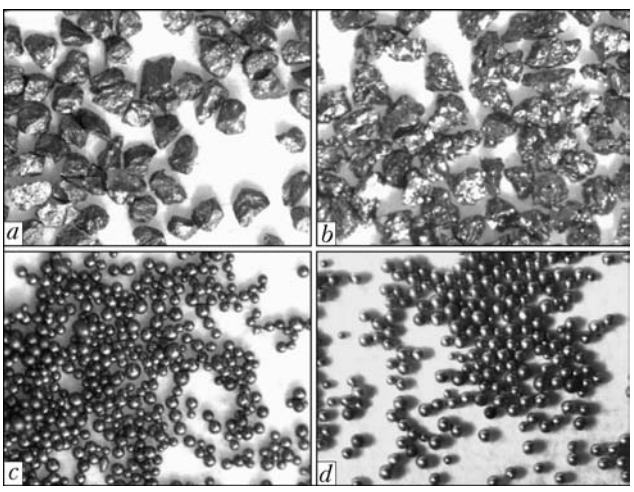

Figure 1. Appearance of tungsten carbide particles (×80) produced by different technologies: *a* — crushed; *b* — macrocrystalline; *c*, *d* — spherical and sprayed, respectively

Table 1. Content of carbon and values of microhardness of tungsten carbide particles produced by different technologies

No.	Type of tungsten carbide particles	C, %	*HV*100
1	Crushed	3.9	1800–2300
2	Macrocrystalline	6.0	1900–2150
3	Spherical (fusion), batch 1	3.9	1950–3000
4	Spherical (fusion), batch 2	3.9	1700–2300
5	Spherical (fusion), batch 2	3.9	1900–2800
6	Spherical (spraying)	4.0	2600–3300

© V.I. DZYKOVICH, A.P. ZHUDRA and A.I. BELY, 2010

tip. Normally, thickness of this film is less than 150–200 μm. Formation of such microvolumes of molten metal is accompanied by its intensive stirring, this leading to homogenisation of chemical composition of the detaching particles, which determines their high homogeneity and consistency of the stoichiometric composition. The character of melting of the tungsten carbide ingot tip in thermal centrifugal spraying is shown in Figure 2.

To compare properties of tungsten carbide powders produced by different technologies, their microhardness was measured, and their carbon content was determined (Table 1). Particle sizes were within 50–150 μm. Table 1 gives values of the measurements made on twenty particles for each material. To make analysis comprehensive, the list of the investigated powders includes samples of spherical particles produced by fusion by all of the known companies manufacturing this material.

Analysis of the results shows that the most consistent values of microhardness were exhibited by the particles produced by thermal centrifugal spraying of ingots. A wide range of microhardness values of the particles produced by the fusion method proves the above conclusion that the particles preserve heterogeneity of a material made by melting of initial tungsten carbide ingots.

The content of carbon in all the samples (except for macrocrystalline tungsten carbide WC, where the carbon content is 6 %) is 3.9–4.0 wt.%, this corresponding to the content of carbon in tungsten carbide, which is a eutectic mixture consisting of 78–82 wt.% W_2C and 18–22 wt.% WC [10].

Scanning electron microscope CAM SCAN 4 + LINK — system ENERGY 200 (energy-dispersive analyser) was used to study peculiarities of structure of the samples investigated. Analysis of electron microscopy images of the particles (Figure 3) shows that the spherical particles produced by the thermal centrifugal spraying method are characterised by the highest homogeneity of structure.

The investigations revealed the qualitative advantage of the spherical particles produced by the thermal centrifugal spraying method, compared to macrocrystalline tungsten carbide particles and crushed particles of fused carbides, which have a large number of defects in the form of cracks and pores. Moreover, comparing spherical particles produced by different technologies shows the presence of a non-spherical component for the samples produced by the spheroidisation method (up to 15 %), whereas for the particles produced by thermal centrifugal spraying this amount is no more than 5 %.

Comparative characteristics of tungsten carbide particles produced by different methods can be supplemented with X-ray examinations of the samples made by the procedure described in study [11]. Figure 4, *a, b* shows characteristic X-ray patterns of

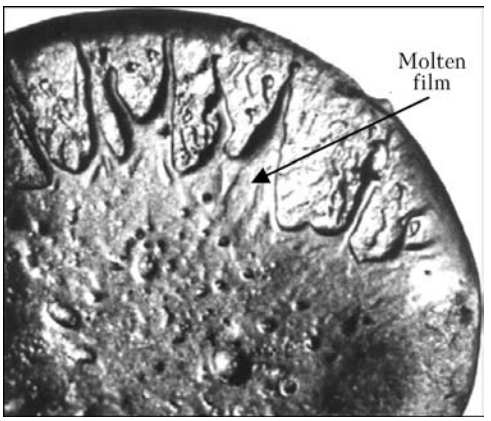

Figure 2. Character of melting of ingot tip in thermal centrifugal spraying

tungsten carbide particles produced by crushing and thermal centrifugal spraying, and Table 2 gives composition of the carbide phase and lattice parameters of carbides produced by the four technologies.

It should be noted that microhardness and properties of the particles of cast tungsten carbides WC–W_2C tend to maximum, providing that each particle

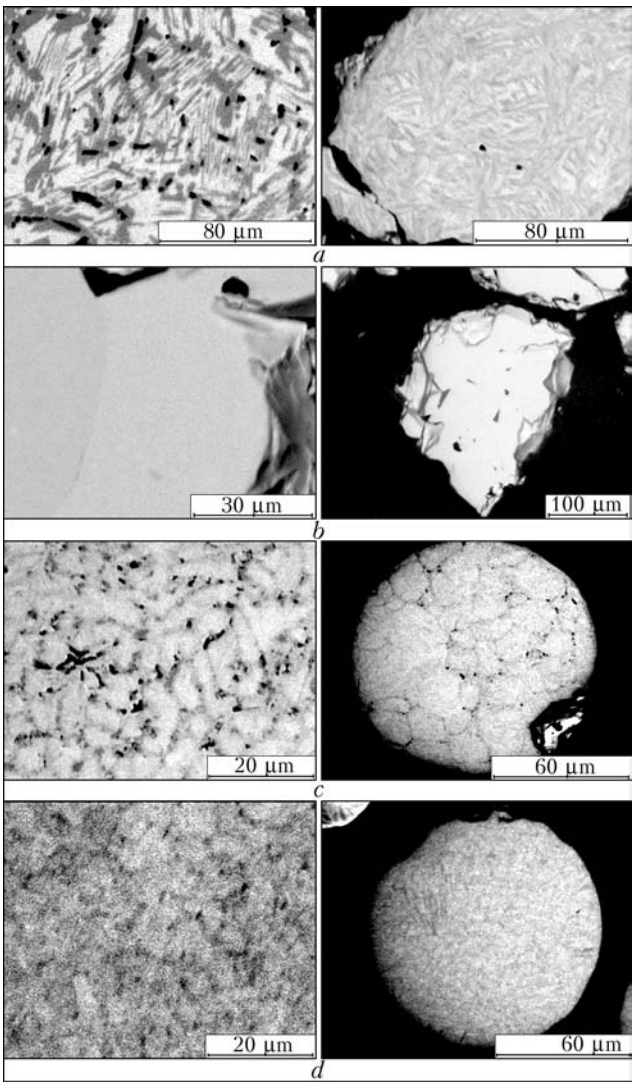

Figure 3. Electron microscopy view of tungsten carbide particles produced by different technologies: *a* — crushed; *b* — macrocrystalline; *c* — spherical (fused); *d* — spherical (sprayed)

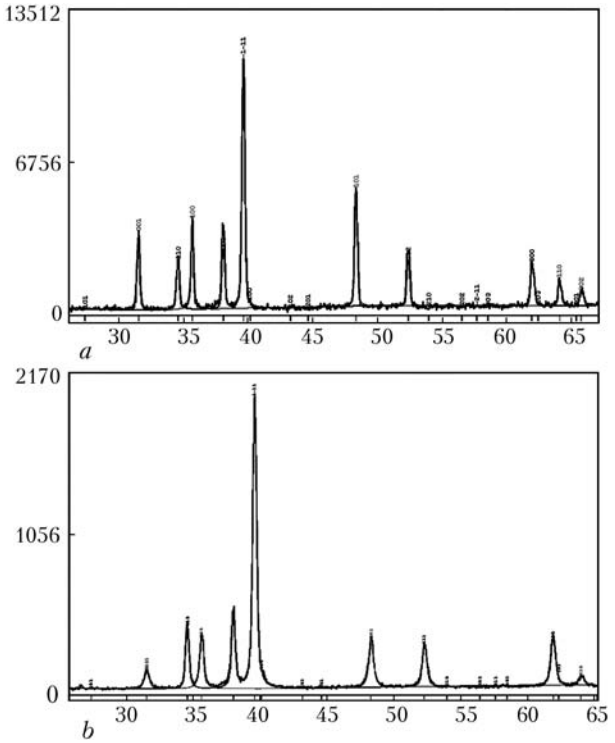

Figure 4. X-ray patterns of tungsten carbide particles produced by different technologies: *a* — crushed; *b* — spherical (spraying)

has a stoichiometric composition, which is a eutectic alloy consisting of 78–82 % W_2C and 18–22 % WC. It can be seen by comparing X-ray patterns of the examined samples that particles of the powder produced by the thermal centrifugal spraying technology developed by the E.O. Paton Electric Welding Institute have practically a eutectic composition. Two phases W_2C and WC in a proportion of 77.34 and 22.66 wt.%, respectively, were detected in the powder (Table 2, Figure 4, *b*).

To compare, the spherical tungsten carbide particles produced by the fusion spheroidisation method contain lines of free tungsten, as well as phases of free tungsten and carbon (see Table 2). Composition of spherical particles of batch 1 is closest to eutectic. However, proportion between the W_2C and WC phases is violated and equals 62.67 and 37.33 wt.%.

CONCLUSIONS

1. The technology for plasma thermal centrifugal spraying of refractory materials, developed by the E.O. Paton Electric Welding Institute, allows producing spherical tungsten carbide particles, which are closest in their stoichiometric composition to the eutectic one.

2. The cast tungsten carbides particles produced by spraying are characterised by high microhardness *HV* 26,000–33,000 MPa and stable homogeneous structure, and are superior in their properties to particles produced by other technologies.

Table 2. Phase composition of powders and their lattice parameters

Type of particles	Phase	Phase content, wt.%	Lattice parameters, nm	
Crushed	WC	36.20	2.9048	0. 28368
	W_2C	63.80	5.1861	0.47237
	W	–	–	–
Macrocrystalline	WC	95.42	2.9063	0.28398
	W_2C	4.08	5.1868	0.47163
	W	–	–	–
Spherical (fusion), batch 1	WC	37.33	2.9067	0.28364
	W_2C	62.67	5.1909	4.73830
	W	–	–	–
Spherical (fusion), batch 2	WC	26.32	2.9056	0.28375
	W_2C	69.42	5.1850	0.47286
	W	4.26	3.1645	–
Spherical (fusion), batch 3	WC	31.12	2.9063	0.28370
	W_2C	57.20	5.1855	0.47298
	W	11.41	3.1645	–
	C	0.27	2.4612	0.67163
Spherical (spraying)	WC	22.66	2.9056	0.28368
	W_2C	77.34	5.1893	0.47333
	W	Traces	–	–

1. Meerson, G.A., Zelikman, A.N. (1973) *Metallurgy of rare metals*. Moscow: Metallurgiya.
2. *WOKA carbide materials for wear protective. Welding and PTA applications*: Bull.
3. Gladky, P.V., Pereplyotchikov, E.F., Ryabtsev, I.A. (2007) *Plasma surfacing*. Kiev: Ekotekhnologiya.
4. Dignard, N.M., Boulos, M.I. (1997) Ceramic and metallic powder spheroidization using induction plasma technology. Plasma Technology Research Center (CRTP). In: *Proc. of United Thermal Spray Conf.* (15–19 Sept., 1997, Indianapolis, USA).
5. Bourdin, E., Fauchais, P., Boulos, M.I. (1983) Induction plasma technology. *Int. J. Heat and Mass Transfer*, 26(**4**), 567–582.
6. Pawlovski, L. (1995) *The science and engineering of thermal spray coatings*. Chichester: John Wiley & Sons.
7. Muns, R. (1995) *Particulate systems*. Montreal: McGill University.
8. Bely, A.I., Danilchenko, B.V., Goncharenko, V.S. et al. *Unit for centrifugal spraying of refractory metal rods*. USSR author's cert. 1381840. Publ. 02.02.1987.
9. Yushchenko, K.A., Zhudra, O.P., Bily, O.I. et al. *Method for producing of granulated refractory materials*. Pat. 20516A Ukraine. Publ. 15.07.97.
10. Samsonov, G.V., Vitryanyuk, V.N., Chaplygin, F.I. (1974) *Tungsten carbides*. Kiev: Naukova Dumka.
11. Dzykovich, V.I. (2009) Effect of the centrifugal thermal spraying processes on properties of spherical carbide particles. *The Paton Welding J.*, **4**, 43–45.

PLASMA ZrO_2 COATINGS WITH METALLIC BOND COAT OF ALLOY AlCuFe

A.L. BORISOVA, L.I. ADEEVA, A.Yu. TUNIK, T.V. TSYMBALISTAYA and **A.P. GRISHCHENKO**
E.O. Paton Electric Welding Institute, NASU, Kiev, Ukraine

The article present results of investigations of structure, phase composition and microhardness of thermal barrier plasma coatings produced by using quasi-crystalline alloy AlCuFe with a different content of the ψ-phase as a bond coat material instead of traditional alloy MeCrAlY (Me–Ni, Co, Fe). Formation of phases in the ceramic ZrO_2 layer was studied depending upon the ψ-phase content in the bond coat of a thermal barrier plasma coating.

Keywords: *thermal barrier plasma coatings, powders, zirconia, alloy AlCuFe, quasi-crystalline phase, structure, coating properties*

To increase power of internal combustion engines it is necessary to raise temperature and degree of compression of a working gas formed in fuel combustion. One of the efficient methods to address the above problem is to apply thermal barrier coatings (TBC). This makes it possible either to increase the working temperature of the gas and, thus, engine power, or to reduce losses of the engine power in combustion chamber through decreasing consumption of cooling air. Moreover, TBCs allow reducing cost of the engine owing to utilisation of less expensive and scarce materials, other parameters being equal.

TBC is a multilayer system, which consists of a metallic bond coat, external ceramic and transition cermet layers [1–3]. The external ceramic layer performs heat-protecting functions in TBC. The system based on partially stabilised zirconia has received the widest acceptance as a thermal barrier layer. Wide application of ZrO_2 is provided by low thermal conductivity coefficient (1 $W \cdot m^{-1} \cdot K^{-1}$) and high values of linear thermal expansion coefficient (LTEC) ($9.5 \cdot 10^{-6}$ K^{-1}), heat resistance and fracture toughness.

Zirconia is susceptible to reversible polymorphic transformation, which is a negative factor when it is used as a coating material. In heating to 1000–1050 °C, its low-temperature monoclinic modification ZrO_{2M} transforms into the tetragonal one ZrO_{2T}, which is accompanied by volumetric compression (by 7.7 %) [4]. Cooling to a temperature below 1000 °C causes reverse transformation into the monoclinic modification and, accordingly, increase in volume and decrease in density of a coating, this leading to its fracture and deterioration of performance. Polymorphic transformation is suppressed by using partial or complete stabilisation of structure of ZrO_2 by oxides which are close to it in structure (Y_2O_3, MgO, CaO, CeO_2, Yb_2O_3), form solid solutions with ZrO_2 and decrease thermal conductivity of ceramics approximately by half [5]. The most efficient stabilising addition to zirconia is yttrium oxide.

The key function of the bond coat in TBC is plastic relaxation of stresses in the coating, which form because of unmatched changes in volumes of ceramic and metallic materials in heating and cooling of a part [2, 3]. As ductility of alloys catastrophically falls as a result of their high-temperature oxidation, and a layer of ceramics is permeable for gases, the bond coat material should be characterised by high heat resistance. Alloys of the type of metal (Ni, C, Fr)–Cr–Al with additions of reactive elements (Y, Yb, Zr, Hf, etc.) are used as such bond coats. Fracture of such a coating occurs in diffusion interaction with the substrate metal, this leading to decrease in the concentration of alloying elements in the coating and formation of phases with lower oxidation resistance [2].

In this study the authors used alloy AlCuFe [6–9], corresponding in its chemical composition to a range of existence of the quasi-crystalline ψ-phase ($Al_{63}Cu_{25}Fe_{12}$), instead of MeCrAlY, which is a traditional bond coat material. This alloy is characterised by high hardness (up to 10 GPa), corrosion resistance and heat resistance (up to 500 °C), while in LTEC (about $1 \cdot 10^{-5}$ K^{-1}) and thermal conductivity (1–2 $W \cdot m^{-1} \cdot K^{-1}$) it is close to ceramics ZrO_2. The presence of aluminium as a main element in the alloy indicates to a high potential of using it as a bond coat material for protection from high-temperature corrosion, e.g. in manufacture of internal combustion engines.

The main method for deposition of zirconia thermal barrier coatings is plasma spraying (up to 90 % of developments) [9]. Plasma spraying of the ZrO_2–6–8 % Y_2O_3 ceramic layer provides formation of coatings, which may contain up to 99 wt.% of the tetragonal phase [3] or meta-stable T′-phase also with the tetragonal lattice [10]. It is characterised by an increased content of stabiliser, low degree of tetragonality and non-transformability into a monoclinic phase under the effect of stresses. So, investigations were

© A.L. BORISOVA, L.I. ADEEVA, A.Yu. TUNIK, T.V. TSYMBALISTAYA and A.P. GRISHCHENKO, 2010

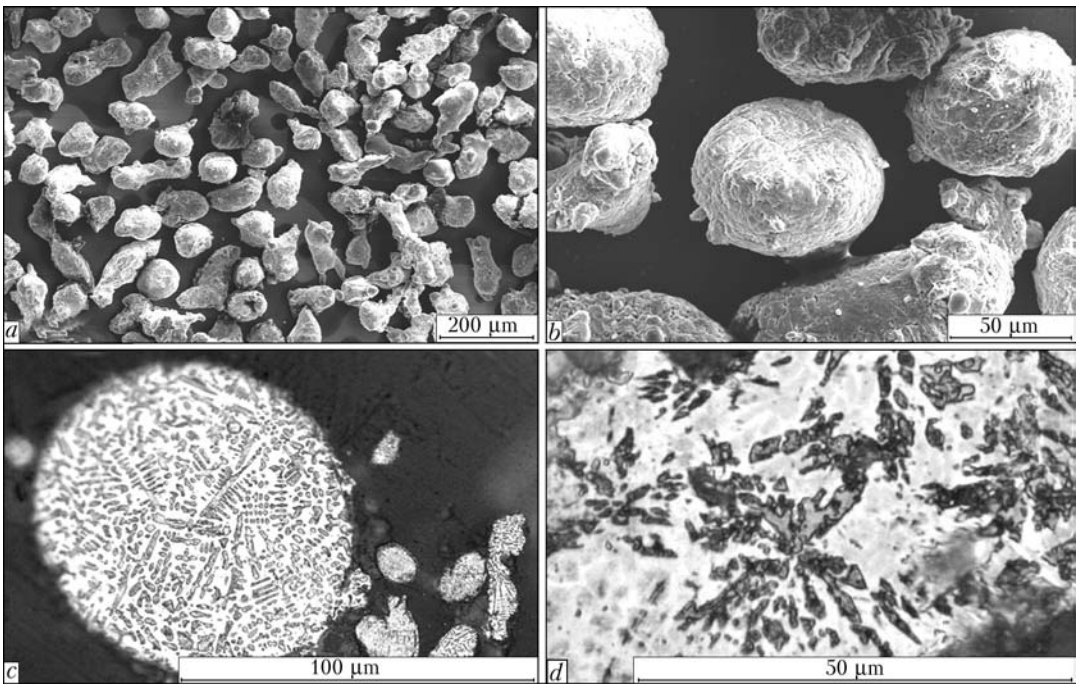

Figure 1. Appearance (*a, b*) and typical structure (*c, d*) of particles of the AlCuFe powder produced by high-pressure water atomisation of melt

conducted to study the effect of a new material of the bond coat, i.e. powder of quasi-crystalline alloy AlCuFe, and its ψ-phase content on structure and phase composition of the ZrO_2 external ceramic layer.

The ZrO_2 powder stabilised by 6.2 wt.% Y_2O_3 (external ceramic layer), as well as powder of alloy AlCuFe with a different content of the quasi-crystalline ψ-phase (metallic bond coat) were used as initial materials for deposition of thermal barrier coatings. The AlCuFe powder was produced by high-pressure water atomisation of the melt [11, 12]. Its ψ-phase content is determined by cooling conditions (quenching). It depends upon the size of the powder particles and may vary from 24 (for a faction of −160 + 120 μm) to 55 wt.% (for a fraction of −40 + 25 μm). Powders of three compositions were used in this study for spraying of the bond coat of thermal barrier coatings: powder with a 24 wt.% content of the ψ-phase was produced by milling and separation of the required fraction (−63 + 40 μm) from the powder with a particle size of 120–160 μm; powder of the −63 + 40 μm fraction with the 52 wt.% content of the ψ-phase was produced by atomisation; and to provide the 80 wt.% content of the ψ-phase the same powder was subjected to annealing in argon at a temperature of 700 °C for 2 h.

Table 1. Parameters for plasma spraying of coatings

Spraying powder	*I*, A	*U*, V	Plasma gas		Spraying distance, mm
			Composition	Flow rate, l/min	
ZrO_2	500	65	N_2	25	100
AlCuFe	500	40	Ar + N_2	25	140

The integrated procedure was employed to examine powders and coatings:

- metallography (microscope «Neophot-32» equipped with a digital photography attachment);
- scanning electron microscopy (scanning electron microscope JSM-840);
- durometry analysis (LECO hardness meter M-400 with a load of 0.25, 0.5 and 1 N);
- X-ray diffraction analysis (XRDA) (diffractometer DRON-UM1 with monochromated radiation Cu_{K_α}).

The graphite single crystal placed on a path of the diffracted beam was used as a monochromator. Diffraction patterns were produced by step-by-step scanning in a $10 < 2\theta < 120°$ angle range. The content of the quasi-crystalline ψ-phase in the powders and coatings based on alloy AlCuFe was determined by the Sordelet method [13].

As established by the morphology examination, the main mass of the AlCuFe powder consists of particles of an irregular rounded or elongated shape with the developed surface (Figure 1, *a, b*). The XRDA results (Figure 2, *a–c*) showed that the powders contained a mixture of two phases, i.e. metallic β- and quasi-crystalline ψ-phases.

Microstructure of the particles revealed by etching is a heterogeneous and two-phase one. Polyhedral crystals of the ψ-phase in the form of dendrites or rosettes (see Figure 1, *c, d*) can be seen in the light crystalline matrix (β-phase).

According to the XRDA results (Figure 2, *d*), the ZrO_2 powder stabilised by 6.2 wt.% Y_2O_3 contained 89.8 wt.% ZrO_{2T} and 10.2 wt.% ZrO_{2M}.

TBCs from the AlCuFe and ZrO_2 powders with a particle size of 40–63 μm were deposited on a steel

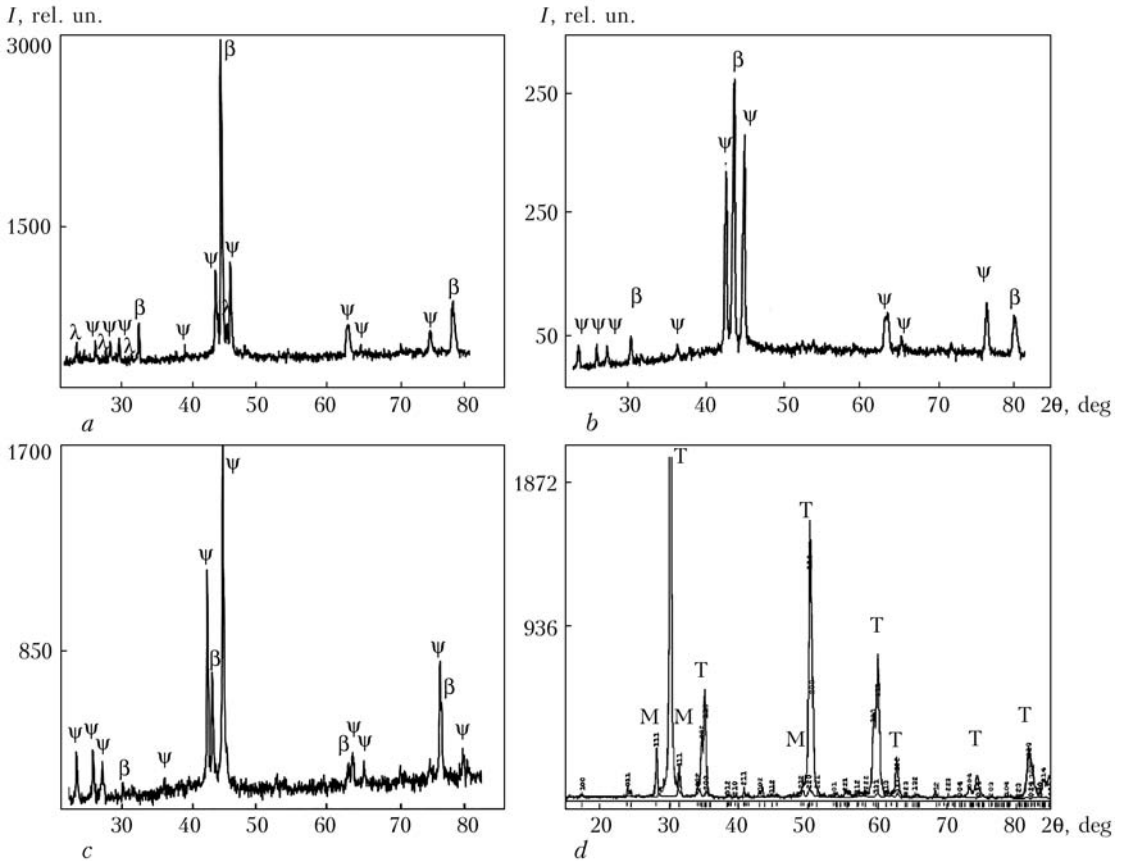

Figure 2. Diffraction patterns of AlCuFe powders with ψ-phase content of 24 (*a*), 52 (*b*) and 80 wt.% (*c*) and ZrO_2 + 6.2 % Y_2O_3 (*d*)

substrate by the plasma method using the UPU-8M unit. The plasma spraying parameters providing formation of dense coatings without defects and exfoliations are given in Table 1.

As found by examination of coatings of the AlCuFe powder containing different amounts of the ψ-phase, its content in the coatings decreased to 15, 23 and 54 wt.%, compared with 24, 52 and 80 wt.% in the initial powders. Traces of aluminium-base oxides α- and γ-Al_2O_3 and $CuAl_2O_4$ were detected in the coatings, in addition to the β- and ψ-phases. Microhardness of the metallic AlCuFe bond coat grew from (5620 ± ± 920) to (6820 ± 900) MPa with increase in the ψ-phase content (Table 2).

Metallography of the two-layer coatings (Figure 2) showed that they were free from cracks and exfoliations both at the interface with the substrate and at the ceramic coating–bond coat interface. Microhardness of the external ceramic layer grew to some extent when it was spayed on the bond coat with an increased ψ-phase content (see Table 2).

As established as a result of XRDA (Figure 4), the content of the monoclinic phase in the external ceramic layer (5.00–6.38 wt.%) was lower than in the initial powder (10.2 wt.%). The ZrO_2 tetragonal phase dominated in the ceramic layer. The calculations showed that the degree of tetragonality c/a (where c and a are the crystalline lattice parameters) also decreased and equalled c/a = 1.0103–1.0107 (see Table 2), while in the powder it was c/a = 1.0122.

Therefore, the ZrO_2 ceramic coating that forms on the AlCuFe metallic bond coat is close in structure to the non-equilibrium T′-phase, which is, according to [10], is oversaturated with the stabiliser and does not

Table 2. Characteristics of two-layer thermal barrier coatings

Sample No.	Layer	Microhardness *HV*, MPa	Phase composition, wt.%	Degree of tetragonality of ZrO_2
1	Metallic	5620 ± 920	15 ψ, 85 β, traces of oxides α-, γ-Al_2O_3 and $CuAl_2O_4$	1.0107
	Ceramic	11090 ± 1150	94, 98 ZrO_{2T}, 5.02 ZrO_{2M}	
2	Metallic	5950 ± 930	23 ψ, 77 β, traces of oxides α-, γ-Al_2O_3 and $CuAl_2O_4$	1.0103
	Ceramic	11200 ± 500	95 ZrO_{2T}, 5 ZrO_{2M}	
3	Metallic	6820 ± 900	54 ψ, 46 β, traces of oxides α-, γ-Al_2O_3 and $CuAl_2O_4$	1.0104
	Ceramic	11990 ± 1400	93, 62 ZrO_{2T}, 6.38 ZrO_{2M}	

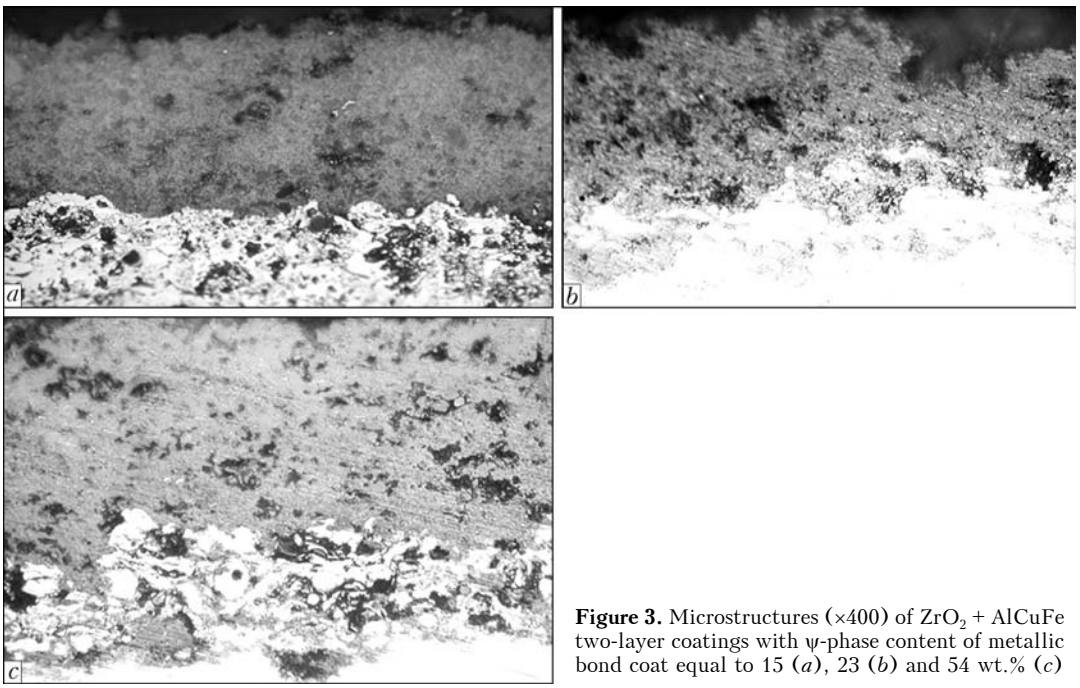

Figure 3. Microstructures (×400) of ZrO_2 + AlCuFe two-layer coatings with ψ-phase content of metallic bond coat equal to 15 (*a*), 23 (*b*) and 54 wt.% (*c*)

readily transform into the monoclinic one, like the equilibrium ZrO_{2T} phase. Only as a result of diffusion of the stabiliser in high-temperature (over 1200 °C) and long-time annealing the T′-phase transforms into the cubic and equilibrium tetragonal phase. The latter transforms into the monoclinic modification of ZrO_2 in cooling, which is accompanied by degradation of strength properties of ceramics and causes reduction of service life of the TBC [3]. In other words, the T′-phase plays an important role in production of coatings with high fracture resistance in thermal cycling.

Investigations of heat resistance of the two-layer TBCs* sprayed on aluminium alloy showed that in heating with flame of a gas torch to 400 °C for 3 s,

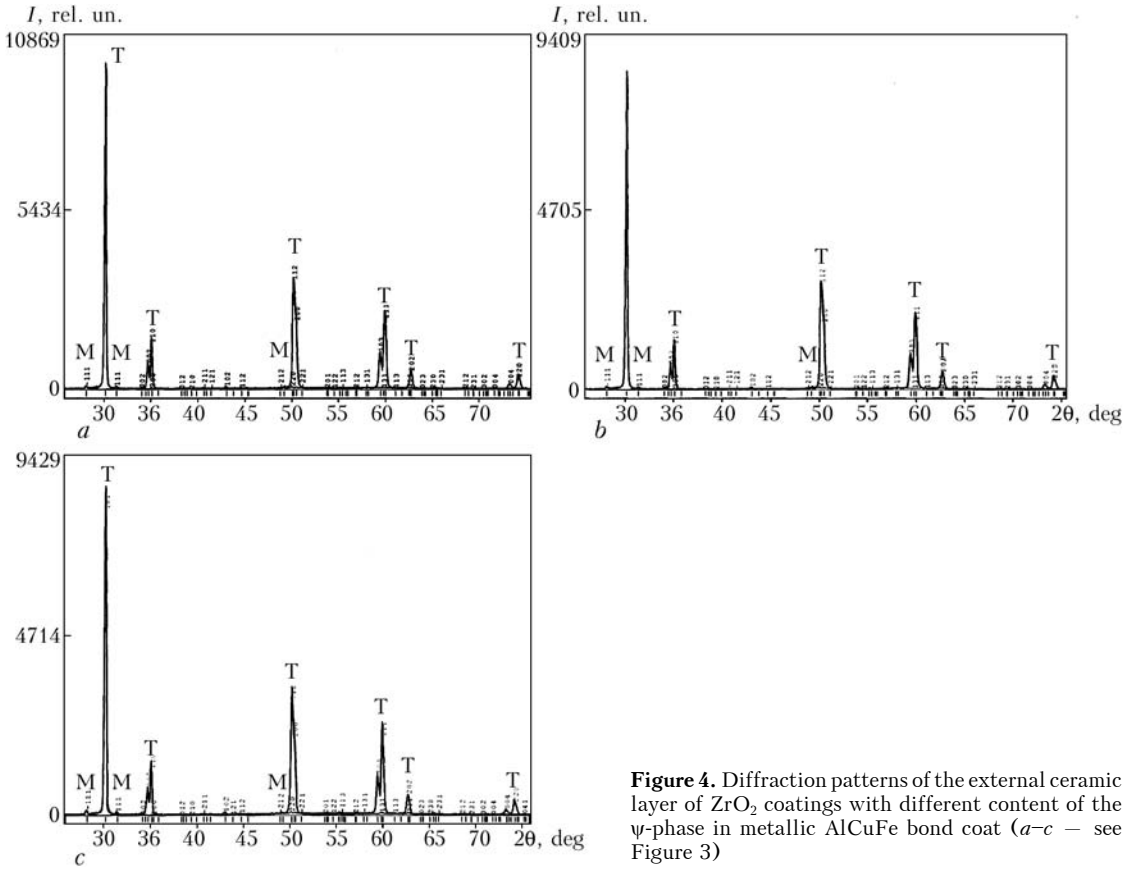

Figure 4. Diffraction patterns of the external ceramic layer of ZrO_2 coatings with different content of the ψ-phase in metallic AlCuFe bond coat (*a*–*c* — see Figure 3)

*Engineers A.N. Burlachenko and N.V. Virgilyanskaya took part in the investigations.

followed by cooling with compressed air to a temperature of 70–80 °C, the coatings had no signs of fracture for 600 cycles. Analysis of cyclograms of heating of the coated samples indicated that the use of alloy AlCuFe as a bond coat allowed decreasing the substrate temperature by 87 °C, whereas the use of NiCrAlY as a bond coat allowed this temperature to be decreased only by 70 °C.

Therefore, the ZrO_2 + AlCuFe two-layer coatings can be of interest as thermal barrier coatings for parts of aluminium alloys, e.g. components of internal combustion engines.

1. Ivashko, V.S., Iliyushchenko, A.F., Okovity, V.A. (1989) Technological possibilities of plasma spraying of thermal barrier coatings. In: *Transact. on Thermal and Vacuum Coatings in Power and Engine Engineering*. Kiev: PWI.
2. Iliyushchenko, A.F., Okovity, V.A., Kundas, S.P. et al. (2002) *Formation of thermal coatings: theory and practice*. Minsk: Besprint.
3. Iliyushchenko, A.F., Ivashko, V.S., Okovity, V.A. et al. (1998) *Thermal barrier coatings on the base of ZrO_2*. Minsk: NII PM s OP.
4. Rutman, D.S., Toropov, Yu.S., Pliner, S.Yu. et al. (1985) *High refractory materials of zirconium dioxide*. Moscow: Metallurgiya.
5. Kanygina, O.N., Pak, K.M. (1996) Effect of yttrium, calcium and aluminium oxides on structure and properties of zirconium ceramics. *Vesti KGNU*. Nat.-Techn. Sciences Series, Issue 1, 53–56.
6. Noskova, N.I., Ponomaryova, V.G., Yartsev, S.V. et al. (1995) Quasicrystalline phases in Al–Mn and Al–Cu–Fe alloys. *Fizika Metallov i Metallovedenie*, 79**(2)**, 80–86.
7. Noskova, N.I., Yartsev, S.V. (1994) Quasicrystalline phases. *Ibid*., 78**(6)**, 34–38.
8. Prevarsky, A.P. (1971) Investigation of Fe–Cu–Al system. *Izvestiya AN SSSR. Metally*, **4**, 220–222.
9. Borisov, Yu.S., Borisova, A.L., Adeeva, L.I. et al. (2003) Thermal coatings with quasicrystalline phase, properties and applications (Review). *Fizika i Khimiya Tv. Tila*, **3**, 456–465.
10. Pliner, S.Yu., Dabizha, A.A. (1987) Strengthening of ceramics from zirconium dioxide at the expense of tetragonal-monoclinic transformations. *Ogneupory*, **3**, 58–62.
11. Borisov, Yu.S., Panko, M.T., Adeeva, L.I. et al. (2001) Technologies for production and properties of powders of the Al–Cu–Fe system for thermal spraying of coatings with quasicrystalline structure. *The Paton Welding J*., **1**, 45–50.
12. Borisova, A.L., Tunik, A.Yu., Adeeva, L.I. (2006) Structure and properties of powders of Al–Cu–Fe system alloy for thermal spraying of quasi-crystalline coatings. *Ibid*., **12**, 19–26.
13. Sordelet, D.J., Besser, M.F., Anderson, I.E. (1996) Particle size effects on chemistry and structure of Al–Cu–Fe quasicrystalline coatings. *J. Thermal Spray Techn*., 5**(2)**, 161–174.

ADVANCE OF FERROUS METALLURGY AND WELDING CONSUMABLES PRODUCTION IN PRC (Review)

I.K. POKHODNYA and **A.S. KOTELCHUK**
E.O. Paton Electric Welding Institute, NASU, Kiev, Ukraine

The paper presents the data on development of ferrous metallurgy and welding consumables production in China during the last decade. Components of successful growth of steel and welding consumable production in this country have been analyzed.

Keywords: *ferrous metallurgy, steel, welding consumables, production dynamics, organizational structure*

In 2009 PWI conducted Ukrainian-Chinese seminar, in which presentations were made by PWI staff members, as well as Prof. Tian Zhiling, Vice General Manager for Research of the «China Iron and Steel Research Institute» Group, on development of ferrous metallurgy and welding consumables production in PRC. This paper was prepared by the materials of this presentation [1], as well as the data of [2].

Ferrous metallurgy. After creation of PRC steel production in this country was growing at a relatively slow pace, starting from 158 thou t in 1949 and up to 100 mln t in 1996. The next 12 years were a period of rapid development of ferrous metallurgy. In 2008 PRC enterprises produced about 500 mln t of steel, which amounted to approximately 39 % of world production (Figure 1). Such a growth of cast iron and steel production is due to rapid economic development and increased demand, primarily, in the local market. Steel consumption by PRC enterprises in 2006 was equal to 442.5 mln t, with the fraction of metallurgy reaching 8 % of the gross national product.

Progress was due, primarily, to large-scale upgrading of capital assets and creation of modern metallurgical production. The Table gives the data on the scope of upgrading the equipment for production of cast iron and steel. A lot of attention was given to introduction of power-saving technologies. By 2006 44 units for dry quenching of coke were put into operation. Recycling of coke oven gas annually yields 2.6 bln kW·h of power, and recycling of blast-furnace gas — 3.6 bln kW·h.

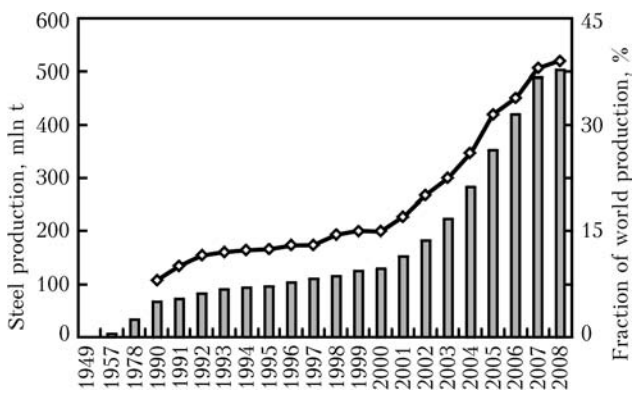

Figure 1. Steel production (*bars*) and its fraction in world production (*curve*) in PRC in 1949–2008

By 2006, 10 steam-gas power plants were in operation, allowing annual processing of 300 bln m^3 of gas and producing about 10 bln kW·h of power.

Advanced metallurgical technologies are widely used, namely injection of coal dust into blast furnaces, slag splashing on the converter refractory lining, continuous steel casting, hot loading of ingots and continuous rolling. During the period from 1990 to 2006 the fraction of billets produced in continuous casting machines increased from 25 to 99.7 %, and coal dust injection increased on average from 50 to 135 kg per tonne of produced cast iron. Slag splashing on the refractory lining allowed extension of converter operating life from 700–800 to 10 thou melts on average. Average power consumption decreased approximately 2 times — from 1611 to 734 kg of coal equivalent.

Compared to 2000 marked progress was has been made in recycling the wastes and introduction of recirculating water supply. Exhaust emissions were reduced from 18.7 in 2000 to 16.1 m^3/t of produced metal in 2004, SO_2 emissions were reduced almost two times from 6.1 to 3.2 kg/t, and water recirculation reached 92 %.

Starting from 2006, compared to 2000, the fraction of rolled plates and cold rolled sheets, electroplated metal, silicon steels, seamless pipes has increased greatly. Range of rolled products produced in PRC in 2000 and 2006 (thou t) is equal to: rails — 1580 and 3340 (increase of 111.4 %); large sections — 3600 and 9170 (154.7); rolled plates — 17440 and 85420 (389.8); cold-rolled sheets — 4950 and 26050 (426.3); electroplated metal — 3280 and 16250 (395.4); silicon steel — 640 and 3300 (415.6); seamless pipes — 4150 and 14840 (257.6). Technologies, ensuring an increase of metal purity, are currently introduced. The fraction of processed metal in 2006 reached 65 %. In the same year, 83 mln t of reinforcing-bar steel were produced, the fraction of reinforcing steel of strength class III being equal to 12.5 %. Technology of producing steel

© I.K. POKHODNYA and A.S. KOTELCHUK, 2010

Indices of upgrading of capital assets for cast iron and steel production

Metallurgical plants (volume, tonnage)		2002		2006	
		Quantity	Power, thou t	Quantity	Power, thou t
Blast furnaces	≥ 3000 m^3 2000–2999 m^3	3 17	9300 31490	12 37	35760 700090
Total		20	40790	49	105850
Oxygen converters	≥ 300 t 100–299 t	3 32	8190 48190	3 91	8190 124640
Total		35	56380	94	132830
Electric-arc furnaces	≥ 100 t	7	6730	14	11860

of this class envisages comprehensive alloying with vanadium, nitrogen and niobium. Ultrafine-grained steel is produced by a technology, using deformation-induced ferrite transformation.

New generation steels with up to 400 MPa yield point, high-strength steels with up to 800 and up to 1500 MPa ultimate strength are developed. Required mechanical properties of such steels are achieved through provision of their high purity and uniformity, as well as ultra fine-grained structure (about 2 μm grain size).

In connection with development of automotive industry in China, deep-drawn cold-rolled steels, high-strength steels of several types, namely low-carbon and improved high-strength steels have been developed. Fraction of shipments of Chinese hot-rolled sheet steel for automotive industry in 2005 was equal to 87, and that of cold-rolled steel was equal to 62 %.

Steels for the main pipelines of X80, X100 and X120 grades have been developed. The world's longest pipeline from steel of X80 grade — «West–East» II pipeline is under construction, its length reaching 7000 km. Chinese spirally-welded pipes of up to 1219 mm diameter with 18.4 mm wall thickness are used for its construction. Developed steel of X80 grade has impact energy on the level of 368 J at –40 °C; fraction of the tough component in the fracture SA (DWTT) is not less than 90 % at –15 °C. Such steels are characterized by a low content of carbon (approximately 0.03 wt.%); niobium alloying (about 0.10 wt.%) and rolling, initiating ferrite formation at deformation, are applied.

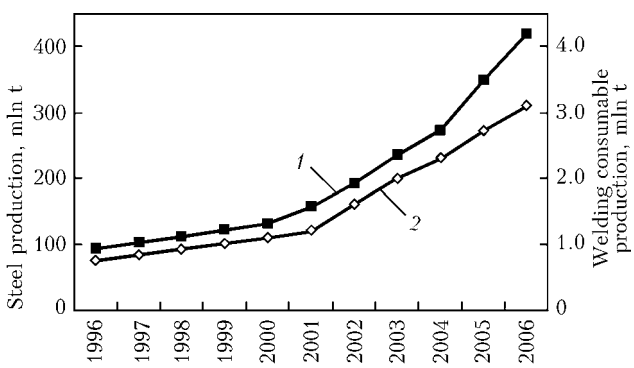

Figure 2. Production (*1*) of steel and welding consumables (*2*) in PRC in 1996–2006

Production of stainless steels is developing. In 2006 their production volume reached 5.3 mln t [1], in 2008, despite the production drop compared to 2007 by 3.6 % , it was 6.9 mln t, which amounted to 27 % of world production of stainless steels [3]. Steels alloyed with nitrogen on the level of up to 0.7 wt.% are being developed, they having not less than 600 MPa yield point and 1000 MPa ultimate strength.

The given data are indicative of an unprecedented progress of ferrous metallurgy in PRC. Most of the produced steel rolled stock is sold in the domestic market. In 2006 China produced 467 mln t of steel, exporting 43 mln t, and imported only 18.5 mln t. Domestic consumption was 442.5 mln t. That is why the world crisis phenomena had little effect on PRC metallurgical production.

Welding consumable production. Welding consumable manufacture in PRC has intensively developed over the last decade and in 2006, compared to 1999, it increased more than 4 times (Figure 2). Structure of the manufactured products has also changed. Fraction of solid wire for gas-shielded mechanized welding increased several times, production of coated electrodes for manual welding decreased, and fraction of materials for submerged-arc welding stayed on the same level and remains to be 10–12 % (Figure 3).

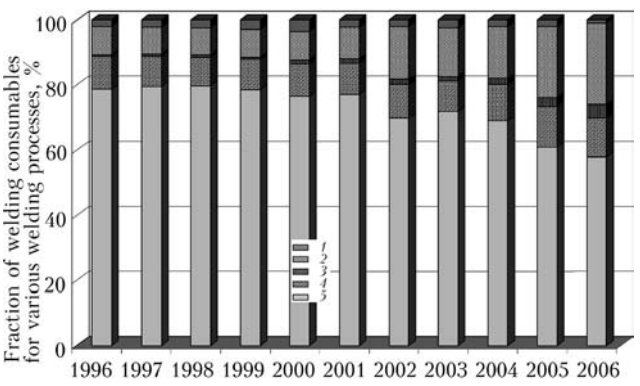

Figure 3. Structure of welding consumable production in RPC in 1996–2006: *1* — consumables for nonconsumable electrode arc welding; *2* — solid wire for gas-shielded welding; *3* — flux-cored wire; *4* — submerged-arc welding consumables; *5* — coated electrodes for manual arc welding

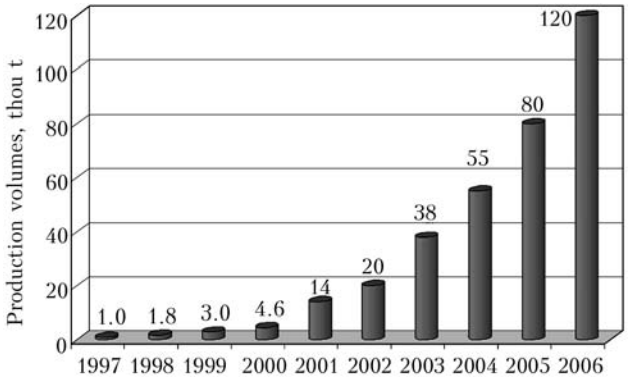

Figure 4. Dynamics of flux-cored wire production in 1997–2006

Figure 4 shows the dynamics of flux-cored wire production. Initially, flux-cored wire production in PRC was organized in 1995 by a license from PWI. Annual efficiency of the line was 1000 t. During this decade the volume of flux-cored wire production increased several times, and in 2006 it was equal to about 120 thou t. PRC specialists have properly appreciated the advantages of welding consumables of this kind. By their predictions by the end of 2015 the overall production of welding consumables in China will reach 3.5–4.0 mln t, here the fraction of coated electrodes for manual arc welding will drop to 22 %, fraction of solid wire for CO_2 welding will rise to 50 %, and that of flux-cored wires will increase up to 15 %. Fraction of consumables for submerged-arc welding will remain on the level of 12 %, and that of consumables for nonconsumable electrode welding will be about 1 %.

China Iron and Steel Research Institute Group. China Iron and Steel Research Institute Group (CISRI) was established in December, 2006 and approved by the Assets Supervision and Administration Commission (SASAC). CISRI was formed as a result of merging of the earlier Central Iron and Steel Research Institute, and Automation Research and Design Institute of Metallurgical Industry, the assets of which were evaluated to be 6.6 bln yuan (about 900 mln USD) [2].

As one of the first 103 test innovation enterprises CISRI is the research base for development of metallic materials, innovation base for key technologies of metallurgical industry, as well as the authorised agency for analysis and tests for metallurgy.

CISRI has 10 national engineering research centers, including National Engineering Research Center of Advanced Steel Technology, National Engineering Research Center of Continuous Casting Technology, National Amorphous and Nanocrystalline Alloy Engi-

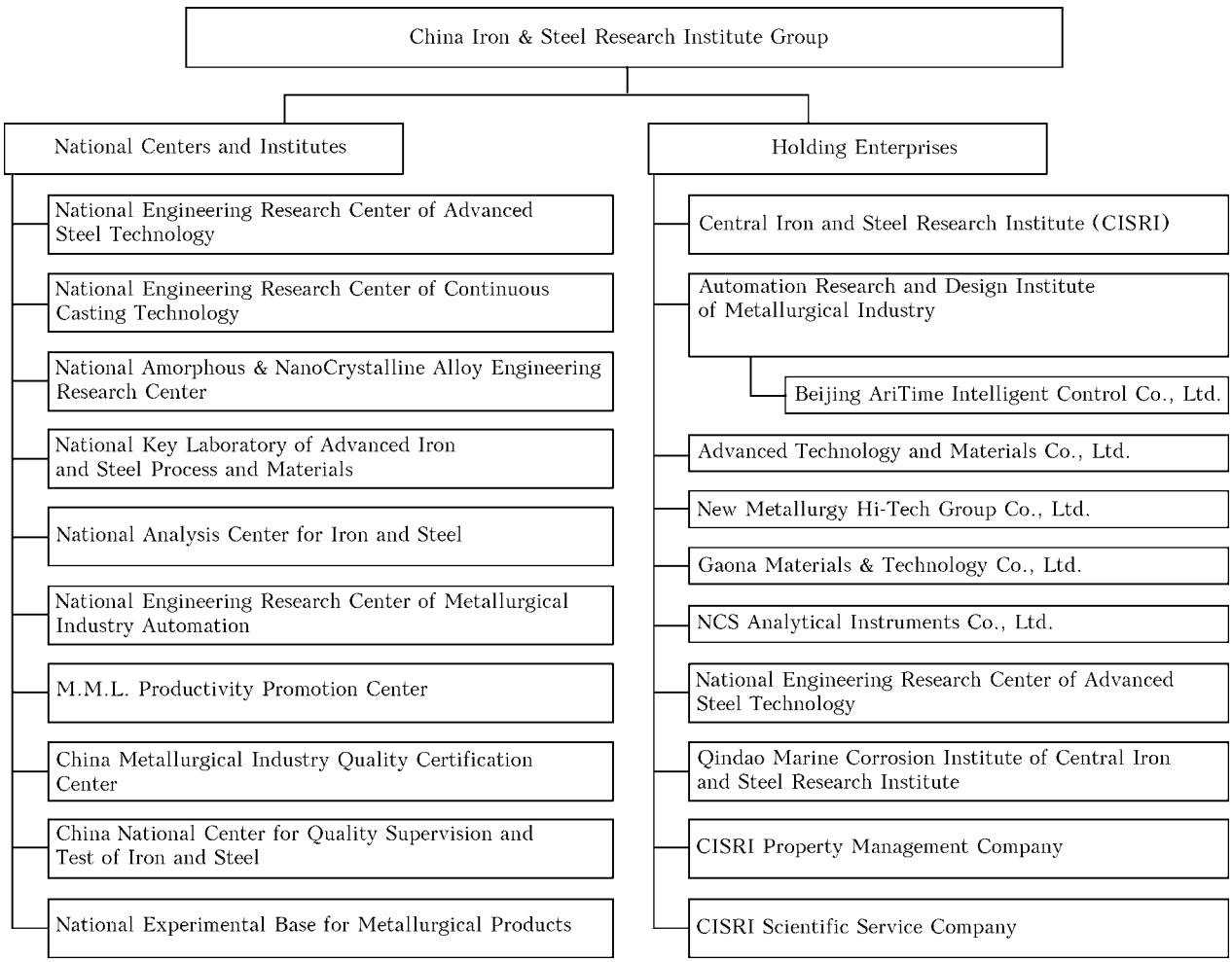

Figure 5. Institutes, engineering centers and enterprises of CISRI Group

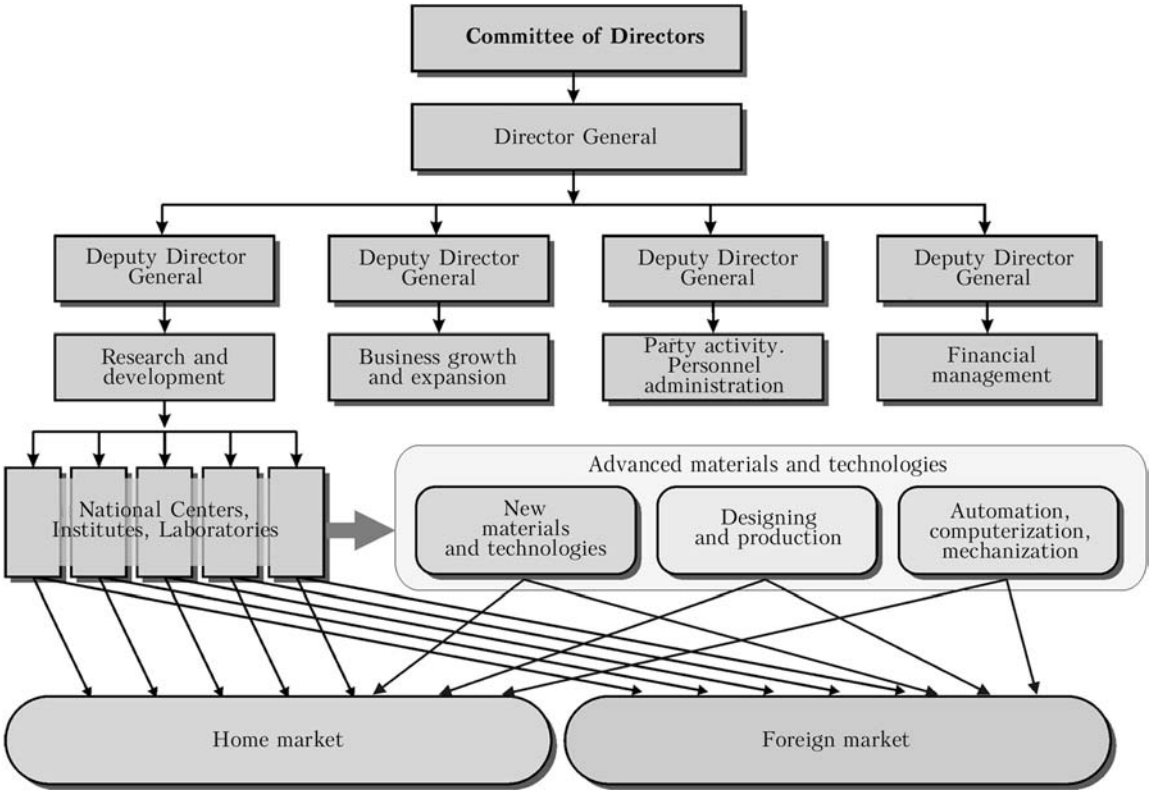

Figure 6. CISRI organizational chart

neering Research Center, National Research Center of Metallurgical Industry Automation, etc.

For promotion of large-scale and international projects and products into industry, CISRI is quickly developing advanced materials, automation technologies, applied technologies, conducts development in the instrument-making and analytical field. Figure 5 gives the structure of enterprises and organizations, included into CISRI group. In order to facilitate the realisation of R&D results, CISRI founded several limited liability joint stock companies. Two companies were initially established: Advanced Technology and Materials Co., Ltd and Beijing AriTime Intelligent Control Co., Ltd, and then several more high-technology enterprises, such as New Metallurgy Hi-Tech Group Co., Ltd and Gaona Materials & Technology Co., Ltd [2].

CISRI has approximately 5800 employees, of which 2800 are staff members, and about 3000 are temporarily employed under contracts. These temporary employees are a constant source for adding new staff to the Institute. In 2007 CISRI annual budget was equal to 500 mln USD. The main sources of funding are state budget (about 10 %), orders from state industrial enterprises (approximately 30 %) and funds from sale of proprietary developments (approximately 60 %).

Figure 6 gives the organizational chart of CISRI. Restructuring conducted in 2006 promoted an increase of research efficiency, and acceleration of introduction of the results of investigations and developments into industry.

1. Tian Zhiling. (2009) Progress of Chinese steel industry & evolution of welding consumables. In: *Proc. of Joint Ukrainian-Chinese Seminar* (25 June, 2009, Kiev).
2. China Iron & Steel Institute Group. Organisation. http://cisri.com/en/sta.org.php
3. (2009) World stainless steel output falls by 6.9 % — China Mining. http://www.chinamining.org/News/2009-03-13/123690966d22451.html

RESISTANCE WELDING OF STEEL REINFORCEMENT USING COMPOSITE INSERT

V.S. KUCHUK-YATSENKO, A.A. NAKONECHNY and **A.G. SAKHATSKY**
E.O. Paton Electric Welding Institute, NASU, Kiev, Ukraine

The process of resistance welding of reinforcing steels with application of fluxed intermediate inserts has been investigated. It was determined that inserts allow producing joints equal in strength to the parent metal at sufficiently lower degrees of plastic deformation and specific power of the equipment. Technology of welding the reinforcement of classes AI–AV of diameter from 8 up to 32 mm is offered.

Keywords: *resistance butt welding, steel reinforcement, composite insert, fluxing components*

Increase in efficiency and quality of welded joints in welding structures of reinforcing steels is an urgent problem, as the technologies, used in construction, envisage the presence of a large volume of welding jobs, including those under the site conditions. The development of the new technology of resistance butt welding with use of composite inserts at the E.O. Paton Electric Welding Institute [1] gave large opportunities for improvement both of the welding process itself and also machines for resistance welding, in particular the improvement of mass and dimension characteristics, simplification of control circuit and drive of welding machines.

The resistance butt welding is widely used for joining of wires, rods, pipes of steels, non-ferrous metals and alloys. This method has found a wide spreading owing to its simplicity, high efficiency, hygienic characteristics, low cost of the applied equipment. However, the traditional resistance butt welding has significant drawbacks, main of which is the deterioration of mechanical properties of welded joints, in particular ductility. The decrease in mechanical properties is due to metal overheating and formation of coarse grains, caused by this in the joining zone, and also defects in the form of oxide films and microcracks [2]. This is greatly manifested in resistance welding of reinforcement of diameter of more than 8 mm, and, therefore, this method of welding is not used for joining the large-diameter reinforcement.

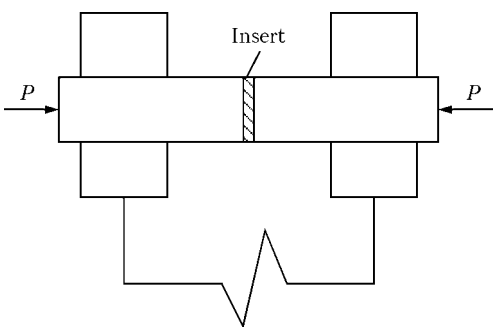

Figure 1. Scheme of resistance welding with use of a composite insert

The improvement of process of the resistance welding requires the reduction of volumes of overheated metal in welded joint, increase in concentration of heat generated in the zone of contact, protection of joint zone from oxide films. In the given work the feasibility of intensification of heating of contact zone was investigated by using the inserts (Figure 1) during resistance heating, which represent interlayers of a composite structure consisting of a metallic base and fluxing components. When current is passed through the butt with an insert, its intensive heating and melting take place due to its high internal resistance. Here, a high localization of resistance heating is occurred as compared with the traditional method.

For comparison, Figure 2 shows the temperature distribution in the butt in resistance flash-butt welding of reinforcement. It is seen from the Figure that during resistance heating using a composite insert the heating is more concentrated, and the temperature field is approximately same as in flash-butt welding.

The composition of a composite insert includes fluxing elements, whose melting temperature is lower

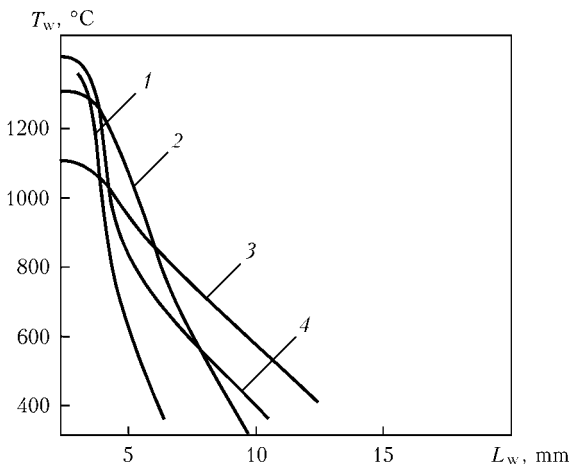

Figure 2. Distribution of welding temperature T_w before upsetting in resistance welding of reinforcement of 32 mm diameter using continuous flashing (*1*), composite insert (*2*), resistance (*3*), flashing with preheating (*4*): L_w — distance from welding zone

© V.S. KUCHUK-YATSENKO, A.A. NAKONECHNY and A.G. SAKHATSKY, 2010

Figure 3. Appearance of welded joint of reinforcement of 32 mm diameter of steel 25G2S

than the melting temperature of parent metal of parts being welded. The presence of fluxing components makes it possible to protect the heated metal in the contact zone from oxidizing, thus providing the formation of quality joints in the process of parts pressing during upsetting. Here, the feasibility is provided for producing joints at the temperature of heating of near-contact metal layers, which is lower than solidus temperature of parent metal. In this case the smaller deformation of edges is required for the joint formation than in traditional resistance welding.

The base of a composite insert is a profiled sheet of low-carbon steel of 0.8–2.0 mm thickness, the height and profile pitch are selected with account for allowable current density, then the intensity of heat generation in the contact zone is determined.

The flux composition includes oxides, chlorides and fluorides of alkali and alkali-earth metals, the flux melting temperature is 900–1000 °C. To deoxidize and improve the weld metal structure, the powders of carbon, manganese, silicon, nickel and molybdenum are added into the flux.

To conduct experiments, the machine AMG 20/170 Schlatter of 170 kV·A capacity for the resistance flash-butt welding was modified. The drive of this machine was modified for the resistance welding. The system of welding process control on the basis of

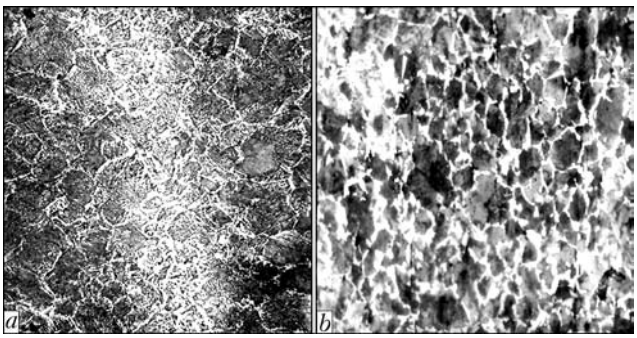

Figure 4. Microstructures (×150) of joint zone metal (*a*) of steel 25G2S and HAZ metal (*b*)

KSU KS 02 in the variant for butt welding provides its automatic control and recording.

As test specimens, the rods of reinforcement of diameter from 8 to 32 mm of classes AI–AV were selected [3]. Results of evaluation of specifics of heating (Table) allowed optimizing the welding conditions and welding flux composition. Specimens of 8, 12, 20 and 32 mm diameter were welded (steels 20, 25G2S, 70), whose edges were subjected to rough lathe machining. Figure 3 shows almost complete absence of weld reinforcement, that is due to a significant decrease in tolerance for upsetting.

Metallographic examinations were conducted on specially manufactured sections of welded joints. The samples were etched in 4% HNO_3 solution in alcohol. Hardness was measured using the LECO hardness meter M-40 at 0.5 N load. The grain size was determined in accordance with GOST 5639–82.

Microstructure of metal of 25G2S steel welded joint and HAZ is presented in Figure 4.

Metallographic examinations showed that the structure of welded joint metal is ferrite-pearlite with a dominating ferrite component. At the area of indented metal and adjacent zone to it, the size of ferrite grain corresponds to No.6, hardness is *HV*0.05 180–200. In the fusion zone there are no traces of melt and non-fused remnants of a composite insert.

In HAZ the recrystallization of a grained pearlite into a lamellar one is occurred. Microhardness in HAZ corresponds to a classical region of overheating and is varied from *HB* 160 up to 170, the presence of

Technological parameters and mechanical properties of welded joints of rods and reinforcement

Grade of steel	Diameter of reinforcement, mm	Time of welding, s	Density of welding current, A/mm^2	Tensile strength σ_t, MPa		Impact strength *KCV*, J/cm^2, at 20 °C	
				Parent metal	Welded joint	Parent metal	Welded joint
20	8 12 20	2.3 3.3 4.3	17 12 10	490–510 (500)	485–505 (495)	90	55–70 (63)
25G2S	20 32	4.3 6.1	10 8	600–620 (610)	597–625 (611)	130	75–90 (83)
70	12 20	2.3 3.3	15 12	840–890 (865)	843–870 (857)	55	22–30

Note. In brackets the mean values of σ_t and *KCV* are given.

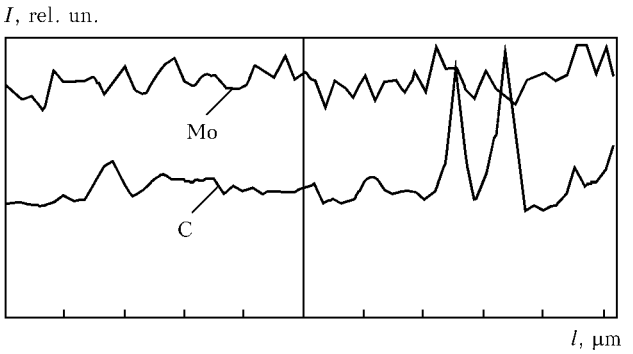

Figure 5. Distribution of carbon and molybdenum across the weld made of steel 25G2S (base of measurement is 120 μm with 2 μm pitch)

brittle phases and hardening structures was not observed. X-ray diffraction miroanalysis showed that elements-activators from welding flux composition in the form of separate structural components were not observed in metal of weld and HAZ. There are small peaks of concentrations of carbon and molybdenum, located at a certain distance from the fusion zone. This proves that a negligible alloying of metal of weld and HAZ is occurred during welding due to the diffusion process (Figure 5).

The carried out investigations made it possible to develop the technology of resistance butt welding of reinforcement of diameter of up to 32 mm with use of a composite insert.

The application of a special composite fluxed insert in resistance welding provides a highly-concentrated heating in the zone of contact, flux protection of the joint zone, decrease in process duration and in tolerances for heating and upsetting, as well as significant (6–8 times) reduction of forces in upsetting.

Welding requires the lower specific power of welding equipment, thus widening the technological capabilities of improvement both of the welding process itself, and also machines for the resistance welding.

1. *Method of resistance butt welding*. Pat. 78378 Ukraine. Int. Cl. B 23 K 11/02. Publ. 15.03.2007.
2. Gelman, A.S. (1970) *Principles of pressure welding*. Moscow: Mashinostroenie.
3. *GOST 14098–91*: Welded joints of reinforcement and embedded elements of reinforced concrete structures. Introd. 01.07.92.

10th International Conference-Exhibition «Corrosion-2010»

June 8–10, 2010 Lvov, H.V. Karpenko Physico-Mechanical Institute of the NAS of Ukraine

Conference topics

- fundamental aspects of corrosion and corrosion-mechanical fracture
- hydrogen and gas corrosion
- new corrosion-resistant materials
- thermal, galvanic and other coatings
- inhibitory and biocidal protection
- electrochemical protection
- methods of investigation and corrosion control
- anti-corrosion protection of oil and gas industry equipment
- anti-corrosion protection of power and chemical equipment
- corrosion and economic problems
- problems of training corrosion experts

Phone/Fax: (031) 263-15-77
E-mail: corrosion2010@ipm.lviv.ua
http:/www.corrosion2010.ipm.lviv.ua

FRICTION STIR WELDING AS AN EFFECTIVE METHOD TO IMPROVE STRUCTURE PERFORMANCE*

A.A. POKLYATSKY, A.Ya. ISHCHENKO, A.A. CHAJKA and **T.M. LABUR**
E.O. Paton Electric Welding Institute, NASU, Kiev, Ukraine

Main advantages of weld formation in the solid phase as a result of plastic deformation of metal in friction stir welding of auminium alloys are considered. Examples of using this process in the developed countries to produce welded structures in various engineering sectors and the resulting saving of the resources are given. Structures, weakening degree, strength, values of resistance to off-center tension of samples, and levels of residual stresses and strains in high-strength aluminium alloy welded joints produced by friction stir welding and nonconsumable-electrode argon-arc welding are analyzed.

Keywords: *high-temperature aluminium alloys, friction stir welding, nonconsumable-electrode argon-arc welding, microstructure, hardness, strength, off-center tension*

The main characteristic of any industrial structure is the ability to ensure the required performance under specified service conditions for a certain period of time. New materials, unique production technologies and different methods of joining individual elements and components often have to be used in structure fabrication to achieve the set objective. Each of these components has an essential influence on the finished product cost and largely determines their operating characteristics.

Wrought and heat-hardenable aluminium alloys are rather widely used as structural materials. Owing to high specific strength, good corrosion resistance, reliable resistance to repeated loads and low rate of fatigue crack propagation, these materials are used in development of aviation systems, space vehicles, water and land transportation [1–3]. Various welding processes are used to produce permanent joints in fabrication of aluminium alloy structures. In most of the cases, however, weld formation occurs due to melting of a certain volume of the metal being welded and filler wire fed into the welding zone with their subsequent solidification in an inert shielding atmosphere. Metal heating up to melting temperature leads to significant phase and structural transformations, causing considerable plastic deformation of the joints, and promotes development of high residual stresses in them. In the welding zone the base metal softens, and the weld has a cast coarse-crystalline structure, leading to an abrupt lowering of the welded joint ultimate strength. In addition, during melt solidification intercrystalline fracture of welds can take place in the sites of precipitation of secondary low-melting phases [4]. Therefore, many of the above drawbacks can be avoided, if the welding process is performed without metal preheating up to the melting temperature.

One of the promising methods to produce solid-phase permanent joints is friction stir welding (FSW). Here the principle of weld formation is based on heating of a small metal volume up to the plastic state due to friction, its stirring across the entire thickness of the edges being welded, and deformation in a closed space [5]. That is why, the FSW process has a number of significant advantages compared to fusion welding [6, 7]:

- weld formation in the solid phase allows avoiding formation of hot cracks, macroinclusions of oxide film, pores and other defects, which are due to metal melting and solidification in fusion welding;
- metal heating in the welding zone due to friction eliminates ultraviolet radiation of the arc, evolution of fume and metal vapours and lowers the noise level;
- permanent joint without metal melting can be formed without shielding gas application and welding can be performed in any position in space;
- absence of an arc discharge and molten metal prevents loss of alloying elements in the weld, and eliminates the need of increasing their content in it through application of filler materials;
- stirring of plasticized metal at excess pressure in a limited volume leads to fragmentation of macroparticles of oxide inclusions, and the requirements to surface preparation of the edges being welded become less stringent;
- tool tip penetration to the entire depth of the butt allows welding metal of different thickness without any special edge preparation;
- running of the welding process at lower temperatures leads to reduction of the degree of material softening and level of residual deformations in structures;
- increased effectiveness of energy utilization at FSW and reduction of metal heating temperature in

*The paper was prepared by the results of fulfillment of comprehensive program of the NAS of Ukraine «Problems of life and safety of operation of structures, constructions and machines».

© A.A. POKLYATSKY, A.Ya. ISHCHENKO, A.A. CHAJKA and T.M. LABUR, 2010

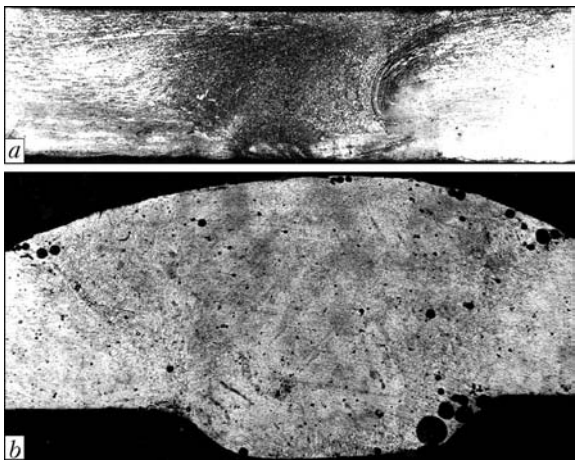

Figure 1. Transverse macrosections (×12) of welded joints of aluminium alloy 1460 made by FSW (*a*) and TIG welding with Sv1201 filler (*b*)

the welding zone lower the process energy content compared to fusion welding;

• possibility of easy automation of the welding process, thus ensuring a stable quality of welds without high operator qualifications.

Owing to such advantages FSW process opens up wider technological capabilities for fabrication of welded structures from alloys which cannot be joined by fusion welding because of formation of hot cracks in welds; ensuring a higher strength level of welded joints on heat-hardenable and work-hardened aluminium alloys; joining metastable alloys produced by rapid solidification of metal from the melt, composites and nanomaterials; producing from batch-produced individual profiles those welded components which it is not rational in terms of cost or practically impossible to produce by extrusion or casting in one piece; manufacturing practically without distortion large lightweight panels in shipbuilding, aircraft and flat wagon construction, etc.

Owing to its advantages FSW process is becoming ever wider accepted in many developed countries of the world. In shipbuilding and in railway transportation large-sized integrated panels are manufactured, which are friction stir welded from individual extruded profiles [8, 9]. In automotive industry this process is applied for manufacturing space frames of cars, motor-cycles and bicycles, truck bodies, bodies and flooring of buses, vans and trailers, elements of chassis, wheel discs, etc. [10]. Application of FSW by Boeing allowed reducing the manufacturing time of Delta rocket fuel tanks and decreasing by an order of magnitude the number of defects in welds compared to fusion welding. Eclipse Aviation company successfully applies this welding process for joining the components of the fuselage and cabin of business class five-seat plane Eclipse 500, and Airbus Company is studying the possibilities of the process in order to apply it in manufacturing the fuselage, vertical stabilizers and wings of A3xx Airbus aircraft [11]. In US NASA enterprises FSW was used to perform about half a mile of welds on the external tank of the carrier rocket of the space Shuttle [12].

The effectiveness of application of this resource-saving process is indicated by the results of statistical studies obtained in the USA. Performance of about 10 % of the entire volume of welding operations by friction stir process in 2005 allowed saving $1.35 \cdot 10^{16}$ J of energy and 20000 t of shielding gas, and the total saving was more than 4.9 bln USD, although NASA rightfully believes that the main benefit from FSW process is improvement of labour conditions of welders and personnel directly involved in welded structure fabrication [11, 12].

The purpose of the work was evaluation of operating and life characteristics of welded joints of aluminium alloys made by FSW.

Investigations were conducted using sheets 1.8 mm thick from high-strength aluminium alloys AMg6, 1201, 1420 and 1460. FSW of butt joints was performed in a laboratory system designed at PWI, using a special tool with shoulder diameter of 12 mm and conical tip. The velocity of tool rotation was 1420 rpm, and that of its linear displacement along the butt was 8–14 m/h. For comparison similar samples were welded by automatic nonconsumable-electrode argon-arc (TIG) welding with the speed of 20 m/h using MW-450 unit (Fronius, Austria) at 130–145 A current with filler wires of 1.6 mm diame-

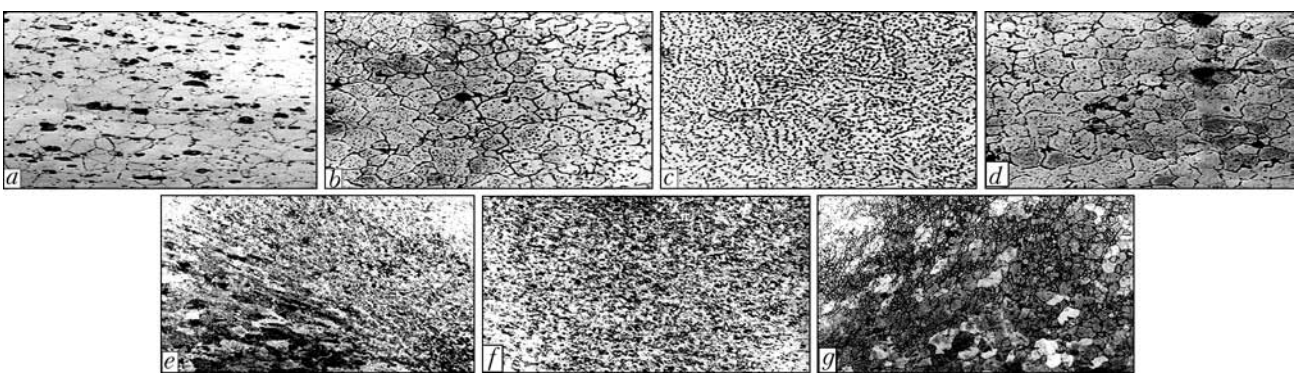

Figure 2. Microstructure (×400) of base metal (*a*) and welded joints of 1201 alloy made by TIG welding with Sv1201 filler (*b*, *d* — zones of fusion of weld with base metal; *c* — weld) and FSW (*e* — TMIZ from the tool advancing side; *f* — weld nugget; *g* — TMIZ from the tool retreating side)

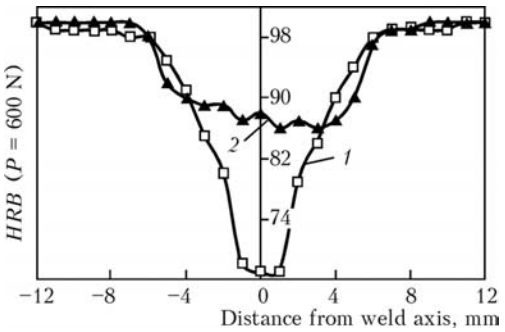

Figure 3. Metal hardness in welded joints of 1201 alloy made by TIG welding with Sv1201 filler (*1*) and FSW (*2*)

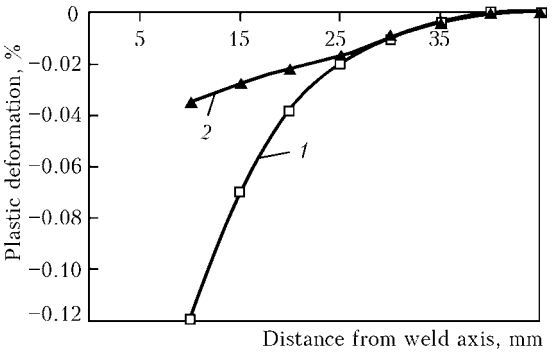

Figure 4. Plastic shrinkage deformation in welded joints of 1420 alloy made by TIG welding with SvAMg63 filler (*1*) and by FSW (*2*)

ter. Produced welded joints were used to make samples for hardness measurement, structural studies, determination of their strength at uniaxial tension and evaluation of fracture resistance values at off-center loading. Metal hardness in welded joints was measured from the side of the weld face, having first ground the reinforcement and in back bead flush with the base metal. Width of welds made by fusion welding was 6.5 mm on average, and that in FSW was 3.5 mm (at 11 mm width of the thermomechanical impact zone — TMIZ). Degree of metal softening in the welding zone was assessed by the results of its hardness measurement in ROKWELL instrument at 600 N load and sphere diameter of 1/16". Microstructure of the made joints was studied using MIM-8M optical microscope. Level of residual stresses and plastic deformations, developing in the longitudinal direction of the butt, was determined by measurement of base distance (25 mm) after welding and cutting up the samples.

Conducted experimental studies allowed assessment of the features of joints produced in the solid phase and by fusion welding. Appearance of macrosections of welds of 1460 alloy in Figure 1 shows that FSW is a resource-saving technology. Permanent joint at FSW forms only from the base metal, not requiring any filler material. It should be further taken into account that there is no need to protect the welding zone by inert gas. And since the welding process is conducted in the solid phase without metal melting, this leads to lower power consumption.

Thermomechanical conditions, under which the joints form at FSW, promote formation of a specific fine-crystalline structure of welds and adjacent sections (Figure 2). Unlike the cast structure of welds formed in fusion welding, the welds made by FSW have a deformed structure. The weld central part (nugget) forms around the tool tip at high pressure and increased temperature, resulting in dynamic recrystallization of grains and formation of fine equiaxed crystallites. In the TMIZ directly adjacent to the nugget, where the metal experiences considerable plastic deformations and heating, rather large elongated along its movement trajectory and fine recrystallized grains form. Next comes the HAZ, in which the metal was not deformed, and structural changes occurred only under the impact of heating.

Owing to formation of a deformed fine-crystalline weld structure and lower metal heating in the welding zone, the degree of softening of aluminium alloy joints is lower and ultimate strength is higher than in their fusion welding. Minimum hardness of weld metal of 1201 alloy, made by TIG welding with Sv1201 filler,

Table 1. Strength of aluminium alloy welded joints made by FSW and TIG welding

#	Welded alloys	Welding process	Filler	Tensile strength of samples without weld reinforcement σ_t^w, MPa	Strength factor $\sigma_t^w / \sigma_t^{b.m}$	Fracture site	Tensile strength of a samples with weld reinforcement σ_t, MPa	Fracture site
1	AMg6	FSW	–	332	0.92	TMIZ	–	–
		TIG welding	SvAMg6	324	0.90	Weld	345	FZ
2	1420	FSW	–	342	0.75	FZ	–	–
		TIG welding	SvAMg63	320	0.70	Weld	373	FZ
3	1201	FSW	–	310	0.73	FZ	–	–
		TIG welding	Sv1201	239	0.57	Weld	296	FZ
4	1460	FSW	–	309	0.55	TMIZ	–	–
		TIG welding	Sv1201	257	0.45	Weld	311	FZ

Note. Average values of characteristics by the results of testing 3–5 samples are given.

Table 2. Characteristics of fracture resistance at off-center loading of samples of aluminium alloy welded joints made by FSW and TIG welding

#	Welded alloys	Welding process	Filler	Tensile strength at off-center tension σ_t, MPa	Stress intensity factor K_c, MPa$\sqrt{m}$	Energy value of crack initiation J_c, J/cm^2	Specific work of crack propagation SWCP, J/cm^2
1	AMg6	–	–	402	31	7.8	6.3
		FSW	–	436	42	6.9	10.6
		TIG welding	SvAMg6	360	24	6.2	4.7
2	1420	–	–	450	15	6.5	2.7
		FSW	–	388	22	4.4	5.2
		TIG welding	SvAMg63	399	29	5.2	5.7
3	1201	–	–	486	15	6.1	2.7
		FSW	–	449	20	7.4	3.8
		TIG welding	Sv1201	333	16	3.7	2.9

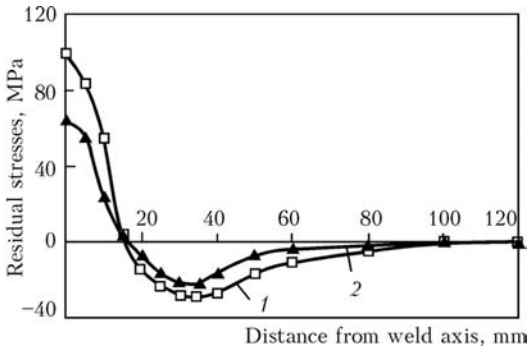

Figure 5. Residual stresses in welded joints of 1420 alloy made by TIG welding with SvAMg63 filler (*1*) and FSW (*2*)

is only *HRB* 67, and that of FS-welded metal is *HRB* 82 (Figure 3). Metal of AMg6 alloy weld made by fusion welding with SvAMg6 filler has minimum hardness *HRB* 82, and that made in the solid phase — *HRB* 87. For 1460 alloy these values are *HRB* 71 (with Sv1201 filler) and *HRB* 82, respectively. Hardness of 1420 alloy weld metal made by TIG welding with SvAMg63 filler is on the level of *HRB* 82, and that of metal welded by friction stir process is *HRB* 86.

Ultimate strength of samples without weld reinforcement made by TIG welding of AMg6 alloy with SvAMg6 filler is equal to 324 MPa, and that of samples welded by friction stir process is 332 MPa (Table 1). Here fracture of samples made by solid-phase welding occurs in the TMIZ and not in the weld metal. Welded samples of 1420 alloy, even though they fail in the weld in both the cases, have a higher ultimate strength (342 MPa) when FSW is used. An even greater difference in strength is achieved in welding copper-containing heat-hardenable aluminium alloys. Samples of 1201 and 1460 alloys made by FSW have ultimate strength on the level of 310 MPa, whereas for samples without reinforcement, made by TIG welding of 1201 and 1460 alloys with Sv1201 filler, this value is equal to just 239 and 257 MPa, respectively.

Lowering of thermal impact on the metal at FSW promotes a lowering of the level of residual plastic deformations, developing in the near-weld zone of welded joints under the impact of stresses exceeding the material proof stress. Maximum plastic deformation at metal shrinkage at 10 mm distance from weld axis is equal to 0.12 % in joints of 1420 alloy made by TIG welding, and is less than 0.04 % for joints made by FSW (Figure 4). Therefore, application of solid-phase welding promotes a lower distortion of welded structures and, therefore, allows lowering the expenses, related to its subsequent elimination.

Presence of residual plastic shrinkage deformations at weld cooling stage leads to development of residual tensile stresses in the middle part of the welded joint. Therefore, application of FSW provides a lower level of residual stresses. For instance, maximum value of residual tensile stresses in welded joints of 1420 alloy, made by TIG welding, is on the level of 99 MPa, and in those made by FSW it is 64 MPa (Figure 5), i.e. such joints are less prone to propagation of service cracks in them and have a higher fracture resistance.

A higher level of life characteristics of welded joints made in the solid phase is confirmed by the results of testing samples at their off-center tension. Samples with stress raisers in the form of a sharp (R = = 0.1 mm) notch made by FSW mostly have higher fracture resistance values than those made by a non-consumable electrode, and sometimes even higher than the respective base metal values (Table 2).

The conducted series of investigations allowed development of technological recommendations on FSW of sheet aluminium alloys. The advantages of such a process of making permanent joints will be realized in fabrication of heat exchangers and aerospace systems.

CONCLUSIONS

1. Since in FSW the weld and the adjacent sections are heated below the melting temperature of the welded metal, the possibility of solidification crack formation in aluminium alloys is eliminated.

2. Intensive stirring of plasticized metal at excess pressure in a limited space at FSW promotes formation

of an ultradispersed structure in the weld nugget, and formation of long and fine recrystallized grains elongated along the trajectory of plasticized metal displacement in the adjacent TMIZs.

3. Deformation strengthening of metal, grain refinement, increase of volume fraction of their boundaries and refinement of intermetallic phases in the weld and in the sections adjacent to it at FSW ensure a higher level of metal hardness in the welding zone and ultimate strength of joint metal than in fusion welding.

4. Lowering of thermal impact on the metal at FSW promotes a lowering of the level of residual plastic shrinkage deformations and tensile stresses in the joints, thus leading to a smaller distortion of welded structures and increasing their fracture resistance.

5. Welded joints produced by friction stir process have higher values of fracture resistance at off-center tension of samples than those made by nonconsumable electrode, and sometime even higher than the respective values for the base metal.

6. Application of resources-saving technology of producing permanent joints in the solid phase by FSW in fabrication of welded structures from aluminium alloys allows improving their operating and service life characteristics.

1. Fridlyander, I.N. (2002) Aluminium alloys in aircraft in periods of 1970–2000 and 2001–2015. *Tekhnologiya Lyog. Splavov*, **4**, 12–17.
2. Ryazantsev, V.I., Fedoseev, V.A. (1997) Welding of structures of orbital aircraft Buran. *Svarochn. Proizvodstvo*, **4**, 31–36.
3. Gorynin, I.V., Zolotarevsky, Yu.S., Rybin, V.V. et al. (1999) Metal science concepts in development of wrought aluminium alloys for high-speed sea ships. *Voprosy Metallovedeniya*, **3**, 197–209.
4. Ishchenko, A.Ya. (1985) Character of hot cracks formed in fusion welding of high-strength aluminium alloys. In: *Current problems of welding of non-ferrous metals*. Kiev: Naukova Dumka.
5. Dawes, C.J. (1995) An introduction to friction stir welding and its development. *Welding and Metal Fabr.*, **1**, 13–16.
6. Dawes, C.J., Thomas, W.M. (1996) Friction stir process welds aluminum alloys. *Welding J.*, **3**, 41–45.
7. Defalco, J. (2006) Friction stir welding vs. fusion welding. *Ibid.*, **3**, 42–44.
8. Lahti, K. (2003) FSW — possibilities in shipbuilding. *Svetsaren*, **1**, 6–8.
9. Kallee, S.W., Davenport, J., Nicholas, E.D. (2002) Railway manufacturers implement friction stir welding. *Welding J.*, **10**, 47–50.
10. Hinrichs, J.F., Norik, J.S., McDonald, W.M. et al. (2001) Challenges of welding aluminium alloys for automotive structures. *Svetsaren*, **12**, 281–287.
11. Arbegast, W.J. (2006) Friction stir welding after a decade of development. *Welding J.*, **3**, 28–35.
12. Ding, J., Carter, R., Lawless, K. et al. (2006) Friction stir welding flies high at NASA. *Ibid.*, **3**, 54–59.

FOR SPECIALISTS

On June 16–17, 2010 Ukrainian-German Seminar on the subject «*Plasma and Electron Beam Technologies for Protective Coatings*» will be held in Kiev at the E.O. Paton Electric Welding Institute.

Seminar subject complies with such a priority field as «New materials and production technologies», developed by the Federal Ministry of Education and Science of Germany within the framework of scientific-technical cooperation with Ukraine. The project was planned as a pilot project and is intended to support internationalization of SMEs. It should promote practical implementation of internationalization strategy.

The Seminar envisages exchange of information on the above subject between specialists of both enterprises and scientific institutions. The main circle of seminar participants will include scientists and specialists of manufacturers and users of functional products with optimized tribological properties, as well as specialists working in such production sectors, as automotive industry, mechanical engineering, etc. Poster presentations and possibility for cooperation negotiations will also be provided during the seminar.

Contacts: Tel./Fax: +38(044) 289 22 02. E-mail: Yu.kon@paton.kiev.ua
Prof. Konstantin A. Yushchenko,
Deputy Director of the E.O. Paton Electric Welding Institute of the NASU

CODE DESIGNATIONS OF LOCALLY MANUFACTURED FLUXES AND FLUX + WIRE COMBINATIONS IN KEEPING WITH INTERNATIONAL STANDARDS

A.V. ZALEVSKY[1], **V.I. GALINICH**[1], **N.A. PROTSENKO**[2] and **V.V. KUKHARENKO**[3]
[1]E.O. Paton Electric Welding Institute, NASU, Kiev, Ukraine
[2]ISTC «Paton-Cert», Kiev, Ukraine
[3]RPE «Conversion Technologies» of the Ukrainian Research Institute of Shipbuilding Technology, Nikolaev, Ukraine

The paper deals with the features of application of International Standards ISO 14171:2002 and ISO 14174:2004 for classification of welding fluxes. Code designations of local fluxes in keeping with the above standards are given, as well as identification of codes included into the designations, and recommendations on application of code designations of welding fluxes.

Keywords: *arc welding, welding fluxes, International Standards ISO 14171:2002 and ISO 14174:2004, classification, code designations.*

Submerged-arc welding is the main technological process in manufacture of the most metal structures (pipes, bridges, oil and gas pipelines, ships, various structures). It is notable for a high level of mechanization and productivity, quality of welded joints, and is actually the only method for joining of elements of metal structures in welding of metal with a thickness of more than 12–15 mm.

The main factor for increasing competitiveness of welded metal structures is their high quality at a low cost. The cost of flux itself has a low influence on the cost of a metal structure. Despite this fact, the high quality of a metal structure and expenses for achieving it significantly depend on the welding flux i.e. its ability to provide the defect-free formation of the weld metal, pore and crack resistance of the latter, providing of high brittle fracture resistance of the weld, reduction of costs for repair of joints etc.

AN-60, AN60M, AN-348-A, AN-348-AM, AN-348-APM, AN-47, AN-47DP, OSTs-45, OSTs-45M, AN-43, AN-67B grades of fused fluxes used for welding of carbon unalloyed and low-alloyed steels, AN-8 flux for electroslag welding, and AN-20S, AN-20P, AN-26S, AN-26P fluxes for welding of stainless steels are widely applied in the CIS countries. Fluxes of the above grades are mainly produced by the two, most renown in Europe, Ukrainian manufacturers — OJSCs «Zaporozhie Plant of Welding Fluxes and Glass Products» and «Nikopol Ferroalloys Plant» (according to GOST 9087–81E [1], TU U 05416923.049–99 [2] and GOST R 52222 [3]). Joining of Ukraine to the World Trade Organization requires bringing of national standards and other regulatory technical documents in correspondence with international standards.

Harmonization of national standards. In this connection, there are two problems with the domestic welding fluxes. The first one is the absence of full information about consumer properties of fluxes in the national standards. Such information in accordance with International Standards ISO 14171:2002 and 14174:2004 should be included in codes giving the designations of fluxes. Code designations are indicated in labels, packages, in technical documents, in handbills and booklets etc. Designations for the new flux grades are to be given by their developers, and for the existing ones (according to GOST 9087–81E) — by a special organization having appropriate technical capabilities and specialists to conduct necessary tests and codifications.

The second problem lies in that even though fluxes meet the main technical requirements to the technology for manufacture of welded metal structures (strength of weld metals, their defect-free formation etc.), the national standards do not contain indicators of consumer properties of the fluxes (strength characteristics of welds, their brittle fracture resistance etc.). It is caused by the fact that, conceptually, the main standard, according to which domestic fluxes are manufactured, i.e. GOST 9087–81E [1] (as well as different specifications), is aimed at determination of requirements to the technology of manufacture of a flux, rather than to its consumer properties. For example, precise chemical composition of the flux, color of its grains, method for evaluation of the moisture content of the flux and other factors do not allow common flux customers (in particular, representatives of trade organizations, who in the most cases are not specialists in the field of development and application of fluxes) to effectively evaluate the possibility of using a certain grade of flux to solve their technological problems, as these indicators bear no information on mechanical properties of the weld metal or welded joint (yield strength and tensile strength, impact

© A.V. ZALEVSKY, V.I. GALINICH, N.A. PROTSENKO and V.V. KUKHARENKO, 2010

toughness etc.), while these indicators are the main criteria of for selection of flux. Hence, we will compare the main standards on welding fluxes in force in the international market.

In accordance with the said standards, a manufacturer, putting a tag (label) on a product, evidences that the latter meets requirements of a corresponding standard specifying properties of the given product. Complete information on these properties, as a rule, is contained in the accompanying documents. At the same time, the information (or its main part), which is indicated on the labels or in short advertisements, should be concise and clear for a consumer. Therefore, it is formed in accordance with special standards.

The following main international standards are used for welding fluxes:

ISO 14171:2002. Welding consumables — Wire electrodes and wire-flux combinations for submerged arc welding of non alloy and fine grain steels — Classification;

ISO 14174:2004. Welding consumables — Fluxes for submerged arc welding — Classification;

ISO 544:2003. Welding consumables — Technical delivery conditions for welding filler metals — Type of product, dimensions, tolerances and marking;

ISO 14344:2002. Welding and allied processes — Flux and gas shielded electrical welding processes — Procurement guidelines for consumables;

ISO 15792-1:2000. Welding consumables — Test methods. Pt 1: Test methods for all-weld metal test specimens in steel, nickel and nickel alloys;

ISO 15792-2:2000. Welding consumables — Test methods. Pt 2: Preparation of single-run and two-run technique test specimens in steel;

ISO 3690:2000. Welding and allied processes — Determination of hydrogen content in ferritic steel arc weld metal.

It should be noted that harmonized international standards do not automatically cancel regional, intergovernmental and national standards, including GOST 9087–81E. For example, in addition to international standards, European standards EN 760 and EN 756 are in effect in the European market of welding fluxes, and German standards DIN 32522 and DIN 8557 are in effect in the German market. Main principles of the international standards are implemented in national production through development of similar national standards on their basis.

American standards [4, 5] are widely applied by flux manufacturers, in addition to the above international standards. They are differ from the international standards (including ISO 14171:2002 and ISO 14174:2004) in that they do not contain information on physical-chemical properties of fluxes, and have differences in welding technologies during testing. However, like in ISO 14171:2002, the results of tests of the flux + wire combinations are applied for the classification purposes. According to the American system of classification, fluxes have no designation except for a trade mark. All the flux grades have a mandatory designation of the flux + wire combinations, which, like in ISO 14171:2002, contains the main data on consumer properties of a flux in the coded form: for welding of which materials the flux is designed, what level of mechanical properties of the weld metal this flux in combination with specific welding wires provides under standard conditions, etc. These characteristics are basic in evaluation of fitness of fluxes for purpose in accordance with the international standards. This approach provides the customer with a possibility to compare technical characteristics and select an optimal welding variant using code designations of fluxes. From this point of view, domestic marking of fluxes, for example AN-60 grade, gives no information to a customer who knows nothing about this flux. It only indicates that this flux was developed by the Academy of Sciences of Ukraine (AN) and gives the development number (60). At the same time, even a short designation of this flux according to ISO 14174:2004 (SF 1 MS) indicates that this product is a welding (S) fused (F) flux for welding of carbon and low-alloyed steels (1), and is of the manganese-silicate type (MS).

Given the above-said, to determine codes and give corresponding designations to fluxes, we carried out tests of welding-technological properties of domestic fluxes of the most common grades in accordance with the requirements of ISO 14174:2004 and ISO 14171:2002.

Welding and tests of mechanical properties of the welded joints were carried out in certified laboratories of the E.O. Paton Electric Welding Institute and branch RPE «Conversion Technologies» of the Ukrainian Research Institute of Shipbuilding Technology.

Only the most widely used welding wires of the Sv-08A, Sv-08GA (GOST 2246–70) and Sv-08G1NMA (TU U 14-16-130–97) grades of the domestic production, and 4.0 mm diameter wires of the S1 and S2 grades from the known European manufacturers, i.e. «Multimet» (Poland), 5.0 mm diameter wire S2 from the «Boehler» (Austria), and 5.0 mm diameter wire S1 from the OERLIKON (Germany) were utilized in study. Welding and testing of joints were carried out in accordance with the requirements of standards ISO 14171:2002, ISO 15792-1:2000 and ISO 15792-2:2000.

The codes of properties were determined, and code designations were given to tested combinations based on the investigations results for combinations of fluxes and welding wires in accordance with the requirements of standard ISO 14171:2002 (Table 1).

Code designations of domestic welding fluxes in accordance with the requirements of International Standard ISO 14174:2004 are given in Table 2. These fluxes manufactured in accordance with GOST 9087-

Table 1. Code designations of combinations of domestic welding fluxes with wires of local and import production in accordance with requirements of International Standard ISO 14171:2002

Flux + wire combination	Designations acc. to ISO 14171:2002
Yield strength of base metal and 47 J impact energy of welded joint metal (TWO-run technique, section A)	
AN-60 + S1	ISO 14171-A-S 3T 0 MS S1
AN-348-A + S1	ISO 14171-A-S 5T 2 MS S1
OSTs-45M + S1	ISO 14171-A-S 5T 2 MS S1
AN-47 + S2	ISO 14171-A-S 5T 2 CS S2
AN-47DP + S2	ISO 14171-A-S 5T 2 CS S2
AN-43 + S2	ISO 14171-A-S 3T 4 AR S2
AN-67B + S2	ISO 14171-A-S 3T 4 AR S2
Tensile strength and 27 and 47 J impact energy of welded joint metal (TWO-run technique, section B)	
AN-60 + Sv-08A	ISO 14171-B-S49S 2 MS SU11
AN-60 + SV-08A	ISO 14171-B-S49S 0U MS SU11
AN-348-A + SV-08A	ISO 14171-B-S49S 2 MS SU11
AN-348-A + Sv-08A	ISO 14171-B-S43S 0U MS SU11
OSTs-45M + Sv-08A	ISO 14171-B-S49S 2 MS SU11
OSTs-45M + Sv-08A	ISO 14171-B-S43S 0U MS SU11
AN-43 + Sv-08GA	ISO 14171-B-S57S 5 AR SU11
AN-43 + Sv-08GA	ISO 14171-B-S57S 4U AR SU11
AN-47 + Sv-08GA	ISO 14171-B-S57S 5 CS SU11
An-47 + Sv-08GA	ISO 14171-B-S57S 3U CS SU11
AN-67B + Sv-08G1NMA	ISO 14171-B-S57S 7 AR SUN2M3
AN-67B + Sv-08G1NMA	ISO 14171-B-S57S 6U AR SUN2M3
Yield strength of pure (deposited) weld metal and 47 J impact energy (Multi-run technique, section A)	
AN-60 + S1	ISO 14171-A-S35 2 MS S1
AN-60 + S2	ISO 14171-A-S42 0 MS S2
AN-348-A + S1	ISO 14171-A-S38 0 MS S1
AN-348-AM + S1	ISO 14171-A-S38 0 MS S1
OSTs-45M + S1	ISO 14171-A-S35 0 MS S1
AN-47 + S2	ISO 14171-A-S42 2 CS S2
AN-47DP + S2	ISO 14171-A-S50 2 CS S2
AN-47DP + S3Ni1Mo	ISO 14171-A-S50 2 CS S3Ni1Mo
Tensile strength of pure (deposited) weld metal and 27 and 47 J impact energy (Multi-run technique, section B)	
AN-60 + Sv-08A	ISO 14171-B-S49A 2 MS SU11 ISO 14171-B-S49A 0U MS SU11 ISO 14171-B-S49S 2 MS SU11 ISO 14171-B-S49S 0U MS SU11
AN-348-A + Sv-08A	ISO 14171-B-S49A 2 MS SU11 ISO 14171-B-S49A 0U MS SU11 ISO 14171-B-S49S 2 MS SU11 ISO 14171-B-S49S 0U MS SU11
OSTs-45M + Sv-08A	ISO 14171-B-S49A 2 MS SU11 ISO 14171-B-S49A 0U MS SU11 ISO 14171-B-S49S 2 MS SU11 ISO 14171-B-S49S 0U MS SU11

Table 2. Code designations of domestic welding fluxes in accordance with requirements of International Standards ISO 14174:2004 and DSTU ISO 14174:2009

Flux grade	Full designation	Concise designation
AN-60 AN-60M	Welding flux ISO 14174-S F MS 1 AC H10 Welding Flux DSTU ISO 14174 S F MS 1 AC H10	Welding flux ISO 14174-S F MS 1 Welding flux DSTU ISO 14174-S F MS 1
AN-348-A AN-348-AM AN-348AP AN-348APM	Welding flux ISO 14174-S F MS 1 AC H10 Welding flux DSTU ISO 14174-S F MS 1 AC H10	Welding flux ISO 14174-S F MS 1 Welding flux DSTU ISO 14174-S F MS 1
AN-47 AN-47DP	Welding flux ISO 14174-S F CS 1 AC H10 Welding flux DSTU ISO 14174-S F CS 1 AC H10	Welding flux ISO 14174-S F CS 1 Welding flux DSTU ISO 14174-S F CS 1
OSTs-45M OSTs-45	Welding flux ISO 14174-S F MS 1 AC H10 Welding flux DSTU ISO 14174-S MS 1 AC H0	Welding flux ISO 14174-S F MS 1 Welding flux DSTU ISO 14174-S F MS 1
AN-43	Welding flux ISO 14174-S F AB 1 AD H5 Welding flux DSTU ISO 14174-S F MS 1 AB 1 AD H5	Welding flux ISO 14174-S F AB 1 Welding flux DSTU ISO 14174-S F MS 1
AN-67B	Welding flux ISO 14174-S F AR 1 AC H5 Welding flux DSTU ISO 14174-S F MS 1 AR 1 AC H5	Welding flux ISO 14174-S F AR 1 Welding flux DSTU ISO 14174-S F MS 1
AN-8	Welding flux ISO 14174-S F MS 1 AC H10 Welding flux DSTU ISO 14174-S F MS 1 AC H10	Welding flux ISO 14174-S F MS 1 Welding flux DSTU ISO 14174-S F MS 1
AN-20S AN-20P	Welding flux ISO 14174-S F AB 2 AD H10 Welding flux DSTU ISO 14174-S F AB 2 AD H10	Welding flux ISO 14174-S F AB 2 Welding flux DSTU ISO 14174-S F AB 2
AN-26S AN-26P	Welding flux ISO 14174-S F AB 2 AC H5 Welding flux DSTU ISO 14174-S F AB 2 AC H5	Welding flux ISO 14174-S F AB 2 Welding flux DSTU ISO 14174-S F AB 2

81:2004, TU U 05416923-049–99 and GOST R 52222 were designated on the basis of the results of tests carried out according to the requirements of International Standard ISO 14174:2004. The information, which is contained in technical documents for manufacture of fluxes (GOST 9087–81E, TU U 05416923.049–99 and GOST R 52222 etc.) and relates to application, methods of manufacture and chemical composition of the fluxes, as well as the results of special tests conducted to determine applicability of the fluxes to AC and/or DC welding, data on the content of diffusible hydrogen, metallurgical characteristic and current load was used to make a decision. Designations of the above fluxes according to draft DSTU ISO 14174:2009, introduction of which in Ukraine as a national standard is planned for 2010, are also given.

Some peculiarities of application of international standards. Analysis of international standards relating to fluxes shows that they contain no data, which are included in intergovernmental and national standards acting in Ukraine, as well as in specifications. In fact, the latter regulate the technology for manufacture of fluxes — their chemical composition, color etc. These data are classified information (know-how) of foreign manufacturers. Therefore, from a point of view of a foreign consumer, GOST 9087–81E and different Ukrainian specifications are internal normative documents of enterprises, from which no information can be obtained, for example, on a level of strength of a welded joint provided by this flux in combination with welding wires of these or other grades, as well as on that under which conditions this flux should be used.

As noted above, implementation of international standards does not cancel any currently acting national norms. However, it imposes some requirements to the product delivery conditions. These requirements are specified in ISO 14344:2002, which sets a list and scope of mandatory tests for welding consumables. The latter are determined by the customer when concluding a delivery contract. The results of these tests are by all means included into the quality certificate or an accompanying document that replaces it.

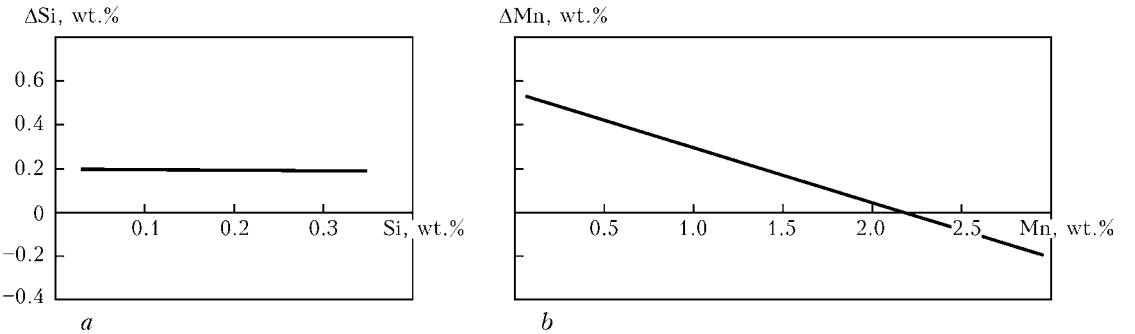

Dependence of increment (burnout) of silicon (*a*) and manganese (*b*) in weld metal on their content in welding wire [6]

Table 3. Designations of metallurgical characteristics of domestic fluxes

Flux grade	ISO 14174:2004	EN 760:1996
AN-60	ISO 14174-S F MS 1 AC H10	F MS 1 68 AC 14 SM HP10 3-40
AN-60M	ISO 14174-S F MS 1 AC H10	F MS 1 68 AC 14 SM HP10 2-16
AN-348-A	ISO 14174-S F MS 1 AC H10	F MS 1 78 AC 12 HP10 2-28
AN-348-AM	ISO 14174-S F MS 1 AC H10	F MS 1 78 AC 12 HP10 2-16
AN-47	ISO 14174-S F CS 1 AC H10	F CS 1 66 AC 12 HP10 3-25
OSTs-45	ISO 14174-S F MS 1 AC H10	F MS 1 78 AC 14 HP10 2-25
OSTs-45M	ISO 14174-S F MS 1 AC H10	F MS 1 78 AC 14 HP10 2-16
AN-43	ISO 14174-S F AB 1 AD H5	F AB 1 54 AD 8 HP5 2-25
AN-67B	ISO 14174-S F AR 1 AC H5	F AR 1 54 AC 14 HP5 2-25
AN-8	ISO 14174-S F MS 1 AC H10	F MS 1 78 AC 12 HP10 2-28
AN-20S	ISO 14174-S F AB 2 AD H10	F AB 2 65AD 9 HP10 2-28
AN-20P	ISO 14174-S F AB 2 AD H10	F AB 2 65AD 9 HP10 3-40
AN-26S	ISO 14174-S F AB 2 AC H5	F AB 2 65 AC 10 HP5 2-25
AN-26P	ISO 14174-S F AB 2 AC H5	F AB 2 65 AC 10 HP5 2-28

Therefore, after Ukraine joined WTO, the situation is as follows. If the customer requires to deliver flux AN-60 according to GOST 9087–81E, the supplier should manufacture and deliver the flux in compliance with this regulatory document, but if it is necessary to deliver this flux according to ISO 14344:2002, the supplier manufactures it in compliance with GOST 9087–81E, since it is this standard that determines the technology for manufacture of the given flux, carries out welding tests (if the customer requests this) in accordance with the requirements of ISO 14171:2002, ISO 15792-1:2000 and ISO 15792-2:2000, and draws up documents (quality certificate etc.) in compliance with ISO 14344:2002. It should be noted that this standard contains only guidelines for delivery of welding consumables, while GOST 9087-81:2002 contains requirements to physical-chemical characteristics of the products and their manufacture technology. Therefore, both standards supplement each other. So, GOST 9087–81E will act for some time as

Table 4. Designations of fluxes for welding of carbon and low-alloy steels

Flux grade (Flux) (ISO 14174:2004)	Welding wire (Wire electrodes) (ISO 14171:2002)	Classification (Classification ISO 14171:2002)	
		Probe of pure (deposited) weld metal (Multi-run technique)	Welded joint (TWO-run technique)
AN-60 AN-60M S F MS 1 AC H10	S1	A-S35 2 MS S1	A-S 3T 0 MS S1
	S2	A-S42 0 MS S2	–
	S1 (Sv-08A)	B-S49A 2 MS SU11 B-S49A 0U MS SU11	B-S49S 2 MS SU11 B-S49S 0U MS SU11
AN-348-A AN-348-AM S F MS 1 AC H10	S1	A-S38 0 MS S1	A-S 5T 2 MS S1
	S1 (Sv-08A)	B-S49A 2 MS SU11 B-S49A 0U MS SU11	B-S49S 2 MS SU11 B-S49S 0U MS SU11
AN-47 S F CS 1 AC H10	S2	A-S42 2 CS S2	A-S 5T 2 CS S2
	SU11 (Sv-08GA)	–	B-S57S 5 CS SU11
OSTs-45M S F MS 1 AC H10	S1	A-S35 0 MS S1	A-S 5T 2 MS S1
	S1 (Sv-08A)	B-S49A 2 MS SU11 B-S49A 0U MS SU11	B-S49S 2 MS SU11 B-S49S 0U MS SU11
AN-67B S F AR 1 AC H5	S2	A-S 50 4 AR S2	A-S 3T 4 AR S2
	SUN2M3 (Sv-08G1NMA)	B-S57A 7 AR SUN2M3 B-S57A 6U AR SUN2M3	B-S57S 7 AR SUN2M3 B-S57S 6U AR SUN2M3
AN-43 S F AB 1 AD H5	S2	A-S 50 4 AR S2	A-S 3T 4 AR S2
	SU11 (Sv-08GA)	B-S57A 5 AR SU11 B-S57A 4U AR SU11	B-S57A 5 AR SU11 B-S57A 4U AR SU11

Designation of combination of flux AN-60 + wire S1 according to standard ISO 14171:2002 (testing of pure (deposited) weld metal for determination of yield strength and 47 J impact energy (Multi-run technique, section A)

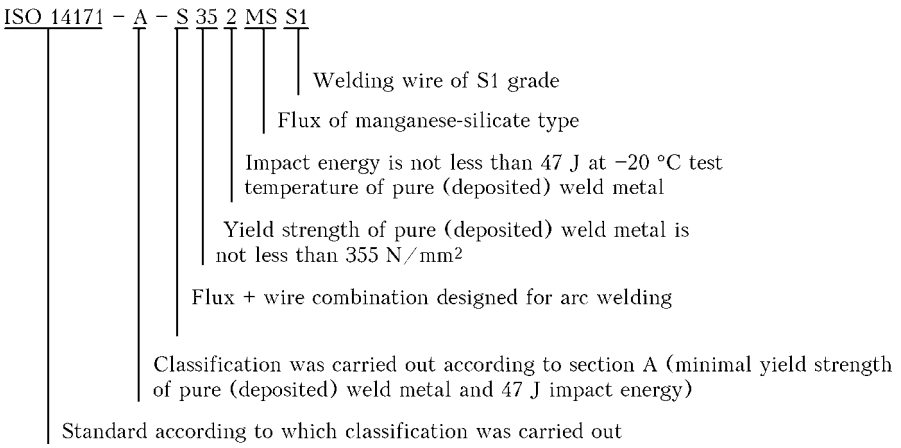

Designation of combination of flux AN-60 + wire Sv-08A according to standard ISO 14171:2002 (testing of welded joint for determination of tensile strength and 27 J impact energy (TWO-run technique, section B)

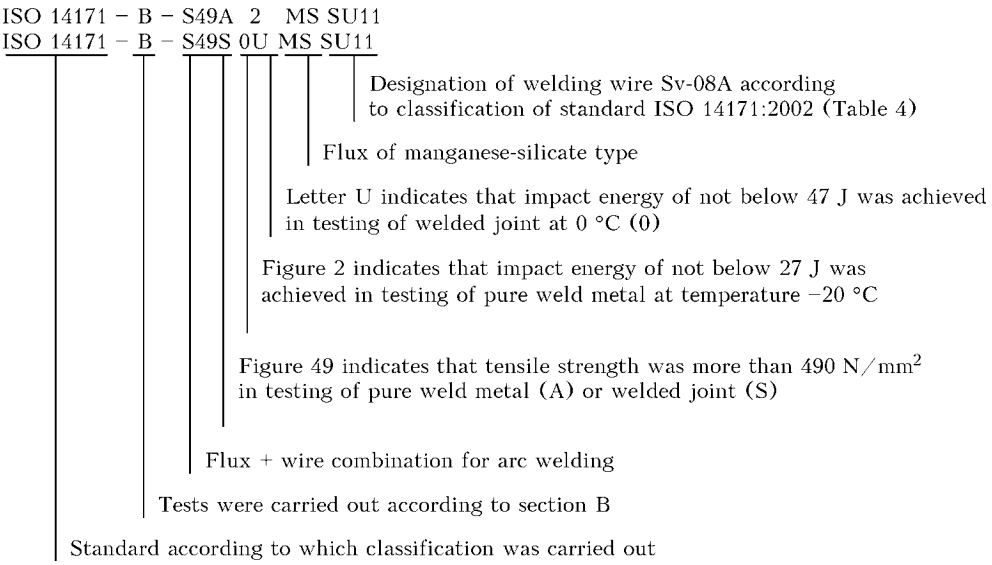

Designation of flux AN-60 according to standard ISO 14174:2004 Welding flux ISO 14174-S MS 1 AC H10

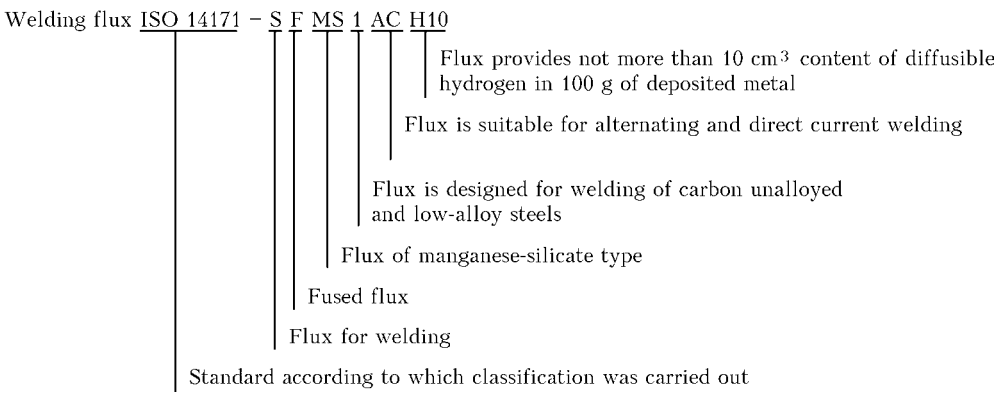

an intergovernmental standard for customers from the CIS countries, and further on will become a standard of enterprise.

Some explanations to standards ISO 14171:2002 and ISO 14174:2004. *Metallurgical characteristic*. Standard ISO 14174:2002 contains a statement about metallurgical characteristic of a flux, although it indicates that this characteristic is not included in the flux designation, but is only mentioned in technical documentation (not saying in what document). Also, this standard does not mention a regulatory document, according to which this characteristic is determined.

The metallurgical characteristic shows an influence of chemical composition of a flux on transfer of primarily silicon and manganese into the weld metal — increments ΔSi and ΔMn, which are determined as a difference between the content of an element in the deposited metal, obtained according to ISO 15792-1:2000, and in the welding wire.

Sometimes the metallurgical characteristic of flux is given in advertisement materials [6] in form of diagrams of the dependence of increase in alloying elements on their content in the flux (Figure). European standard EN 760:1996 is used more often. In it an appropriate number is given to a specific range of values of increase in alloying elements, by using which the metallurgical characteristic is evaluated. However, in tests a disagreement is observed in obtained results. This is explained by the fact that a number of factors, which are difficult to take into account, for example, maintaining the precise welding conditions or chemical composition of metal, influence the transfer of alloying elements into the weld metal. Therefore, for comparative assessment of domestic fluxes by the codes with allowance for the metallurgical characteristic, we recommend to use a comparative table, which is made based on the statistical data, using European standard EN 760:1996 (Table 3).

Current load. Current load is a maximal current for welding with one electrode, at which the flux melt boils and loses its ability to form the weld. This characteristic is not included into the flux designations in existing standard ISO 14174:2004. However, this drawback was eliminated in a new edition of this standard ISO 14174:2008 by using flux designations according to EN 760:1996 (figure after code AC or AD multiplied 100 times shows current load value).

Grain size. The last three figures in designations according to EN 760:1996 point to a grain size (minimum/maximum). The code of this characteristic is not included into the flux designations of existing standard ISO 14174:2002. However, its new edition requires that the grain size be indicated on a packing and in technical documents.

Utilization of designations. The designation according to standard ISO 14174:2002 for each flux exists in one variant. It shows only the main consumer characteristics of the flux itself. Such designations should be included in all information materials (on labels, in quality certificates, promotional products, technical documents) after the flux grade, for example, grade AN-60 (DSTU ISO 14174-S F MS 1 AC H10).

More often this designation is used by customers when approaching a manufacturer, or by manufacturers for promotion of a product.

Classification according to standard ISO 14171:2002 concerns only those fluxes, which are classified by standard ISO 14174:2004 to class 1, i.e. designed for welding of unalloyed and low-alloy steels. Therefore, the designations of other classes of the fluxes are given only according to standard ISO 14174:2004 (see Table 2, fluxes of AN-20S, AN-20P, AN-26S, AN-26P, AN-8 grades).

The quantity of designations of flux + wire combinations according to standard ISO 14171:2002 depends on the quantity of welding wires and steel grades, with which a flux was tested, and could achieve ten and a half or more.

Meaning of codes. Standards ISO 14171:2002 and ISO 14174:2004 contain a detailed description of codes, which are included in designations of fluxes or combinations of the latter with wires. Interpretation of the codes is given by an example of flux AN-60 (p. 47).

For domestic flux manufacturers, it is necessary to introduce the said designations of fluxes and their combinations with welding wires in the quality certificates and labels on packing, as well as in technical documents and promotion products. An example of designation to be used in advertisements and informational materials is given in Table 4.

It should be noted that Technical Commission ISO/TC44/SC3 prepares new editions of standards ISO 14171:2002 and ISO 14171:2004 by taking into account remarks of the customers, developers and manufacturers of welding fluxes. The updated standards will provide clear statements on the metallurgical characteristic, current load, methods for their determination and application in designations of fluxes. Publication of these standards is planned within the next years.

1. *GOST 9087–81E*: Fused welding fluxes. Specifications. Introd. 01.01.82.
2. *TU U 05416923.049–99*: Fused welding fluxes of grades AN-47, AN-348-A, AN-348V, ANTs-1A, AN-60, OSTs-45 and their modifications D, M, P. Valid from 04.04.2000.
3. *GOST R 52222*: Fused welding fluxes for automatic welding. Specifications. Approved 01.01.2005.
4. *ANSI/AWS A5.17–89*: Specification for carbon steel electrodes and fluxes for submerged arc welding. Approved 17.03.89.
5. *ANSI/AWS A5.23–90*: Specification for low alloy steel electrodes and fluxes for submerged arc welding. Approved 01.01.99.
6. (1993) *Handbuch Schweisszusatzwerkstoffe*. OERLIKON.

INFLUENCE OF WORKING FREQUENCY ON DIMENSIONS OF TRANSFORMERS FOR AC RESISTANCE WELDING

Yu.N. LANKIN
E.O. Paton Electric Welding Institute, NASU, Kiev, Ukraine

The paper deals with a resistance welding machine powered from a high-frequency mains. Effect of working frequency increase compared to industrial frequency on the volume of machine transformer core was studied. It is shown that frequency increase does not lower the overall dimensions and weight of the transformer and it is not rational to supply power to AC resistance welding machines of medium and high power from a higher frequency inverter.

Keywords: *resistance welding, inverter, welding machine, transformer, secondary circuit, magnet core volume*

Increase of working frequency is known to be an effective means of reduction of transformer dimensions and weight [1]. Reduction of weight and dimension characteristics is particularly rational for built-in transformers of welding tongues. Frequency triplers, motor generator sets or inductor generators were earlier used as the main power source [2], and now thyristor or transistor inverters are applied [3]. Unfortunately, frequency increase leads to increase of inductive resistance of the machine secondary circuit. To avoid welding current dropping in this case, secondary voltage of the transformer and, hence, its power have to be increased. Thus, increase of supply frequency has an ambiguous influence on the overall volume of transformers for AC resistance welding. Therefore, it is of interest to study the nature of influence of working frequency on overall volume and the associated weight of the transformer for AC resistance welding.

For transformers with minimum weight and dimension characteristics the following relationships are valid [1]:

$$V_{tr} \approx 3V_m, \quad 0.13V_m^{4/3} = S_m S_{ap}, \quad S_{ap} = (2.5 - 1.3)S_m,$$

where V_{tr} is the transformer volume; V_m is the magnet core volume; S_m, S_{ap} are the magnet core cross-section and its aperture area, respectively. Hence,

$$V_m = (9.2 - 5.5) \sqrt[3/4]{S_m},$$

i.e. transformer volume is directly related to magnet core section. Reduction of active section of magnet core material S_m with increase of frequency follows from a known formula:

$$S_m = \frac{E_1}{4.44 f w_1 B}, \qquad (1)$$

where E_1 is the self-induction emf in the primary winding; w_1 is the number of primary winding turns; B is the induction. Unfortunately, with frequency increase the power of losses in the magnet core and additional losses in winding copper increases, leading to additional increase of the transformer winding. For frequency range up to units of kiloherz additional losses in copper through skin-effect are negligible. Dependence of specific losses in the magnet core on frequency has the following form [1]:

$$p = Af^{\alpha}B^2, \qquad (2)$$

where A are the losses in a unit of volume at $f = 1$ Hz; $B = 10^4$ T; $\alpha = 1.5–2.0$.

To ensure that the loss power in the magnet core and transformer overheating, respectively, stayed on the same level, it is necessary to lower the induction simultaneously with increase of frequency, as follows from (2). However, according to relationship (1), reduction of induction leads to increase of S_m. Thus, cross-section of transformer magnet core and, therefore, also its volume decrease markedly slower with increase of frequency than in inverse proportion to frequency. In addition, with reduction of transformer dimensions the cooling surface decreases and induction has to be lowered even further.

In [1] the theory of similarity was used to derive the following expression for transformer magnet core volume V_m:

$$V_m(f) = 1.5\sqrt{\frac{Ak_{ad}}{k_m}}\,\frac{P}{\sqrt[4]{f}\,\Delta T}, \qquad (3)$$

where P is the power; k_{ad} is the coefficient of additional losses in copper; k_m is the coefficient of magnet core aperture filling with copper; ΔT is the transformer overheating. Expression (3) was derived for active load and without allowing for scattering inductance of transformer windings. A feature of AC resistance welding machines is inductive-active nature of transformer load

$$Z_2(f) = \sqrt{(R_c + r_p)^2 + (2\pi f L_c)^2}, \qquad (4)$$

© Yu.N. LANKIN, 2010

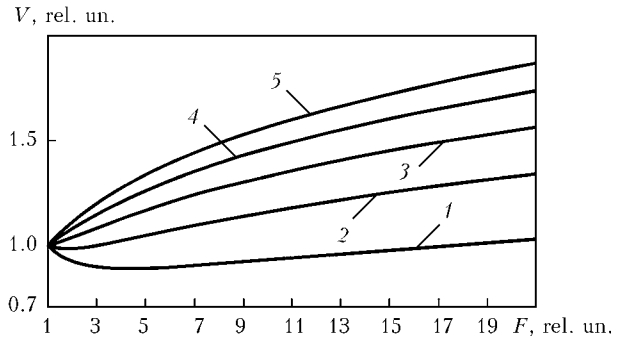

Dependence of dimensionless volume of transformer magnet core on dimensionless frequency at different power factors of the machine at industrial frequency: *1* — cos φ = 0.9; *2* — 0.8; *3* — 0.7; *4* — 0.6; *5* — 0.5

where R_c is the ohmic resistance of machine secondary circuit; r_p is the resistance of the welded part; L_c is the inductance of machine secondary circuit. In this case, expression (3) becomes

$$V_m(f) = 1.5 \sqrt{\frac{Ak_{ad}}{k_m}} \frac{Z_2(f)I_2^2}{\sqrt[4]{f}\,\Delta T}, \quad (5)$$

where I_2 is the resistance machine secondary current.

In order to study the influence of frequency on magnet core volume, it is convenient to go over to dimensionless parameters of the transformer, taking the following as basic transformer parameters at 50 Hz industrial frequency: $V = V_m(f)/V_m(50)$ is the transformer relative volume, $F = f/50$ is the relative frequency.

Let us assume that at change of frequency R_c, r_p, L_c, k_{ad}, A, I_2 and ΔT remain unchanged. Considering that

$$\frac{2\pi 50 L_c}{R_c + r_p} = \text{tg}\,(\varphi), \quad (6)$$

$$\frac{2\pi f L_c}{R_c + r_p} = \text{tg}\,(\varphi)F, \quad (7)$$

where φ is the shear angle between current and voltage in the secondary circuit at working frequency equal to 50 Hz, from equations (4)–(7), omitting intermediate transformations, we will have the dependence of relative volume of transformer magnet core on working frequency and cos φ (power factor) of the machine:

$$V = \frac{\sqrt{\cos^2(\varphi)(1 - F) + F}}{\sqrt[4]{F}}. \quad (8)$$

Dependencies of V on F and cos φ, calculated by formula (8), are given in the Figure. As follows from the Figure, for machines with cos φ = 0.9 of the secondary circuit at industrial frequency a lowering of magnet core volume maximum by 11 % is found with increase of the working frequency. At cos φ ≥ 0.8 the magnet core volume only rises with increase of working frequency. Usually, cos φ of resistance machines of 50 Hz industrial frequency is in the range of 0.4–0.7, and the maximum possible range is 0.2–0.8 [4]. Therefore, increase of working frequency of AC resistance welding machines for reduction of transformer overall dimensions is not rational, as for real secondary circuits of machines the transformer overall dimensions are not reduced, but, on the contrary are increased. The above calculations were made using a number of simplifying assumptions. However, their influence has the second order of smallness, and does not seriously affect the obtained regularities.

Real reduction of the dimensions and weight of the transformer can be achieved when using increased frequency in resistance machines with rectifiers in the secondary circuit.

Increase of working frequency unambiguously improves the adjustment characteristics of machines for resistance welding through increase of the control system dynamic characteristics. This has a marked effect at application of the time of welding current pulse below 5–10 periods of 50 Hz mains. Therefore, AC machines of industrial frequency are not used for microwelding requiring less than 10–30 ms time of welding current running. In this case, it is the most rational to apply higher frequency machines with and without rectifiers in the secondary circuit, which have incomparably better adjustment characteristics than the most widely accepted now capacitor machines.

CONCLUSIONS

1. Increase of working frequency (application of inverters) does not provide a reduction of overall dimensions and weight of the transformer of AC resistance welding machines.

2. Increase of working frequency in some cases can reduce the overall dimensions and weight of resistance welding machines with a rectifier in the secondary circuit, thus improving the dynamic characteristics of the system of welding current control, which is particularly appropriate for microwelding.

1. Gorsky, A.N., Rusin, Yu.S., Ivanov, N.P. et al. (1988) *Calculation of electromagnetic elements of secondary power supplies*. Moscow: Radio i Svyaz.
2. Ryskova, Z.A., Fedotov, P.D., Zhimereva, V.I. (1990) *Transformers for resistance welding*. Leningrad: Energoatomizdat.
3. Budilov, B.A., Glazov, V.V., Komarchev, A.I. et al. *Machine for resistance welding*. Pat. 2047444 RF. Int. Cl. B23K111/24. Appl. 07.02.1994. Publ. 10.11.1995.
4. Glebov, L.V., Peskarev, N.A., Fajgenbaum, D.S. (1981) *Calculation and design of resistance welding machines*. Leningrad: Energoatomizdat.

NEWS

VERSATILE SOURCE SUPER-200P

Limited Liability Research-and-Production Company «Plasma» (Rostov-on-Don, RF) for 18 years has been involved in development and production of electric welding equipment, and is now taking one of the leading positions in Russia not only in the volume and range of its products, but also in their technical level.

Machines developed by designers and production engineers of the «Plasma» Company in collaboration with specialists of the E.O. Paton Electric Welding Institute of the NAS of Ukraine feature a high level of welding characteristics, reliability and simplicity in operation, as well as an excellent exterior design.

Worthy of attention in a product line of argon-arc welding units are multifunctional, light-weight, easy-to-use and mobile inverter rectifiers based on the up-to-date MOS-FET technology, which provide HF arc excitation, adjustable mode of welding current pulsation P/(pulse), and are equipped with forced air cooling and overheating protection.

SUPER-200P is one of the versatile professional welding units of the inverter type, which provides a high welding quality on all types of metals in the mode of tungsten-electrode argon-arc (TIG) welding at the alternating and direct current (AC/DC), as well as in a mode of manual arc (MMA) welding. In addition, it makes it possible to perform air-plasma cutting of up 1o 15 mm thick metals.

Key advantages of SUPER-200P include regulation of the time of purging at the beginning and end of welding and the initial welding current, smooth decrease of the welding current at the end of welding, overheating protection, multifunctionality, and pulsation mode for TIG welding.

Parameters of SUPER-200P: mains voltage — 220 V; welding current (duty cycle) — 200 A (60 %); power — 4.5 kW, dimensions (H × W × D) — 498 × × 327 × 360 mm, weight — 20 kg.

GANTRY-TYPE THERMAL CUTTING MACHINE «NORMAL»

Moscow Limited Liability Company «Factor» offers three-coordinate gantry-type thermal cutting machine «Normal», which is a CNC processing system for cutting out of metal rolled products based on specified drawings. The machine is equipped with a system for automatic return to the initial cut point on each part and a system for tracking of distance between a cutter and plate being cut. The machine allows cutting out of complex-configuration billets with the high accuracy and quality of a surface cut.

It can be fitted with any device for air-plasma cutting of metals, as well as with equipment for gas-oxygen cutting. Sizes of the cutting work zone range from 1.5 × 3 to 3.5 × 12 m.

CNC parameters:

• input of control programs — keyboard, USB port. Loading and unloading of control programs are performed in a dialogue mode of the menu system;

• design — monoblock (processor, sensor communication board, volatile and non-volatile (flash-disk) memory), membrane keyboard, colour display, power source);

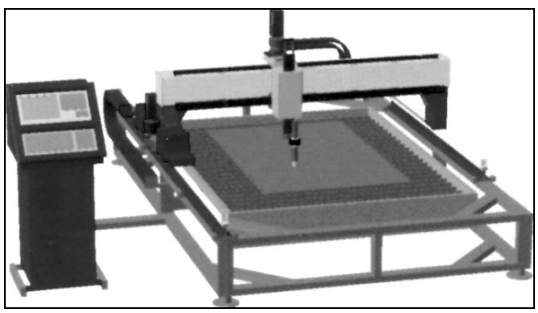

• supply voltage — 220 V, 50 Hz. Consumed power — not more than 400 W;

• types of interpolation: linear and circular on X and Y coordinates;

• quantity of feedback controlled coordinates — 3;

• proportional control of Z coordinate by signal of distance or arc voltage sensor.

SUBSCRIPTION
FOR «THE PATON WELDING JOURNAL»

If You are interested in making subscription directly via Editorial Board, fill, please, the coupon and send application by fax or e-mail.

The cost of annual subscription via Editorial Board is $324.

Telephones and faxes of Editorial Board of «The Paton Welding Journal»:

Tel.: (38044) 287 6302, 271 2403, 529 2623

Fax: (38044) 528 3484, 528 0486, 529 2623.

«The Paton Welding Journal» can be also subscribed worldwide from catalogues of subscription agency EBSCO.

SUBSCRIPTION COUPON
Address for journal delivery

Term of subscription since _____ **200** **till** _____ **200**
Name, initials _____
Affiliation _____
Position _____
Tel., Fax, E-mail _____

ADVERTISEMENT IN «THE PATON WELDING JOURNAL»
(DISTRIBUTED ALL OVER THE WORLD)

«AVTOMATICHESKAYA SVARKA»
RUSSIAN VERSION OF «THE PATON WELDING JOURNAL»
(DISTRIBUTED IN UKRAINE, RUSSIA AND OTHER CIS COUNTRIES)

External cover, fully-colored:
First page of cover (190×190 mm) – $700
Second page of cover (200×290 mm) – $550
Third page of cover (200×290 mm) – $500
Fourth page of cover (200×290 mm) – $600

Internal cover, fully-colored:
First page of cover (200×290 mm) – $400
Second page of cover (200×290 mm) – $400
Third page of cover (200×290 mm) – $400
Fourth page of cover (200×290 mm) – $400

Internal insert:
Fully-colored (200×290 mm) – $340
Fully-colored (double page A3) (400×290 mm) – $570
Fully-colored (200×145 mm) – $170

- Article in the form of advertising is 50 % of the cost of advertising area
- When the sum of advertising contracts exceeds $1000, a flexible system of discounts is envisaged

Technical requirement for the advertising materials:
- Size of journal after cutting is 200×290 mm
- In advertising layouts, the texts, logotypes and other elements should be located 5 mm from the module edge to prevent the loss of a part of information

All files in format IBM PC:
- Corell Draw, version up to 10.0
- Adobe Photoshop, version up to 7.0
- Quark, version up to 5.0
- Representations in format TIFF, color model CMYK, resolution 300 dpi
- Files should be added with a printed copy (makeups in WORD for are not accepted)